UiT The Arctic University of Norway

Faculty of Health Science

Department of Pharmacy

Drug Transport and Delivery Research Group

The development of electrospun chloramphenicol containing wound dressing

Anjanah Murugaiah

Thesis for the degree Master of Pharmacy, FAR 3911, May 2021

THESIS FOR THE DEGREE MASTER OF PHARMACY

THE DEVELOPMENT OF ELECTROSPUN CHLORAMPHENICOL
CONTAINING WOUND DRESSING

BY

ANJANAH MURUGAIAH

MAY 2021

SUPERVISORS

Associate Professor Ann Mari Holsæter

and

PhD fellow Laura Schulte Werning

Drug Transport and Delivery Research Group Department of Pharmacy

Faculty of Health Sciences

UiT- The Artic University of Norway

IV

Acknowledgements

Table of contents

List of Figures

List of Tables

Abstract

Wound healing is among the most complex processes in the human body that is greatly coordinated with a focus to rebuild tissue integrity and restore the skin´s protective barrier. The normal healing process is disrupted in chronic wounds, leading to delayed wound healing due to several underlying factors such as aging, obesity, and diabetes. Among chronic wounds 50 % are infected and up to 78 % of these wounds have presence of biofilm. The management of these wounds is complicated, even with antibiotics. Antibiotic resistance is a growing issue worldwide. Thus, there is a need for innovative treatments that are capable of accelerating wound healing process, and at the same time, prevent and fight bacterial contamination and growth. Electrospinning is a favorable method for making nanofiber dressings. These nanofibers can be added several active ingredients to obtain multifunctional wound dressings.

This project aims as developing multifunctional nanofibers, containing the active ingredient soluble beta-1,3/1,6-glucan (SBG®) with an immune stimulating effect, and chitosan (CHI) applied for its antimicrobial effect. In addition, we incorporated chloramphenicol (CAM) as the antimicrobial ingredient. Hydroxypropyl methylcellulose (HPMC) and polyethylene oxide (PEO) were used as co-polymers, and water, ethanol, and acetic acid were used as solvents. The focus of this master project was to process and characterize these multifunctional nanofiber formulations together with appropriate control formulations.

The nanofibers were produced using the needle-free Nanospider™ technology. To assess the properties of fabricated nanofibers, suitable methods for characterization of both polymer solutions without and with CAM and final nanofibers were applied. Conductivity, pH, surface tension and viscosity were examined to characterize the polymer solutions. The produced nanofibers were evaluated for absorption capacity, tensile properties, morphologies, and diameter. Fabricated nanofibers with CAM were evaluated for its content and *in vitro* release. In addition, all nanofibers were assessed for *in vitro* cell toxicity.

Polymer solutions containing CAM and β-glucan (βG) did not affect solution properties. CHI containing polymer solutions had increased conductivity, pH, and viscosity. The electrospinning process was not influenced by these increased properties. The temperature and relative humidity were successfully controlled during the electrospinning process for all nanofibers. All nanofibers were uniform and had diameter in the range from 129.5 to 200.9 nm. Nanofibers containing CHI did hold their structure in simulated wound fluid (SWF) and was possible to be investigated for absorption capacity. These nanofibers had absorption capacity up to 1055 % and was judged suitable for treatment of moderate to high exudative wounds. The method used for absorption capacity was not able to be performed on nanofibers without CHI since these nanofibers dissolved fast in SWF. The tensile strength of all produced nanofibers was in the skin range and proved to have good strength. However, the elongation at break for all nanofibers was poor and suggested to be less elasticity compared to the native skin. CHI and βG nanofibers did not affect the *in vitro* CAM release, since all nanofibers had burst release of CAM. The high recovery of CAM from the *in vitro* CAM release, from 85 to 99 %, indicates that CAM is stable in all nanofibers and tolerate the electrospinning process well. Lastly, all nanofibers did not show cytotoxicity, indicating good cytocompatibility on human immortalized keratinocytes (HaCaT) cell lines.

Keywords: Chitosan; SBG®; β-glucan; Chloramphenicol; Nanofiber; Needle-free electrospinning; Nanospider™; Wound dressing; Wound healing; Chronic wounds

Sammendrag

Sårheling er en av de mest komplekse prosessene i menneske kroppen som er svært regulert med fokus på å gjenopprette vevsintegriteten og hudens beskyttende barriere. Den normale helingsprosessen er forstyrret i kroniske sår, noe som fører til forlenget sårheling. Dette kan skyldes flere underliggerende faktorer som aldring, fedme og diabetes. Blant kroniske sår er 50 % infisert og opptil 78 % av disse har tilstedeværelse av biofilm. Behandlingen av slike sår er komplisert, selv med antibiotika. Antibiotikaresistens er et voksende globalt problem. Derfor er det behov for innovative behandlinger som er i stand til å fremskynde helingsprosessen, samtidig som den forebygger og angriper bakteriekontaminasjon og-vekst. Elektrospinning er en lovende metode for å produsere nanofibre til bruk som sårbandasje. I disse nanofibrene kan flere aktive ingredienser tilsettes slik at man oppnår multifunksjonelle sårbandasjer.

Formålet med dette prosjektet var å utvikle multifunksjonelle nanofibre, bestående av den aktive ingrediensen, vannløselige beta-1,3/1,6-glukan (SBG®) med en immun stimulerende effekt, og kitosan (CHI) som blant annet er kjent å ha en antimikrobiell effekt. I tillegg ble kloramfenikol (CAM) inkorporert som antimikrobiell ingrediens. Hydroksypropylmetylcellulose (HPMC) og polyetylenoksid (PEO) ble benyttet som co-polymerer, og vann, etanol og eddiksyre ble brukt som løsemidler. Fokuset med dette masterprosjektet var å produsere og karakterisere multifunksjonelle nanofiber-formuleringer, sammen med passende kontroll-formuleringer.

Nanofibrene ble produsert ved å benytte nål-fri Nanospider™ teknologi. For å optimalisere prosess og nanofibre, ble både polymerløsninger og endelige nanofibre nøye karakterisert. Polymerløsningenes konduktivitet, pH, overflatespenning og viskositet ble undersøkt, og nanofibrene ble undersøkt for absorpsjonskapasitet, mekaniske egenskaper, morfologi og diameter. Nanofibre med CAM ble karakterisert ved undersøkelse av CAM-innhold og *in vitro* CAM frigjørelse. I tillegg, ble alle nanofibre evaluert for *in vitro* celle toksisitet.

Polymerløsningenes egenskaper ble ikke endret ved tilførsel av CAM og β-glukan (βG). CHI ga derimot økt konduktivitet, pH og viskositet. Elektrospinningsprosessen fungerte bra for alle formuleringer. Vi klarte å kontrollere både temperaturen og relativ fuktighet under elektrospinningsprosessen. Alle nanofibrene hadde uniform morfologi og diameter fra 129,5 til 200,9 nm. Nanofibre bestående av CHI holdt strukturen i simulert sårvæske (SWF) og var derfor mulig å måle absorpsjonskapasitet til. Disse nanofibrene hadde absorpsjonskapasitet på opptil 1055 % og var vurdert egnet til behandling av sår med moderat til høytvæskende sår. Med anvendt metode var det ikke mulig å undersøke absorpsjonskapasiteten til nanofibre uten CHI, siden disse nanofibrene løste seg raskt i SWF. "Tensile strength" av alle nanofibre var innenfor i samme størrelsesorden som hudens. Likevel, var "elongation at break" dårlig for alle nanofibrene. Dette viser at de er mindre elastisitet enn huden. CHI og βG nanofibre påvirket ikke *in vitro* CAM frigjøringen, siden alle nanofibrene hadde "burst" frigjøring av CAM. En høy CAM "recovery" fra *in vitro* CAM frigjøringen, på mellom 85 til 99 %, indikerte at CAM er stabil i alle nanofibre og tolerer elektrospinningsprosessen bra. Til slutt, viste alle nanofibre ingen cytotoksisitet, som indikerer bra cytokompatibilitet på lav toksisitet mot humane keratinocytter (HaCaT).

Nøkkelord: Kitosan; SBG®; β-glukan; Kloramfenikol; Nanofiber; Nål-fri elektrospinning, Nanospider™; Sårbandasje; Sårheling; Kroniske sår

List of abbreviations

All-CAM-Nanofiber	CHI-βG-PEO-HPMC-CAM-Nanofiber
All-CAM-Sol	CHI-βG-PEO-HPMC-CAM-Solution
All-Nanofiber	CHI-βG-PEO-HPMC-Nanofiber
All-Sol	CHI-βG-PEO-HPMC-Solution
βG	β-1,3/1,6-glucan (β-glucan)
βG-Ref-CAM-Nanofiber	βG-PEO-HPMC-CAM-Nanofiber
βG-Ref-CAM-Sol	βG-PEO-HPMC-CAM-Solution
βG-Ref-Nanofiber	βG-PEO-HPMC-Nanofiber
βG-Ref-Sol	βG-PEO-HPMC-Solution
CAM	Chloramphenicol
CCK-8	Cell Counting Kit-8
CHI	Chitosan/ Chitopharm^{TM} M
CHI-Ref-CAM-Nanofiber	CHI-PEO-HPMC-CAM-Nanofiber
CHI-Ref-CAM-Sol	CHI-PEO-HPMC-CAM-Solution
CHI-Ref-Nanofiber	CHI-PEO-HPMC-Nanofiber
CHI-Ref-Sol	CHI-PEO-HPMC-Solution
ECM	Extracellular matrix
ES	Electrospinning
EtOH	Ethanol
FE-SEM	Field Emission Scanning Electron Microscopy
HaCaT	Human immortalized keratinocytes
HPMC	Hydroxypropyl methylcellulose/ Benecel^{TM} E4M hydroxypropyl methylcellulose
MMP	Mixed metalloproteinase
NF-ES	Needle-free electrospinning
PBS	Phosphate-buffered saline
PDGF	Platelet-derived growth factor
PEO	Polyethylene oxide
Ref-CAM-Nanofiber	PEO-HPMC-CAM-Nanofiber
Ref-CAM-Sol	PEO-HPMC-CAM-Solution
Ref-Nanofiber	PEO-HPMC-Nanofiber

Ref-Sol	PEO-HPMC-Solution
RH	Relative humidity
ROS	Reactive oxygen species
SBG®	2.5 % (w/w) Soluble beta-1,3/1,6-glucan in water
SD	Standard deviation
SWF	Simulated wound fluid
TGF-β	Transforming growth factor-β

General introduction

Chronic wounds affect more than 6 million people worldwide and are therefore expressed as "the silent epidemic" (Fras Zemljič et al., 2020; Powers et al., 2016). The incidence of chronic wounds is expanding due to the aging global population, increased prevalence of obesity and diabetes mellitus type 2, and other risk related conditions (Boateng & Catanzano, 2015). Chronic wounds are a major public health issue that provokes great economic costs, significant morbidity, and mortality. The standard wound care is to cover the wound area with dressing to both protect the wound from infections and to enhance the healing process. When a wound is infected, the healing process becomes complicated since the wound is colonized by bacteria that potentially develop a biofilm. This makes the management of wounds more complex. Thus, there is a need for innovative treatments which are capable of accelerating wound healing process and prevent bacterial contamination and growth. An ideal wound dressing must be biocompatible, biodegradable, promote wound healing process, be able to swell and absorb excess wound exudate, and exhibit high porosity that permits oxygen exchange (Fras Zemljič et al., 2020). Dressings for chronic wounds come in several forms, but no single one of them can meet all demands, as wounds have different desirable demands in different stages of healing depending on the initial cause and property of the wound.

Nanofibers are nanomaterials in the nano size range. These fibers exhibit several of the required properties of an ideal wound dressing, and have the possibility to revolutionize wound management (Rasouli et al., 2019). Nanofibers constitute a fibrillar network like the human extracellular matrix. Therefore, they provide cell growth and tissue formation (Wang et al., 2018). Nanofibers are fabricated by several methods and among them is the needle-free electrospinning (NF-ES) technique, utilized due to various favorable properties such as simplicity, reproducibility, and cost-efficiency (Eatemadi et al., 2016; Yu et al., 2017).

Electrospun nanofibers are a popular approach for making novel multifunctional wound dressings. These nanofibers, dependent on the composition, can have different functionalities in the wound healing process. Multifunctional nanofibers could provide local and controlled delivery of wound healing agents directly in the wound bed and at the same time act as a protective barrier against bacterial invasion (Wang et al., 2018).

To develop multifunctional nanofibers in this project, two active polymers, chitosan (CHI) and β-1,3/1,6-glucan (βG), were utilized. CHI is an antimicrobial and wound healing activating polysaccharide with good biocompatibility, non-immunogenicity, and low toxicity. βG has immunostimulating effects, promotes wound healing, and is also known to reduce the pain in the wounded bed (Seo et al., 2019). To enhance the wound healing and fight infection, the antibiotic chloramphenicol (CAM) was also added as an active ingredient. Local delivery of the antimicrobial agent CAM in the form of nanofiber dressing is more convenient over systemic use due to higher concentration at the desired area while avoiding high-systemic doses that can cause side effects, which in the case of CAM is dose limiting. This approach therefore can reduce side effects and also lower the risk of development of antimicrobial resistances (Rasouli et al., 2019).

1 Introduction

1.1 The human skin and wounds

1.1.1 Skin

The skin is the largest organ of the human body and comprises 15 % of an adult body weight. The human skin offers a physical barrier between the internal organs and external environment (Vig et al., 2017). It has vital functions such as protection of internal organs, bones, muscles from hazardous environmental agents, chemicals and pathogens (Dwivedi et al., 2019). In addition, the skin forms the first line of protection against pathogens, essential in the synthesis of vitamin D, sensation and temperature regulation of the body (Dwivedi et al., 2019). The human skin consists of three primarily layers; *epidermis*, *dermis*, and *hypodermis* (subcutaneous layer) (Figure 1).
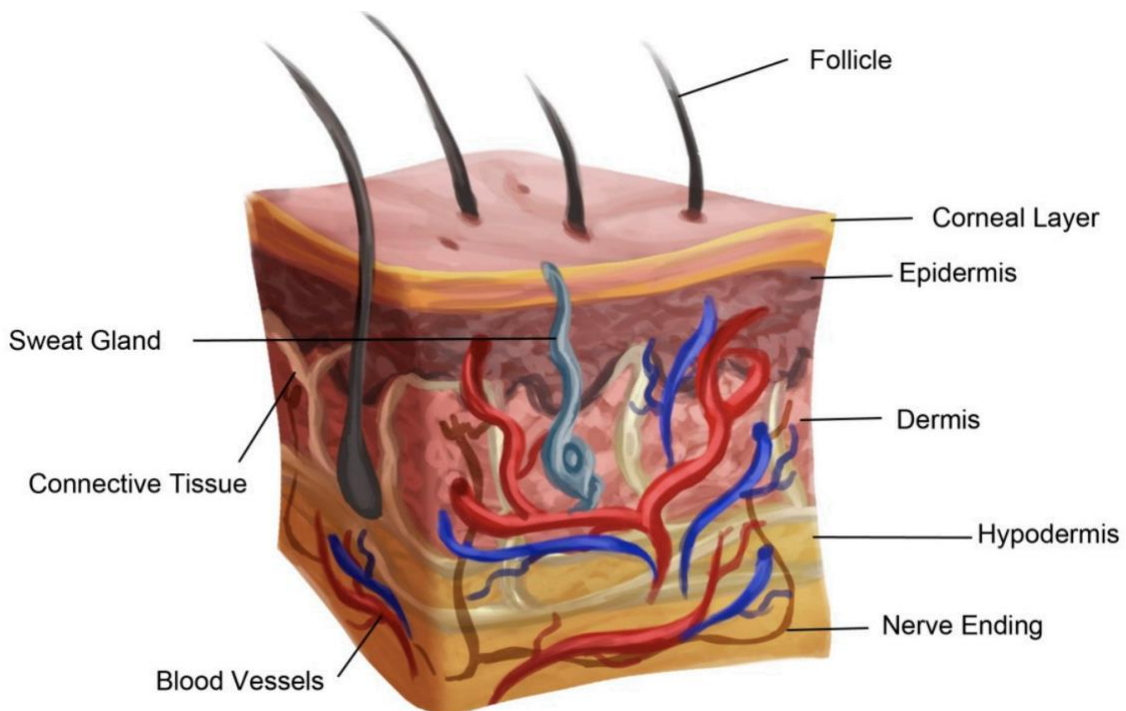
Figure 1: The structure of the skin. Shown here is epidermis, dermis and hypodermis. Reprinted with permission from (Vig et al., 2017). Copyright 2021, Creative Commons Attribution License.

1.1.1.1　Epidermis

The epidermis is the outer layer of the skin, which regulates the body´s water balance as well as it is in direct contact with the environment. This thin and tough layer lacks blood vessels (is avascular), and gets nourished by blood capillaries elongating to the upper layers of the dermis (Qin, 2016). The epidermis mainly consists of Merkel cells, keratinocytes, melanocytes and Langerhans cells. The layer is divided into four sublayers; *stratum corneum*, *stratum granulosum*, *stratum spinosum* and *stratum basale* (from uppermost to bottom) (Albanna & IV, 2016a; Dwivedi et al., 2019; Limbert, 2019). An extra sublayer known as *stratum lucidum* can only be found in the thick skin of palms and soles, beneath the *stratum corneum* and *stratum granulosum (Albanna & IV, 2016a; Limbert, 2019).*

The superficial layer of the skin, the *stratum corneum* is the essential protection against infection, injury and prevents dehydration (Limbert, 2019). Keratinocytes arise from cells in inmost layer of the epidermis, specifically the *stratum basale*. The keratinocytes slowly immigrate against the *stratum corneum* and when these finally reach the surface they gradually shed off the body as it gets replaced by new ones. This is a continuous process which can take up to 28-50 days dependent on the age of an individual (Dwivedi et al., 2019). The resurgence of keratinocyte cells sustains skin hale and hearty.

The *stratum lucidum* layer is only found in palms and soles that consist of closely packed flattened dead cells. This layer provides stretching, water proofing, and reduction of friction in the skin (Dwivedi et al., 2019). In the *stratum granulosum* a permeability barrier is constituted as this layer consist primary of lipid-releasing keratinocytes. Thus, it will keep the lower epidermis moisture and at the same time block the passage of water and water-soluble substances from diffusing beneath surfaces.

1.1.1.2　Dermis

Of all the skin layers, dermis is the thickest. It is positioned underneath the epidermis and above the hypodermis. This layer mainly consists of a dense extracellular matrix (ECM). In addition, the dermis is composed of fibroblasts, blood vessels, hair follicles, sweat glands, sebaceous glands and nerve endings (Vig et al., 2017). The fibroblast secretes collagen and elastin which gives flexibility and strength to the skin (Qin, 2016; Vig et al., 2017). The blood vessels and nerve cells that are in the dermis provide nutrition, and sensation. In addition, the layer supplies nutrition and structural support to the epidermis.

1.1.1.3 Hypodermis

The last layer of the skin is the hypodermis, known as well as the subcutaneous layer. Main task of this layer is to attach the skin to underlying bone and muscle (Qin, 2016; Vig et al., 2017). This layer is mainly composed of adipocytes (fat cells), that have several functions such as thermoregulation, insulation, store nutrition and protect deeper tissues from injuries (Limbert, 2019).

1.1.2 Wound

A wound is created when the epithelial integrity of skin, mucosal surfaces, or organ tissue are disrupted (Singh et al., 2017). This results in attenuation of the skin´s primary functions (Wallace et al., 2019). Etiology of a wound can differ from intentional, unintentional, or sequelae of medical conditions (Singh et al., 2017; Wallace et al., 2019). At the same time as an injury, numerous cellular and extracellular pathways are activated. Wound healing instantly starts with a focus to rebuild tissue integrity and restore the skin´s protective barrier. The process of wound healing is composed of four distinct stages; hemostasis, inflammation, proliferation and remodeling (Singh et al., 2017). A disruption of the healing process can result in delayed wound healing, increased patient morbidity and mortality and poor cosmetic outcome (Singh et al., 2017).

1.1.2.1 Classification of wound

Wounds can be subcategorized into acute or chronic according to the wound healing time and process. Acute wounds go through all the healing phases quickly within 8-12 weeks (Boateng et al., 2008). This kind of wound is often caused by trauma to the skin as a result of insults like abrasions, punctures, crush and thermal injuries, surgery, gunshots, and animal bites. During the healing process, it is important to maintain a moist wound environment as well as to educate patients about wound care, because these are factors that can influence the quality of wound healing. Some of the important principles for acute wound management are the removal of hazard debris and necrotic tissue, an examination of underlying injuries and inspections for infections and closure (Dai et al., 2020).

A chronic wound is described as it fails "to proceed through an orderly and timely process to produce anatomic and functional integrity" (Martin et al., 2010). Underlying conditions such as diabetes, vascular disease and aging are the primary causes of contributing chronic wounds (Frykberg & Banks, 2015). This type of wound is often thought to be delayed, because of the prolonged inflammatory phase of healing (Albanna & IV, 2016b; Singh et al., 2017). Diabetic foot ulcers, pressure ulcers and vascular ulcers are classified as chronic wounds (Dai et al., 2020).

1.1.3 Wound healing

When the human skin is injured, several cell types in the epidermis, dermis and hypodermis coordinates at accurate stages to initiate wound healing. The healing process can be divided into four main stages; hemostasis, inflammation, proliferation and remodeling (Figure 2), as mentioned earlier. These stages occur in a temporal sequence, but at the same time overlap during the healing (Singh et al., 2017). For that reason, wound healing is among the most complex process in the human body.
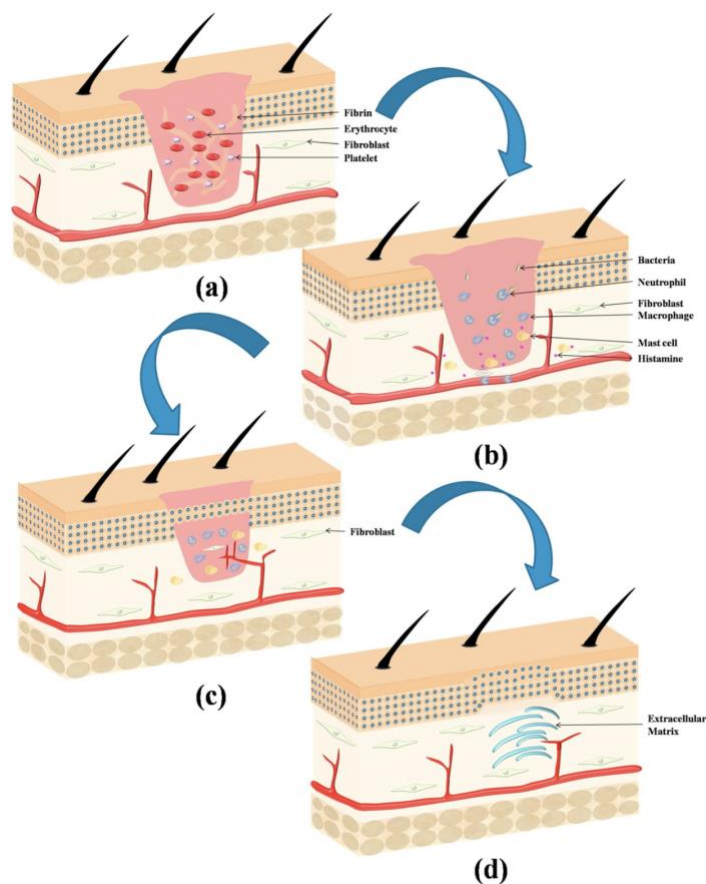
Figure 2: All the wound healing stages; a) Hemostasis b) Inflammation c) Proliferation d) Remodeling. Reprinted with permission from (Ambekar & Kandasubramanian, 2019). Copyright 2021, Elsevier.

1.1.3.1 Hemostasis

Hemostasis is the first stage of the wound healing process with the intention to prevent exsanguination and stop bleeding after vascular injury (Singh et al., 2017). The hemostasis mechanism can be described in three stages such as vasoconstriction, primary hemostasis, and secondary hemostasis (Rodrigues et al., 2019).

An instant response to a wounded skin is vasoconstriction of the vessel walls to reduce bleeding. This happens because endothelin triggers the contraction of smooth muscle (Rodrigues et al., 2019). However, this reduces bleeding only temporarily, since increased hypoxia and acidosis in the wound site causes relaxation of the smooth muscle, and the bleeding resume (Pool, 1977). To maintain vasoconstriction, it is therefore necessary to activate the coagulation cascade where mediators such as bradykinin and thromboxane A_2 reduce bleeding in the long term.

1.1.3.2 Inflammation

The inflammation stage of wound healing follows hemostasis, and the aim is to prevent infection. Polymorphonuclear cells are expressed as "first responders" since neutrophils infiltrate the wound first, and removes cellular debris, foreign particles, and bacteria (Wilgus, 2008). Neutrophils are cleared from the wound site when their task is completed; Either they undergo apoptosis, are sloughed from the wound surface, or they are phagocytosed by macrophages (Singh et al., 2017). At the time of 48-72 hours after injury, the wound is accumulated with macrophages, which are converted from monocytes within the wound (Singh et al., 2017). Macrophages in the wound can recruit more monocytes and increase the macrophage inflammatory response. Macrophages assist in the inflammation process by phagocytes survived pathogens, necrotic tissues, debris and expanded neutrophils (Ambekar & Kandasubramanian, 2019). They have a great reservoir of growth factor which are necessary for regulating the inflammatory response, inducing angiogenesis and increasing the formation of granulation tissue (Singh et al., 2017). Lymphocytes migrate the wound site after 72 hours and are necessary for maintaining the healing process, through the production ECM scaffold and collagen remodeling (Singh et al., 2017). The inflammation stage will last as long as it is required, to secure that residual bacteria and debris from the wound bed is removed.

1.1.3.3 Proliferation

The proliferation stage of wound healing initiates the repair of the tissue defects after hemostasis has been achieved. At this stage also the inflammation stage is in balance, and the wound bed is debris- and bacteria-free. This stage of wound healing is complex and consists of many sub-stages including angiogenesis, granulation tissue formation, re-epithelialization and wound contraction (Singh et al., 2017). All these processes occur concurrently.

Angiogenesis is activated by growth factors such as Transforming growth factor-β (TGF-β), and Platelet-derived growth factor (PDGF) (Ambekar & Kandasubramanian, 2019). Due to hypoxia vascular endothelial growth factor is released and with other cytokines, these stimulate endothelial cells to activate neovascularization and the repair of defective blood vessels (Singh et al., 2017). Local microvascular endothelial cells within the inner surface of blood vessels break down ECM of granulation tissue with the help of mixed metalloproteinase (MMP) (Rodrigues et al., 2019; Siefert & Sarkar, 2012). Therefore, activated endothelial cells can migrate through the ECM and bind to existing vessels to form new capillaries (Rieger et al., 2013). The blood vessel walls are stabilized with smooth muscle cells, and when the blood flow starts, the angiogenesis is regarded completed (Sorg et al., 2007). In this way, angiogenesis is vital for further delivery of nutrients and for the regulated oxygen hemostasis, that allows for cellular proliferation and tissue regeneration (Halim et al., 2012). Therefore, this process is crucial for effective wound healing.

Fibroblasts are triggered to proliferate and migrate to the wound by growth factors such as TGF- β and PDGF (Ambekar & Kandasubramanian, 2019). This results in increased fibroblast concentration at the wound site, and these down regulates the ECM proteins (Singh et al., 2017). Afterward, fibroblast produces collagen and fibronectin, this results in the formation of granulation tissue which replaces the clot. Fibroblast converts to myofibroblast when an adequate matrix has been laid down. Subsequently, it connects to fibronectin and collagen, and aid in wound contraction, as a result the surface area of the wound is reduced (Rodrigues et al., 2019; Singh et al., 2017). Collagen produced by primary fibroblasts, provide mechanical strength to the tissue (Schultz et al., 2011). Myofibroblasts undergo apoptosis once the tissue integrity is sufficient restored (Oliveira et al., 2016).

The reepithelialization process is conducted by local keratinocytes at the wound edge (Reinke & Sorg, 2012). A wedge of keratinocytes migrates across the wound and secrete enzymes, which degrades the temporary ECM (Baum & Arpey, 2005). The migration of keratinocytes continues until it contacts another wedge and finally, a stratified layer of keratinocytes is made (Rieger et al., 2013).

1.1.3.4 Remodeling

The last phase of wound healing is remodeling, it occurs two weeks post-injury and continues up to one year after injury (Ambekar & Kandasubramanian, 2019; Reinke & Sorg, 2012).
In the remodeling stage the neovascular is re-established, while granulation tissue converts into scar tissue and degradation of the ECM follows (Rodrigues et al., 2019). Collagen III in the granulation tissue is replaced with the stronger collagen I (Singh et al., 2017). During remodeling the angiogenesis process decrease, which means that the blood flow declines and the metabolic activity in acute wounds gradually stops (Reinke & Sorg, 2012).

1.1.3.5 Pathophysiology of chronic wound

Abnormal execution of normal wound healing process can result in healing impairment and development of chronic wounds. Chronic wounds as are arrested in the inflammatory stage that obstructs proliferation. Therefore, they do not follow the well-defined wound healing cascade described in the previous sections. Causes of wounds becoming chronic includes a myriad of systemic factors that lead to impairment of wound healing, including local tissue hypoxia, aging, repetitive trauma, bacterial colonization, and chronic disease (Singh et al., 2017; Zhao et al., 2016).

Prolonged suboptimal inflammation in chronic wounds is caused by an imbalance among cytokines, chemokines, proteases, and their inhibitors (Schultz & Mast, 1999). Prolonged inflammatory stage facilitates a polymicrobial infection environment at the wound site, and the formation of biofilms can take place, that can sustain the influx of proinflammatory cells while inhibiting the response to infection (Pastar et al., 2013; van Asten et al., 2016). The inflammation stage in chronic wounds exhibits excessive neutrophils, which overproduce reactive oxygen species (ROS) and causes damage to ECM (Demidova-Rice et al., 2012). Neutrophils secrete serine proteases including elastase and MMPs. Released elastase degrades critical growth factors such as PDGF and TGF-β, and MMPs degrades and inactivates components of the ECM (Demidova-Rice et al., 2012; Diegelmann & Evans, 2004). Even though the production of growth factors in chronic wounds is increased, the bioavailability is decreased due to this problem (Zhao et al., 2016). Activated macrophages and neutrophils produce interleukin 1 beta and tumor necrosis factor alpha, both cytokines increase MMP production and reduce tissue inhibitors of MMPs (Zhao et al., 2016). This results in an imbalance in degradation of the ECM, impairs cell migration, decreases fibroblast proliferation and collagen synthesis (Mast & Schultz, 1996). Substances that are degraded from the ECM induce further inflammation, a self-sustaining process.

Aging

There are several age-related factors that cause impaired wound healing. This can cause clinical and economic problems in an aging population, since the prevalence of chronic wounds is getting higher with increasing age (Schreml et al., 2010). Elderly have slower inflammatory, migration and proliferation responses (Singh et al., 2017). In addition, neutrophils have reduced capability to phagocytose bacteria and the evaluated level of neutrophils leads to an overproduction of proteases, which degrades critical structural and functional proteins like proteoglycan, collagen, and fibronectin (Ashcroft et al., 1999; Ashcroft et al., 2002). An aging population is also more likely to have a chronic disease that additionally slows down wound healing. Therefore, this population group is at risk for wound complications (Singh et al., 2017).

Hypoxia

All varies of wounds are hypoxic to some degree since their local supply of oxygen is disrupted. Adequate oxygen is required for wound healing (Singh et al., 2017). Hypoxia can cause cell membrane disruption and promote inflammatory cascade by several molecular mechanisms, that consequently disrupt wound healing (Toledo-Pereyra et al., 2004). ROS lead to oxidative damage as well as expression of serine proteases, MMPs, and inflammatory cytokines. As a consequence, the inflammatory process is strengthened and the wound healing impaired (Zhao et al., 2016).

Chronic disease

Chronic diseases which affect the cardio-respiratory system can influence adversely the supply of oxygen and other nutrients that are needed for wound healing (Singh et al., 2017). In diabetes the wound healing is greatly impaired due to immunocompromised and higher blood glucose levels that influence leukocyte function (Singh et al., 2017). In addition, expression and function of MMPs is altered and provides poor wound healing in combination with other vascular diabetic complications (Tsioufis et al., 2012).

Bacterial colonization

Among patients with chronic leg ulcers, it was reported up to 50 % infected wounds and the presence of biofilm was found in 70-78 % (Buch et al., 2021; Leaper et al., 2015). Pathogens within the wound bed can damage both host and bacteria by promoting leukocytes which enhance inflammatory cytokines, proteases, and ROS, with the resulting initiating and maintenance of the inflammatory cascade (Schreml et al., 2010). Proteases and ROS degrade both ECM and growth factors, which disrupts cell migration and hinders wound closure (Demidova-Rice et al., 2012). Pathogens in bacterial colonization can form polymicrobial biofilms, whereas the microbial cells are embedded in a secreted polymer matrix, that make an optimal environment for bacteria to avoid host immune response and antibiotic action (Zhao et al., 2013). Formed biofilms obtain nutrients from inflammatory exudate. Additionally, hypoxia in the wound bed provides bacterial colonization (Zhao et al., 2016). Thus, bacterial colonization has a deleterious influence on healing.

1.2 Multifunctional wound dressing

An ideal wound dressing must be biocompatible and biodegradable, promote the wound healing process and enable to swell. In addition, dressings should exhibit high porosity and be oxygen breathable since all the stages in wound healing require oxygen (Ambekar & Kandasubramanian, 2019; Seyedian et al., 2020). Wound dressings are therefore an important aspect of the wound healing process. All these key factors can provide protection against further exogenous microorganisms and relief. Among the beneficial results, the wound dressing is also applied to absorb the exudates in burns and chronic wounds as well as to maintain a moist wound bed environment, to improve the efficiency of wound healing. Several types of wound dressings are available on the market and therefore it could be difficult to choose one, but it is vital to prevent secondary trauma and more harm when changing a dressing is required (Ambekar & Kandasubramanian, 2019).

Multifunctional wound dressing is a novel approach. This dressing type possesses multiple functionalities that might help stimulate the wound healing process. This type of wound dressing can contain active components such as antimicrobial agents, antioxidants, and anti-inflammatory agents for wound healing purpose (Chen et al., 2017). The incorporation of bioactive agents in nanofibers have been broadly investigated to prevent infection and enhance the wound healing process (Croitoru et al., 2020). Local delivery of antibiotic is more convenient over systemic due to higher concentration at the wound area, while avoiding high-systemic concentrations that might cause problem with respect to antimicrobial resistances and unwanted side effects (Rasouli et al., 2019). However, there are several disadvantages with local delivery of antimicrobial agents such as time limited efficacy of antibacterial activity and potential local toxicity due to uncontrolled release (Shi et al., 2018). In this project CAM was incorporated into a multifunctional wound dressing consisting of two active biopolymers.

1.2.1 Chloramphenicol

CAM (Figure 3) was initially isolated from *Streptomyces venezuelae*. It has a wide spectrum of antimicrobial activity, including both gram-positive and gram-negative organisms and rickettsiae (Henderson et al., 2018). CAM is bacteriostatic against most organisms. This antibiotic agent inhibits bacterial protein synthesis by binding to the 50S ribosomal subunit, hence interference with peptidyltransferase activity (Preem et al., 2017). Therefore, it hinders peptide bond formation, which affects protein synthesis and bacterial cell proliferation (Nitzan et al., 2015).
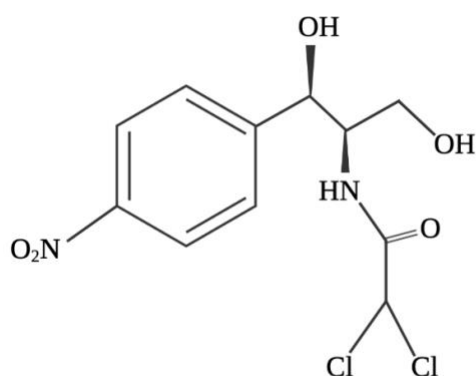
Figure 3: Structural formula of chloramphenicol. Created with Biorender.com.

CAM comes in oral, parenteral and topical administration forms. The side effect profile of systemic CAM is severe; reversible marrow depression and irreversible aplastic anemia are potential side effects (Walker et al., 1998). Therefore, systemic use of CAM is reserved for serious infections where its advantage outweighs its unusual, but severe side effects (Henderson et al., 2018).There are less concerns on severe side effects with topical CAM, therefore it is safer in use and effective in bacterial infection (Shen et al., 2018).

1.2.2 Chitosan

Chitosan (CHI) is partly de-acetylated chitin. The CHI used in this project is produced of chitin polymer of protective shrimp shells made by Chitinor^{TM}. Chitin is a natural insoluble polysaccharide composed of N-Acetyl-D-Glucosamin monomers, as shown in Figure 4. Chitin appears also naturally in some fungi and exoskeleton of insects and crustaceans, as well as it is produced from the cell walls of fungi and brown algae through biosynthesis but it is not frequently used due to its inertness (Ahmed & Ikram, 2016; Periayah et al., 2016; Sahariah & Másson, 2017). The shrimp shells can be extracted and converted into CHI. This process includes de-mineralization, de-proteinization and de-acetylation of the shrimp shells. In the extraction step minerals and proteins are cleared from the shrimp shells. Further, treating with a stabilized concentration of inorganic solvents and with controlled temperature it is possible to convert chitin into CHI. In the de-acetylation step the CHI gets washed with pure fresh water. This makes the CHI pure and stable in quality (Chitinor, 2020).

Structurally CHI is composed of N-Acetyl-D-Glucosamin and D-Glucosamin monomers arranged in a long chain linked through β-(1-4) glycosidic linkages with random sequence (Figure 4) (Chitinor, 2020; Sahariah & Másson, 2017). The percentage of deacetylated D-Glucosamin groups and the chain length, which refers to its molecular weight, will influence properties of CHI, such as solubility, viscosity, film-forming abilities, antimicrobial properties, swelling ratio and biodegradation (Chitinor, 2020; Matica et al., 2019). CHI has large variations in molecular weight, but they are usually categorized as "high molecular weight", "medium molecular weight", and "low molecular weight" (Hosseinnejad & Jafari, 2016).

CHI is soluble in dilute aqueous acetic, lactic, malic, formic, and succinic acids due to protonation of -NH$_2$ group, as seen in Figure 4. At pH lower than 6 CHI is polycationic and therefore able to interact with negatively charged molecules including proteins, anionic polysaccharides, phospholipids and fatty acids (Ahmed & Ikram, 2016).
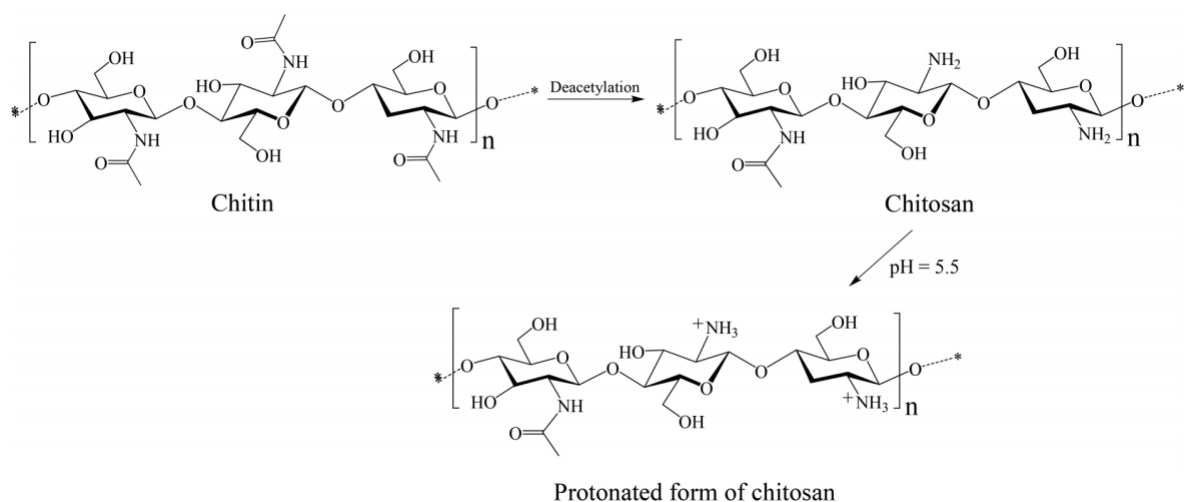
Figure 4: Chemical structure of chitin the unprotonated and the protonated form of chitosan, with the deacetylation- and protonation transformation process indicated. Reprinted with permission from (Sahariah & Másson, 2017). Copyright 2021, American Chemical Society.

Chitosan in wound healing

CHI is widely used in biomedical and pharmaceutical applications, especially for wound healing applications due to favorable properties being biodegradable, biocompatible, eco-friendly, non-toxic, and its great antimicrobial activity (Ali & Ahmed, 2018). The antimicrobial property of CHI was of particular interest in this project since it is desirable to produce wound dressing for infected chronic wounds. CHI exhibits both bacteriostatic and bactericidal effect by several mechanisms of the antimicrobial activity (Matica et al., 2019).

The most described mechanism is the alteration of cell permeability and lysis of the cell membrane, caused by electrostatic interactions between the polycationic chitosan molecule and negatively charged cell membrane of bacteria. Consequently, this interaction causes cell membrane disruption, followed by cell leakage. The other mechanisms refer to interactions between chitosan hydrolysis products and microbial DNA. This interaction leads to the inhibition of mRNA by influencing protein synthesis. The good chelating properties of CHI due to the protonation of -NH$_2$ group enables chelating several metal ions and crucial nutrients for bacteria, thus inhibiting microbial growth. Other mechanisms refer to high molecular CHI that can deposit and make a thick polymer film on the surface of the cell. Therefore, it hinders nutrients and oxygen uptake, further leading to inhibition of bacterial growth (Matica et al., 2019).

CHI can also promote the wound healing by stimulating inflammatory cells, macrophages, and fibroblasts, thereby the inflammatory stage is reduced, and the proliferative process begins earlier (Liu et al., 2018).

1.2.3 β-glucan

β-1,3/1,6-glucan (βG) is an immunomodulator that is extensively utilized in medical products in Asia since ancient times due to its promoting ability of macrophages (Zykova et al., 2014). The ability of βG to stimulate wound repair was of interest in this project since fabricated nanofibers are intended to use on wounds with impaired healing. βG naturally occurs in the cell wall of yeast, fungi, certain bacteria, seaweeds, and cereals. Pure βG is enzymatically extracted from the mentioned sources. βG is structurally composed of D-glucose units linked by β-glycosidic bonds. The βG linkage type, branching manners and molecular weight varies in relative to their sources (Du et al., 2014). The biological and physiochemical properties of βG also strongly vary depending on the source of extraction. Additionally, the physiological activity of βG is also influenced by the degree of purification and extraction method. Based on the physiological properties, βGs are divided into soluble and insoluble; gel creating, linear and high molecular branched βGs are considered as soluble. Many βGs are insoluble including those isolated from yeast such as β-(1,3)-glucans (Bashir & Choi, 2017). This form of βGs are unsolvable in aqueous solution, therefore not possible to be used alone in animal experiments or clinical circumstances (Zykova et al., 2014). Typically, βG consist of β-(1,3) with occasional β-(1,6) branches as can be seen in Figure 5 (Ma & Underhill, 2013).
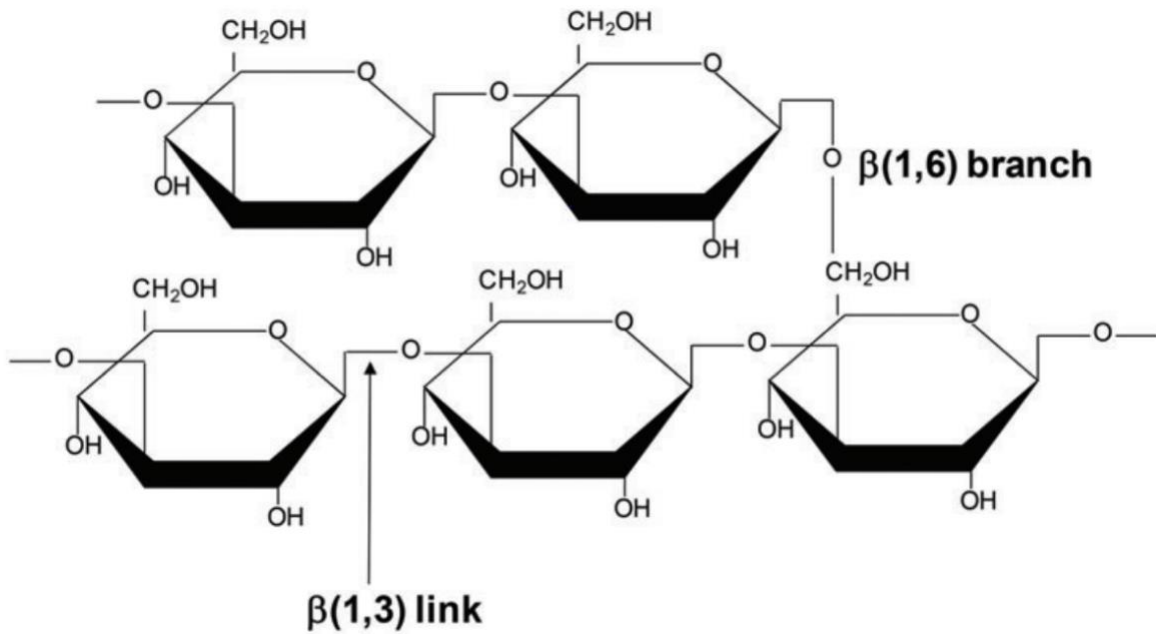
Figure 5: Structure of βG with β-(1,3) linkages and occasional β-(1,6) branches. Reprinted with permission from (Ma & Underhill, 2013). Copyright 2021, Oxford University Press.

β-glucan in wound healing

Health benefits of βG have been widely investigated as immunological activators. βG is used as disease preventing agent and as anti-tumor, immune-modulating, anti-aging and anti-inflammatory agent (Rieder & Samuelsen, 2012; Zhu et al., 2016). βG can stimulate the immune system, modulating humoral and cellular immunity. Therefore, it exhibits beneficial effects in fighting infectious diseases including bacterial, viral and fungal (Bashir & Choi, 2017). The use of βG can promote wound healing, although the mechanism is not fully elucidated.

βG accelerate the wound healing process both in acute and chronic wounds through two potential modes of action, indirectly activate through different cytokines of macrophages or direct influence of keratinocytes and fibroblasts. βG can act as a source of growth factors and inflammatory cytokines, that can stimulate cellular proliferation, angiogenesis, re-epithelialization and give an increase in wound tensile strength (Majtan & Jesenak, 2018). In the human body βG, is recognized by innate immune cells including dendritic cells, neutrophils and macrophages (Ma & Underhill, 2013). The most crucial receptor for binding βG is dectin-1. This binding triggers immune independent responses, such as phagocytosis, producing inflammatory mediators and oxidative burst to kill pathogens. Therefore, dectin-1 receptor has a significant role in immune response towards infection. Dectin-1 receptor on dendritic cells can recognize βG on lymphocytes, and promotes their proliferation (Sun & Zhao, 2007).

Soluble β-glucan (SBG®)

Soluble beta-1,3/1,6-glucan (SBG®) was the applied βG in this study, and a kind gift from Biotec Betaglucans AS, Tromsø, Norway. SBG® was the active ingredient in the previously marketed hydrogel, Woulgan®, indicated for treatment for dry to moderately exuding chronic wounds such as diabetic foot-, leg- and pressure ulcers. In addition to the active ingredient βG of 2.0 % (w/w), Woulgan® consists also of carboxymethyl cellulose as a thickening agent and glycerol as humectant. SBG® contains β-1,3/1,6 glucan that is isolated from cell walls of Baker´s yeast (*Saccharomyces cerevisiae*), following a patented method including several hydrolysis and cleansing steps, conveyed after GMP-standard controlled processes. Thus, SBG® is a pharmaceutical grade active ingredient with a final βG-concentration of 2.5 % (w/w) in water (Grip, 2018). At room temperature, SBG® forms a hydrogel. βG in SBG® has a tertiary-helix structure in solution with a broad size distribution in water (Qin et al., 2013). Due to the higher order, the average molecular weight is 7×10^5 g/mol in aqueous solution (Grip, 2018). This large structure is beneficial for the immune modulation and interactions with βG receptors for immune cells (Legentil et al., 2015).

A randomized, double blind, placebo-controlled phase two study investigated the wound healing effect of SBG® as local treatment of diabetic foot ulcers. The results indicated that SBG® is a promising treatment for promoting cutaneous healing (Zykova et al., 2014). Incorporation of SBG® as active ingredient in electrospun nanofiber as wound dressing did show improved wound healing in animal models (Grip et al., 2018).

1.2.4 Solvents

Choice of solvent to prepare polymer solution has a significant influence on spinnability, since the first and leading step in the electrospinning (ES) process is to dissolve the polymer. Solvent must have some properties like suitable volatility, vapour pressure, boiling point and should maintain the integrity of the polymer. Additionally, it is desirable to utilize solvents that can dissolve the polymer in adequate concentration (Bhardwaj & Kundu, 2010). Polymer solution characteristics such as viscosity, surface tension and conductivity is affected by the choice of solvent in addition to the polymer composition and concentration. This will influence the spinnability of the polymer as mentioned earlier and morphology of electrospun nanofiber (Haider et al., 2018). Primarily, a solvent performs two important roles in ES, dissolve the polymer for creating the electrified jet and convey polymer molecules towards collector (Ohkawa et al., 2004)

Mostly used organic solvents in ES are acetone, dichloromethane, methanol, ethanol (EtOH), acetic acid, and formic acid (Bhardwaj & Kundu, 2010). Although the use of these is common, their toxicity, price, and critical high volatility are disadvantages (Pelipenko et al., 2015). The desired solvent is distilled water due to its safety and biocompatibility, however the use is limited to hydrophilic polymers since the polymers need to be dissolved in the solvent. Thus, co-solvents can be added to increase the solubility. In addition, water-based polymer solutions possess high viscosity at low concentrations. Consequently, a small amount of electrospun nanofiber is produced from a relatively large volume of polymer solution (Bhardwaj & Kundu, 2010; Bhattarai et al., 2005). To accomplish excellent solution viscosity, surface tension, and solvent volatility, a blend of two or several solvents is usually utilized (Pelipenko et al., 2015).

In this project distilled water and acetic were used to produce an acetic aqueous mixture to permit dissolution of CHI. Additionally, EtOH was utilized as solvent to increase the volatility of the polymer solution for optimal ES.

1.2.5 Co-polymers

Co-polymers are often added into the polymer solution to improve the ES process, or nanofiber functionality in consideration of biocompatibility and therapeutic efficacy (Pelipenko et al., 2015).

1.2.5.1 Polyethylene oxide

Polyethylene oxide (PEO) is a synthetic hydrophilic polymer that has been broadly used to produce nanofibers. This is due to its successful ES properties, potential to form ultrafine nanofibers, its linear structure with flexible chains, biocompatible, soluble in aqueous solutions, and ability to form hydrogen bond with other macromolecules (Elsabee et al., 2012). It is well known that the electrospinnability of CHI is restricted primarily due to its polycationic nature at pH less than 6, rigid chemical structure and inter- and intramolecular interaction. Strong hydrogen bond hinders the free movement of CHI chain segment and exposure to electric field cause jet to break up during ES process. Furthermore, ionic groups on the backbone of CHI prevents production of continuous fiber formation and consequently nanobeads are generated. Therefore, adding PEO as co-spinning agent can improve the electrospinnability of CHI. PEO and CHI can strongly interact together due to hydrogen bonds between hydroxyl and amino groups on CHI (Figure 4) molecules and ether groups in PEO. It is also suggested that PEO can act as a plasticizer by breaking down the inter- and intramolecular interaction of CHI chains between new interactions. PEO can lie down through the rigid backbone of CHI (Pakravan et al., 2011). Through these interactions, PEO improves the spinnability of CHI.

1.2.5.2 Hydroxypropyl methylcellulose

Hydroxypropyl methylcellulose (HPMC) is a water-soluble hydrophilic non-ionic cellulose ether (Balogh et al., 2016). HPMC is commonly used in food industry as thickening agent, emulsifier, and stabilizer due to its biocompatibility and low toxicity (Aydogdu et al., 2018). Additionally, HPMC is also utilized for controlled release tablets sine polymeric gel layer is established in contact with aqueous solution (Li et al., 2005). There is not enough study about HPMC as excipient utilized for ES nanofibers. In this study HPMC was utilized since Grip et al obtained good quality of nanofibers prepared with these co-polymers (Grip et al., 2018).

1.3 Nanofiber

Nanofibers are nanomaterials normally described as fibers with a diameter of 10-100 nm (Bhattacharya et al., 2019). Nanofibers provide a lot of unique features such as a structure like native ECM, great ability to liquids, balanced moisture and gas permeability. In wound healing, nanofibers provide an ideal environment by protecting the wound from exogenous infection, and by enhancing cell migration and proliferation. In addition, nanofibers absorb exudate and aid with cell respiration (Rasouli et al., 2019).

Nanofibers can be synthesized from many different materials such as natural and synthetic polymers (Bhattacharya et al., 2019). Several methods are utilized to fabricate nanofibers, whereof ES is one of the most popular.

1.3.1 Electrospinning

There are various methods to manufacture pharmaceutical nanofibers, and among those are drawing, phase separation, template synthesis, and ES (Partheniadis et al., 2020). Of these methods, ES also known as electrostatic spinning, is the most frequently used technique to fabricate nanofibers. ES possesses several unique features such as simplicity, affordability, reproducibility, and cost-efficiency (Eatemadi et al., 2016; Yu et al., 2017). This method forms micro/nanometer-sized polymeric fibers with the use of a high electric field.

A conventional ES apparatus setup consists of a high voltage power supply, a grounded collector, and a spinneret (Ambekar & Kandasubramanian, 2019). Figure 6 is a schematic diagram of a standard single needle-ES device for the fabrication of nanofibers.
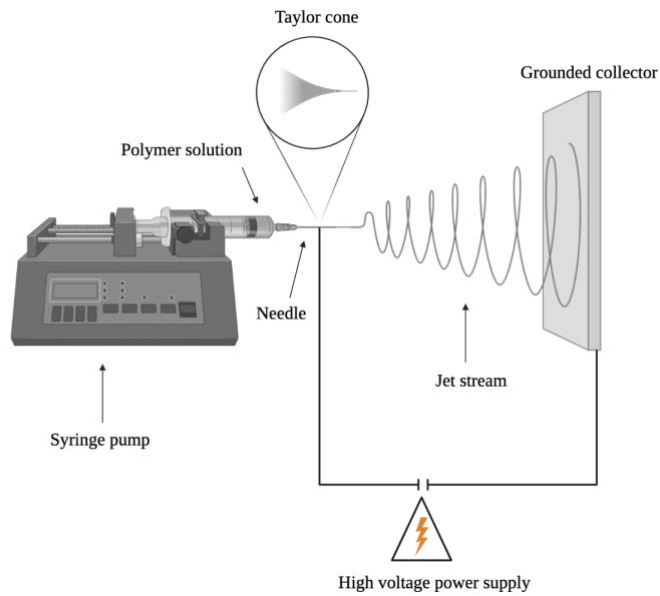
Figure 6: Schematic of single needle electrospinning system. The system is constructed by polymer solution in a syringe, mounted on a syringe pump, performing at a constant flow speed. The high voltage power supply is connected to the needle to charge the fluid. Created with Biorender.com.

The single needle-ES process involves a high voltage power supplier that either possesses positive or negative polarity intending to charge the polymer solution. The high voltage source is connected to both the spinneret and the collector. The syringe is loaded with a polymer solution, fitted to and driven by a syringe pump, which controls ejection speed. Further, the solution forms an electrically charged pendant drop which is held at the tip of the syringe by surface tension. The repulsive force among molecules in the polymer solution with the electric field cause deformation of the pendant drop into a conical-shaped structure called a Taylor cone. When the voltage gets to a sufficient value, the electrical forces overcome the surface tension strength and a liquid jet appears from the Taylor cone and accelerates towards the collector plate. During the travel, the polymer solution gets into a bending instability which causes the jet stream to stretch and whip, hence the travelling distance increases. This results in fiber thinning and evaporation of the solvent, prior to the fibers deposition on the grounded collector (Bhattarai et al., 2019; Eatemadi et al., 2016; Partheniadis et al., 2020; Rasouli et al., 2019).

Although the conventional ES technique has gained a lot of attention, several limitations also exist. Among the challenges, needle clogging, and low-scale production of nanofibers are the main reasons for the development of various modified and advantageous ES techniques such as needle-free ES (Partheniadis et al., 2020).

1.3.1.1 Needle-free electrospinning

In needle-free ES, polymer solution is directly electrospun from a free surface of a liquid. Therefore, it is possible to make multiple nanofiber jets at the same time and this results in large-scale production in an easy and controlled way (Partheniadis et al., 2020). In general, the spinnerets within NF-ES can be categorized into rotating and stationary spinnerets based on the running states throughout the ES process. The stationary spinnerets can be subdivided into categories such as upward-, downward-, and sideward ES (Yu et al., 2017).

Nanospider^{TM} is based on the NF-ES technology and has become a promising approach for the mass production of ultrafine nanofibers from a wide diversity of materials. In this project, an upward ES from stationary wire spinneret was used, which means that the nanofiber generator is beneath the nanofiber collector as shown in Figure 7.
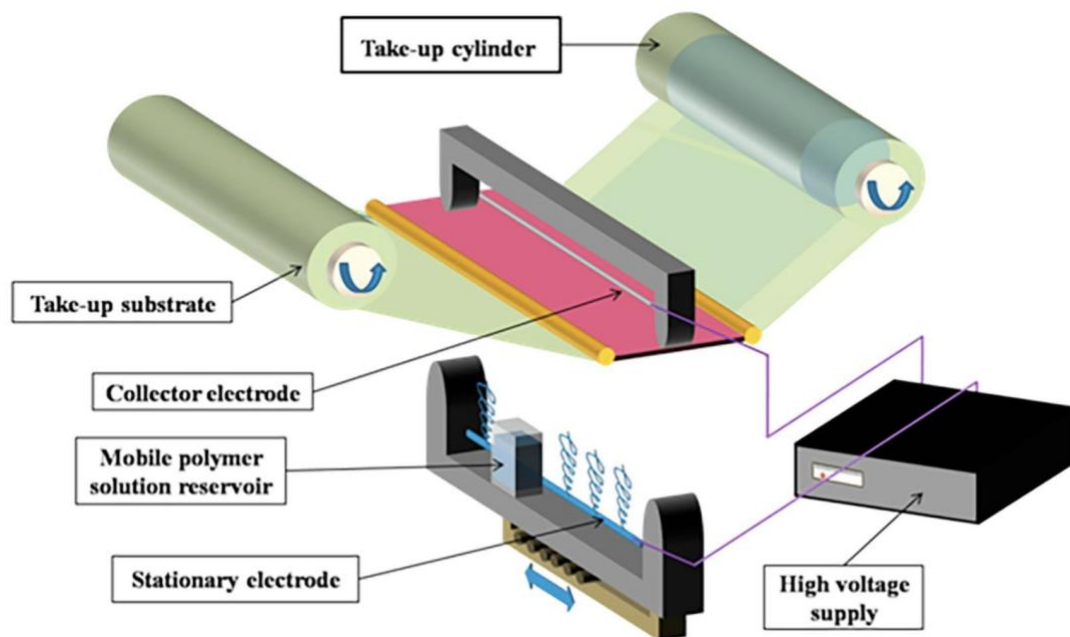
Figure 7: A schematic illustration of the needle-free electrospinning set-up. Reprinted with permission from (Ambekar & Kandasubramanian, 2019). Copyright 2021, Elsevier.

As in standard ES, the spinneret and the nanofiber collector electrode are connected to the high voltage supply. In NF-ES the needle is replaced with a stationary wire that works as the spinning electrode. The surface of the electrode is continuously coated with polymer solution by a reciprocating movement of a polymer solution container. Since the electrode is constantly coated with polymer solution, neither the evaporation of the solution nor the drying of it from the surface takes place. The polymer container consists of an inserted metal orifice, to which both the spinning electrode wire is drawn, and the polymer solution flows out during the movement of the container. As in single needle-ES, when the electrostatic force overcomes the surface tension of the polymer solution, Taylor cones, and numerous jets are established. During the traveling to the collector electrode, the solvent evaporates, and fibers become stretched and deposited onto a mobile substrate collector, which is adjacent to the collecting electrode (Aurélie et al., 2018; Yu et al., 2017).

1.3.1.2   Factors affecting the electrospinning process

Regardless of techniques and types of collectors used to fabricate nanofibers, there are several parameters that can affect the final result such as diameter and morphology of nanofibers. Therefore, it is important to take these parameters into consideration throughout the process. The influencing factors are mainly categorized as; ES-, solution- and environmental-related parameters (Haider et al., 2018).

Electrospinning associated parameters

Factors that influence the formation of nanofibers within the ES process are applied voltage and distance between the spinneret and collector.

Effect of applied voltage

A critical high voltage supply is needed to obtain a Taylor cone and further form ultrathin nanofibers, and the critical value differs within polymer solutions. The applied voltage can influence the size of the nanofiber, formation of beads and absence of jet production (Bhattarai et al., 2019). An increase in applied voltage above the critical value results in augmented beads and smaller diameter of the fibers due to the decrease in the size of the Taylor cone and an increase of the jet speed (Haider et al., 2018).

Effect of spinneret to collector distance

The distance between the spinneret and collector is another crucial, affecting the size and morphology of the electrospun nanofibers (Bhardwaj & Kundu, 2010). The factor can easily influence the morphology of a nanofiber since it relies on the deposition time, evaporation rate, and whipping (Matabola & Moutloali, 2013). Hence, the distance to the collector needs to be optimized, to obtain nice, smooth and uniform nanofibers. The larger the distance is from the spinneret to the collector, the smaller will the diameter of the nanofibers be (Matabola & Moutloali, 2013).

Solution associated parameters

Several factors within solution related parameters can affect the ES process and they are concentration of solution, solution viscosity, molecular weight, surface tension, conductivity, and solvent.

Effect of polymer concentration and solution viscosity

The ES process is depended on the phenomenon of the stretching of a charged jet. This phenomenon can be affected by adjusting the concentration of the polymer solution. In polymer solutions with low concentration, the surface tension and applied electric field can cause tangled polymer chains to break into fragments before reaching the collector, and as a result beaded nanofiber are produced (Iacob et al., 2020). Polymer solution with an increased concentration will have increased the viscosity. This further lead to an increase in the polymer chain entanglement. These entangled chains overcome the surface tension and result in the formation of uniform beadless electrospun nanofibers (Haider et al., 2018).

Effect of molecular weight

The viscosity of the polymer solutions is influenced by the molecular weight of a polymer. A too high molecular weight of polymers applied, causes entanglement and result in trouble for the electric field to pull on individual polymer chains to acquire a thin fiber (Lyons et al., 2004). Meanwhile, too low molecular weight polymers produce fibers with beads due to insufficient number of intermolecular entanglements (Haider et al., 2018).

Effect of solution conductivity

The influence of conductivity plays a significant role in the ES process, mainly in the formation of the Taylor cone. High conductivity of a polymer solution is important for a greater charge-carrying capacity (Bhattarai et al., 2019). Polymer solution with low conductivity will have no charge to create Taylor cone and as outcome the ES process will not take place (Haider et al., 2018). Increasing the solution conductivity will lead to an increase in the charge on the surface to form Taylor cone and causes a decrease as well in the diameter of the nanofibers (Bhattarai et al., 2019; Sun et al., 2014).

Effect of solvent

To produce smooth and beadless nanofibers the selection of the solvent is a significantly important factor. Two critical criteria's need to be considered before selecting an ideal solvent for ES. The solvent should solubilize polymers used and also has a moderate boiling point (Haider et al., 2018). Volatile solvents with moderate to high evaporation rates encourage to facile evaporation of the solvent from the nanofibers during the spinneret to the collector trip (Iacob et al., 2020). However, highly volatile solvents are not used due to their low boiling points and high evaporation that cause the drying of the jet at the spinneret and block it (Haider et al., 2018). Less volatile solvents are also avoided due to their high boiling points that obstruct their drying through the trip to the collector, result in the formation of beaded nanofibers (Lannutti et al., 2007; Sill & von Recum, 2008).

Environmental-related parameters

There are mainly two factors such as relative humidity (RH) and temperature within environmental parameters that influence the diameter and morphology of electrospun nanofibers.

Effect of relative humidity and temperature

The composition of polymer solution affects their sensitivity to the relative humidity in the environment. For hydrophobic polymer solutions dispersed in organic solvent, a high RH causes the fabrication of porous nanofibers. Meanwhile, in aqueous polymer solutions, RH can be employed to manipulate nanofiber diameter and their mechanical properties. Changes in nanofiber morphology related to changes in RH can be described by the combination of two effects. The first effect is the solvent evaporation rate, and the other effect is formation of bead-on-a-string morphology, that is due to the capillary breakup of the viscoelastic fluid (Pelipenko, Kristl, et al., 2013). The low RH value cause rapid solvent evaporation, which lead to polymer solution solidification right after it comes out of the nozzle or deposited on the wire (needle-free ES). Further, it is exposed to voltage-induced stretching for a little period and results in thicker nanofibers. The high RH cause solidification process to be decelerated and the polymer solution in the jet has longer time to be stretched. This results in the formation of thinner nanofibers (Pelipenko et al., 2015; Pelipenko, Kristl, et al., 2013).

Environmental temperature provokes two different effects to modify the average diameter of the nanofibers, it increases the evaporation rate of a solvent and decrease the viscosity of the solution, both mechanism lead to decrease in the mean nanofiber diameter (Haider et al., 2018).

2 Aims of the study

The aim of this master project has been to formulate, process and characterize novel multifunctional nanofiber wound dressings, targeting infectious chronic wounds, with chitosan (CHI) and soluble beta-1,3/1,6-glucan (SBG®) as bioactive fiber-forming polymers, and the antimicrobial agent chloramphenicol (CAM) as a third active ingredient. We also aimed at investigating the effect of these different active ingredients on the feature of both the polymer solution and the nanofibers formed by electrospinning from these polymer solutions. To see only these effects, we also aimed to standardize the solvent compositions, co-polymers and the processing settings, as well as environmental conditions, as much as possible.

Features we aimed at investigating were:

- Conductivity, pH, surface tension and viscosity of the polymer solutions.
- The temperature and relative humidity throughout the electrospinning process.
- Tensile properties, morphologies, diameters, and absorption capacities of the formed nanofibers.
- The CAM *in vitro* release profile from the electrospun nanofibers.
- The *in vitro* cell toxicity of the dissolved nanofibers both without and with CAM.

3 Materials and methods

3.1 Materials

3.1.1 Chemicals

Acetic acid glacial ($\geq$ 99.5 %), Sigma-Aldrich, St. Louis, MO, USA (Lot: 19J014033)

Acetone ($\geq$ 99.5 %), Sigma-Aldrich, St. Louis, MO, USA (Lot: 18I064007)

Albunorm$^{\circledR}$, Octapharma, Lachen, Switzerland (Batch: L623B6663)

Benecel^{TM} E4M hydroxypropyl methylcellulose (HPMC), Ashland Global Specialty Type 2910-3600 mPas

Cell Counting Kit – 8, Sigma-Aldrich, St. Louis, MO, USA (Lot: BCCD4353)

Chemicals Inc, Ashland, KY, USA

Calcium Chloride dihydrate ($\geq$ 99 %), Sigma-Aldrich, St. Louis, MO, USA (Lot: SLBT356)

Chitopharm^{TM} M, average MW of 426 kD, 87,4 % degree of deacetylation, Chitinor AS, Tromsø, Norway (Batch: UPBH 7339 PR)

Chloramphenicol ($\geq$ 98 %), Sigma-Aldrich, St. Louis, MO, USA (Lot: SLBR8868V)

Dulbecco`s modified Eagle`s medium -High Glucose, Biowest, Riverside, MO, USA   (Batch: MS00MH)

Distilled water

Dulbecco´s Phosphate Buffered Saline, Sigma-Aldrich, St. Louis, MO, USA (Lot: RNBJ4223)

Ethanol (96 % v/v), VWR International, Radnor, PA, USA (Lot: 20K034011)

Fetal Bovine Serum, Sigma-Aldrich, St. Louis, MO, USA (Lot: BCBX5318)

Milli-Q water

Methanol, VWR International S.AS, Fontenary-sous-Bois, France (Lot: 20I184025)

Penicillin-Streptomycin, Sigma-Aldrich, St. Louis, MO, USA

Polyethylene oxide (PEO), Dow Chemical Company, Midland, MI, USA (Lot: DTR465630)

Potassium chloride ($\geq$ 99.5 %), Sigma-Aldrich, St. Louis, MO, USA (Lot: SZBG0530V)

Potassium phosphate monobasic, ($\geq$ 99.0 %), Sigma-Aldrich, St. Louis, MO, USA (Lot: SLBJ7258V)

Sodium bicarbonate, Sigma-Aldrich, St. Louis, MO, USA (Lot: 062K0176)

Sodium chloride ($\geq$ 99.5 %), Sigma-Aldrich, St. Louis, MO, USA (Lot: STBG910)

Sodium phosphate dibasic dihydrate (98.5-101.0 %), Sigma-Aldrich, St. Louis, MO, USA (Lot: BCBR0258V)

Soluble beta-1,3/1,6-glucan, 2.5 % (w/w) (SBG®), Biotec BetaGlucans AS, Tromsø, Norway (Batch: 18-BP-023)

Trypsin-EDTA solution, Sigma-Aldrich, St. Louis, MO, USA.

3.1.2 Instruments

Biofuge Stratos, Kendro Laboratory Products, Germany

Bransonic® Ultrasonic cleaner 5510R-DTH, Branson ultrasonics, Danbury, USA

Elmarco Nanospider™ Lab electrospinning machine, Liberec, Czech Republic

Fisherbrand™ accumet™ AP115 Portable pH Meter, Fisher Scientific, Suwanee, GA, USA

Force Tensiometer-K6, Krüss GmbH, Hamburg, Germany

IKA® MS 3 basic shakers, IKA-Werke GmbH & Co .KG, USA

IKA® Viscometers Rotavisc hi-vi II S000 Complete, IKA-Werke GmbH & Co .KG, USA

IP54 Digital Micrometer 0-25/0.001 mm, Wilson Wolpert Instruments, Aachen, Germany

Julabo® F12-ED Refrigerated/Heating Circulator, JULABO Laboratory technology GmbH, Seelbach, Germany

PermeGear´s V6-CA Manual Diffusion System, PermeGear Inc, Hellertown, USA

Polaron SC7640 Sputter Coater, Quorum Technologies LTD, Kent, UK

Qlima H509 Humidifier, PVG International B.V., Oss, Netherlands

RACE 3F 1530, Inelco A/S, Denmark

Sartorius LP620S, scale, Sartorius Lab Instruments GmbH & Co. KG, Göttingen, Germany

Sartoris Quintix 124-1S Analytical Balance, Sartorius Lab Instruments GmbH & Co. KG, Göttingen, Germany

SensION™+EC7 Basic Conductivity Laboratory Meter, Hach Company, Loveland, CO, USA

SensION™+pH31 Laboratory pH Meter, Hach Company, Loveland, CO, USA

Shaking water bath 1083, Gesellschaft für Labortechnik mbH, Burgwedel, Germany

Spark® Microplate readers Te-Cool, Tecan Trading AG, Switzerland

Stuart™ hotplate stirrer multiposition SB162-3, Cole-Parmer, Staffordshire, UK

TA.XT plus Texture analyzer, Stable Micro Systems, Surrey, UK

TES-1364 Humidity-Temperature meter, TES Electrical Electronic Corp., Taipei, Taiwan

Wood´s SW45FB Dehumidifier, Woods TES, Alingsaas, Sweden

Zeiss Sigma FE-SEM, Carl Zeiss, Oberkochen, Germany

3.1.3 Software and programs

Exponent Connect software v. 6.1.16.0, Stable Micro Systems, Surrey, UK

ImageJ software version 1.52u, National Institutes of Health, MD, USA

SparkControl^{TM} v.2.3, Tecan Trading AG, Switzerland

3.1.4 Utensils

Accu-jet® pro Pipette Controller Brand, BrandTech Scientific, Wertheim, Germany

Art® 1000 E Barrier tip, Rached Sterile, 1000 µL pipette tips, Thermo Scientific, Roskilde, Denmark

BD PlastipakTM, 2 mL luer, Becton, Dickinson and Company, Franklin Lakes, USA

Einmach-Fix Zellglas, Max Bringmann KG, Wendelstein, Germany

Falcon® Serological pipette, sterile-R, non-pyrogenic, 5 mL, Corning incorporation, Life sciences, One bection circle, Durham, USA

Falcon® Serological pipette, sterile-R, non-pyrogenic, 2.5 mL, Corning incorporation, Life sciences, One bection circle, Durham, USA

Finnpipette®, 200-1000 µL, Thermo labsystems, Helsinki, Finland

Finnpipette® F2, 20-200 µL, Thermo scientific, Vantaa, Finland

Finnpipette® F2, 0.5-5 mL, Thermo scientific, Vantaa, Finland

HTS Transwell® -96 Well Permeabel Support, Corning®, NY, USA

NuncTM MicroWellTM 96-well microplates w/lid Nuclon D Si, NuclonTM Delta surface, polystyrene plates, 167008, Thermo Scientific, Roskilde, Danmark

VWR Signature^{TM} 1-200 µL Pipette tip, VWR International S.AS, Fontenary-sous-Bois, France

3.2 Methods

3.2.1 Polymer solution preparation

Different polymer spinning solutions were prepared based on the method of Grip et al (Grip et al., 2018). Polymer solutions were made by utilizing CHI, βG, and CAM as active ingredients and HPMC and PEO as co-polymers. In total 8 different polymer solutions, 4 without and 4 with CAM were prepared. These polymer solutions were prepared with CHI and βG as active ingredients, alone or combined. In addition, a polymer solution with only the copolymers was prepared, both without and with CAM (Table 1 and 2).

Table 1: The polymer composition of the different polymer solutions without chloramphenicol (CAM). *"All" indicate that all the polymers (CHI, βG and co-polymers) were included, CHI stands for Chitosan, βG stands for β-glucan, "Ref" indicate that only the co-polymers (polyethylene oxide and hydroxypropyl methylcellulose) were included, "Sol" indicates Solution.*

Solution name	Polymer ingredients % (w/w)			
	CHI	βG	HPMC	PEO
All-Sol	20	20	30	30
CHI-Ref-Sol	20		40	40
βG-Ref-Sol		20	40	40
Ref-Sol			50	50

Table 2: The polymer composition of the different polymer solutions incorporated with chloramphenicol (CAM). *"All" indicate that all the polymers (CHI, βG and co-polymers) were included, CHI stands for Chitosan, βG stands for β-glucan, "Ref" indicate that only the co-polymers (polyethylene oxide and hydroxypropyl methylcellulose) were included, "Sol" indicates Solution.*

Solution name	Polymer ingredients % (w/w)				
	CHI	βG	HPMC	PEO	CAM
All-CAM-Sol	20	20	29.5	29.5	1
CHI-Ref-CAM-Sol	20		39.5	30.5	1
βG-Ref-CAM-Sol		20	39.5	39.5	1
Ref-CAM-Sol			49.5	49.5	1

The total polymer concentration was kept constant for all polymer solutions at 2.5 % (w/w) (Table 3). PEO and HPMC had a ratio 1:1. Table 2 show that solutions with CAM either contained both, one or none of the active ingredients, to assess the influence of the addition of antimicrobial ingredient. The amount of HPMC and PEO varied. All solutions where CAM was incorporated had a concentration of 1 % (w/w) (Table 2).

Acetic acid, EtOH (96 % (v/v)) and distilled water were used as solvents in the polymer solutions. The final solvent concentration of acetic acid, EtOH and distilled water was always 3, 60, and 34.5 % (w/w), respectively (Table 3).

Table 3: Polymer concentration and solvent composition applied in electrospinning, acetic acid, ethanol (EtOH) and distilled water was kept constants for all the polymer solutions.

	Polymer concentration % (w/w)	Acetic acid % (w/w)	EtOH % (v/v)	Water % (w/w)
Polymer solution	2.5	3	60	34.5

Preparation of the polymer solutions is described in Figure 8-9. Polymer ingredients were added as dry materials, besides βG that was obtained from SBG® (2.5 % w/w). As described in Figure 8, to prepare polymer solutions the active polymers were first dissolved in the aqueous solvents, distilled water and acetic acid, before mixing the next day (Figure 9) to assure a homogenous polymer distribution in the final solution. The formulations with βG were first prepared by heating SBG® in a Shaking water bath 1083 (Burgwedel, Germany) at 50 °C for around 10- 15 minutes, to diminish the viscosity. After being heated, almost transparent, and liquefied SBG® was cooled to ambient temperature before weighing. Then, distilled water and acetic acid was weighed, in between adding these aqueous solvents it was shaken well, and lastly CHI was added (Figure 8). Finally, the mixture was left to stir overnight at 50 °C on a heating plate with stirrer to secure full hydration of the polymers (the last step described in Figure 8).
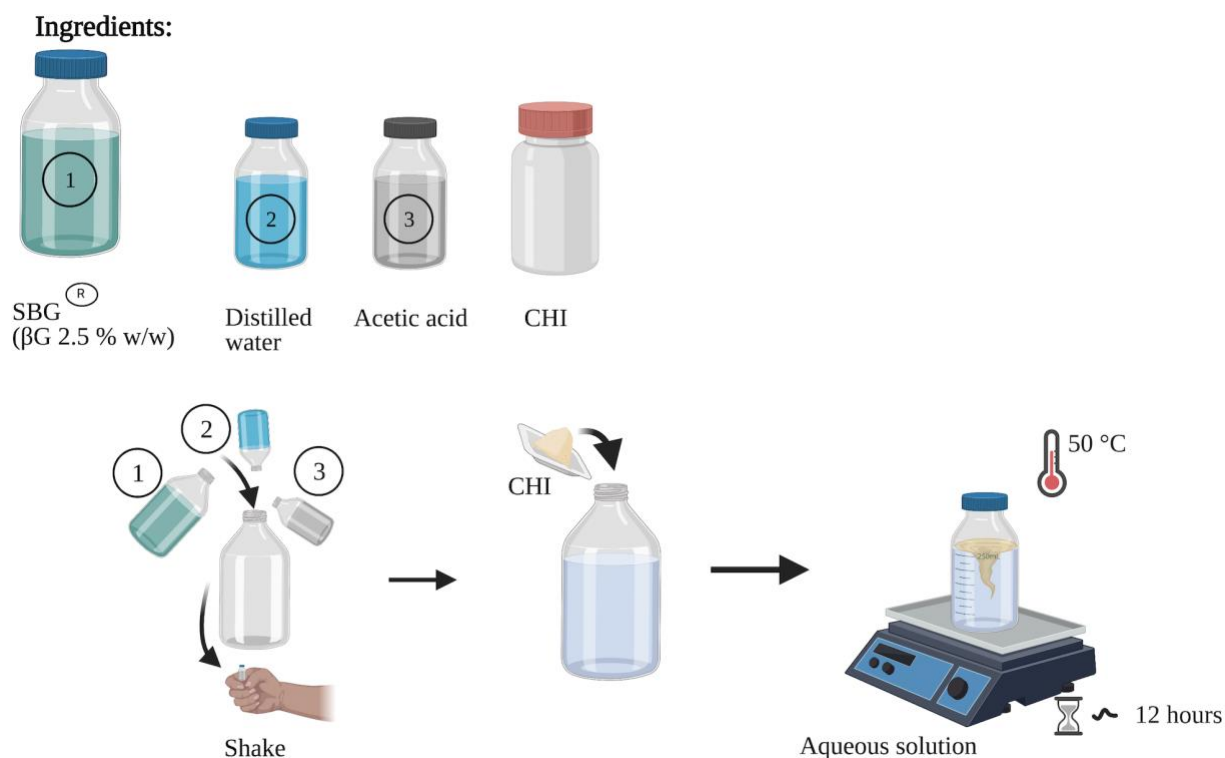
Figure 8: A schematic illustration of Step 1 in the preparation of the polymer solutions; Preperation of the aqueous solution with β-glucan (βG) and chitosan (CHI). *SBG® stands for Soluble beta-1,3/1,6-glucan.* Created with Biorender.com.

The PEO solutions (5 % w/w) were dissolved in EtOH (96 % v/v) and the blend was placed on a magnetic stirrer for 30 minutes at 70°C, as illustrated in Figure 9. Afterwards, the solution was heated in a water bath at the same temperature for 1 hour and then left to cool down. HPMC in EtOH was prepared and stirred on magnetic stirrer at room temperature for almost 10 minutes. In the final stage of step two, as shown in Figure 9, solutions of HPMC and PEO in EtOH and the aqueous solution were mixed to the final polymer concentration of 2.5 % (w/w). Then it was left on the magnetic stirrer at 50 °C overnight, to assure homogeneous blending.
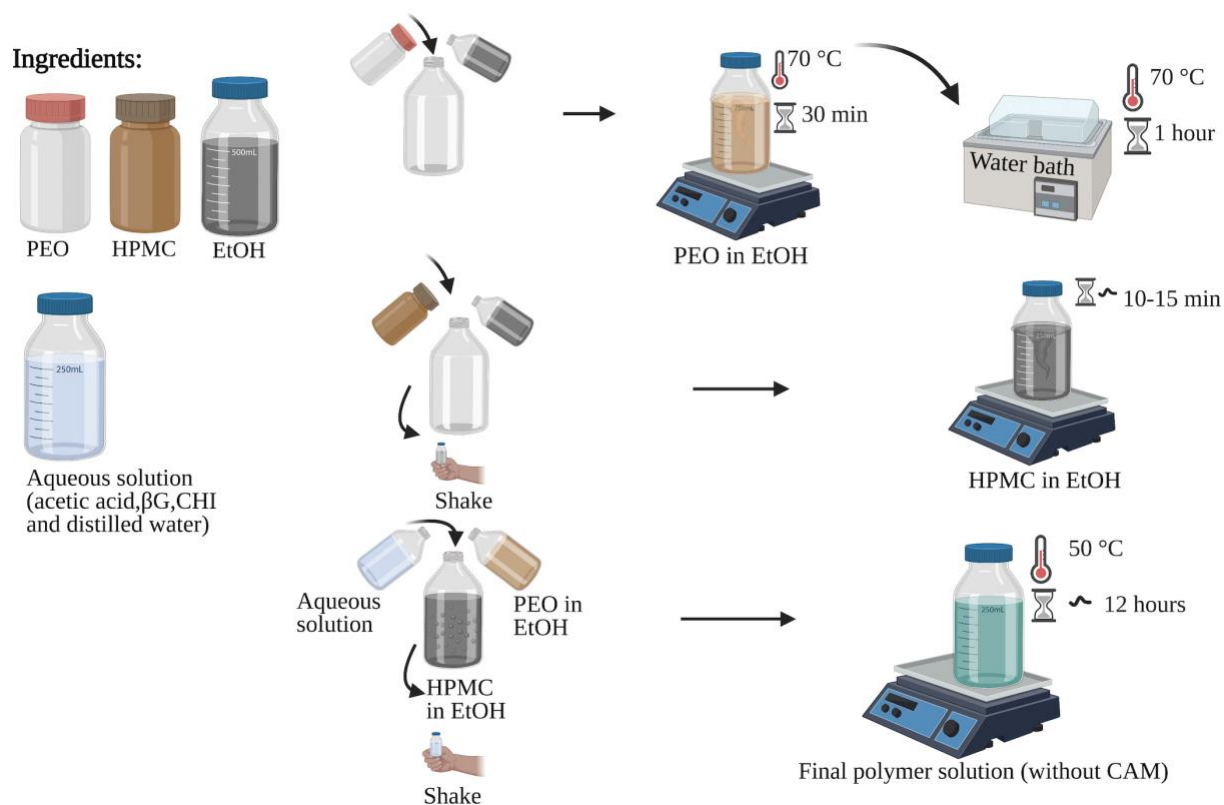
Figure 9: A schematic illustration of Step 2 in the preparation of the polymer solutions; the dissolution of polyethylene oxide (PEO) and hydroxypropyl methylcellulose (HPMC) in ethanol (EtOH), before further mixing in the aqueous solution prepared in Step 1. *CHI stands for Chitosan, βG stands for β-glucan.* Created with Biorender.com.

CAM was added to the solution directly before ES, to avoid any problems regarding the stability. The CAM solution (10 mg/mL), prepared in EtOH, was added to the solution under vigorous stirring, and thereafter left on the stirrer at room temperature for around 30 minutes, to assure uniform solution (Figure 10) and the characterization was done on the same day as the ES process.
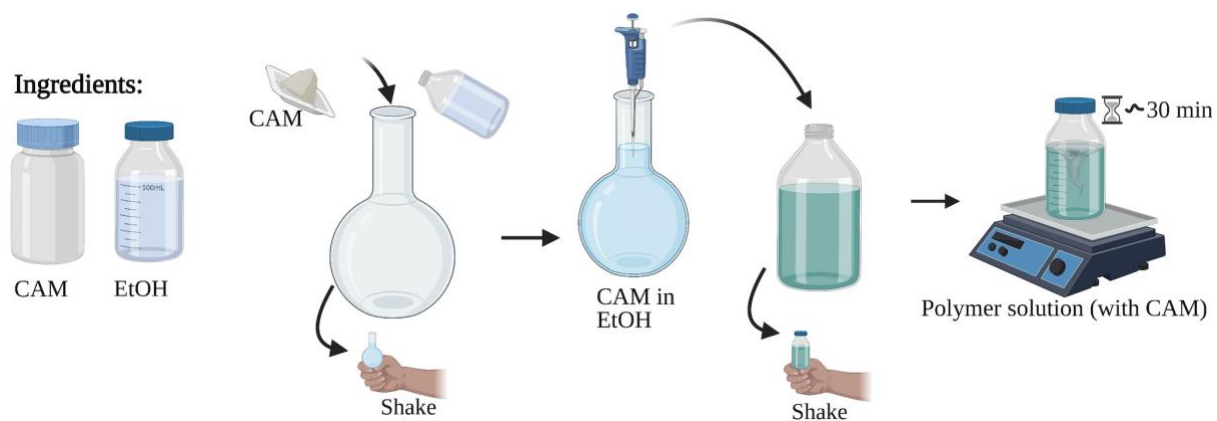
Figure 10: A schematic illustration of Step 3, and how chloramphenicol (CAM) was added into the polymer solution prepared in Step 2. *EtOH stands for ethanol.* Created with Biorender.com.

3.2.2 Characterization of polymer solutions

The conductivity, pH, surface tension, and viscosity were measured for all the polymer solutions (Figure 11).
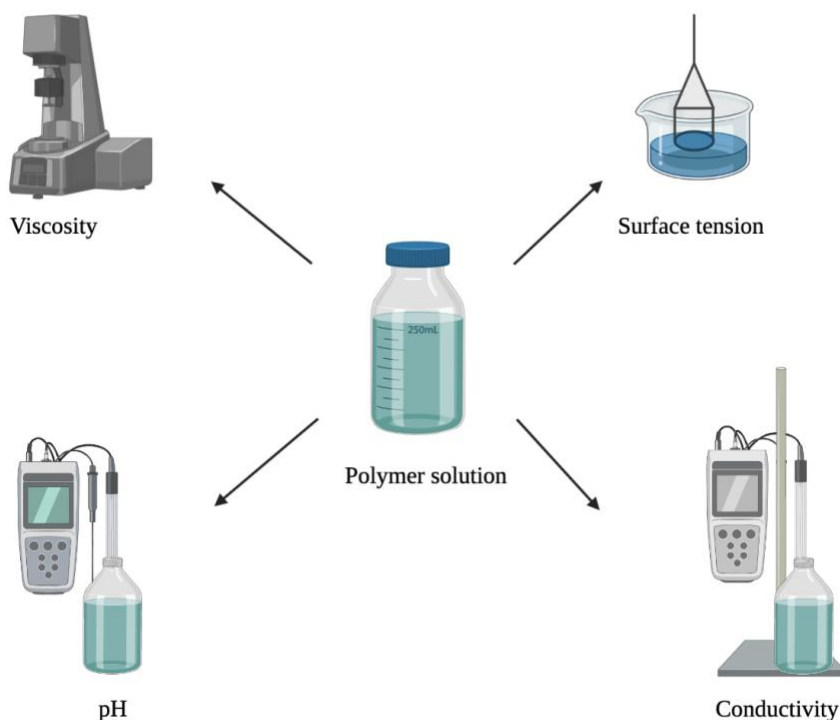
Figure 11: An overview of the characterization methods used for the polymer solutions, measuring; viscosity, surface tension, conductivity, and pH. Created with Biorender.com.

3.2.2.1 Conductivity and pH

Conductivity characterization were performed using a SensION^{TM}+EC7 Basic Conductivity Laboratory Meter (Hach Company, Loveland, CO, USA).

pH was measured using a Fisherbrand^{TM} accumet^{TM} AP115 Portable pH Meter by Fisher Scientific (Suwanee, GA, USA).

All measurements were carried out in triplicates, both for the conductivity and the pH.

3.2.2.2   Surface tension

Surface tension for all the ES solutions was measured utilizing the ring method, and the Force Tensiometer-K6 by Krüss GmbH (Hamburg, Germany). The instrument is equipped with a torsion wire that is combined to a thin wire ring. Around 20 mL of polymer solution was conveyed to the sample vessel and the wire ring was thereafter submerged in the solution. The ring was then slowly withdrawn from the solution by sinking the sample platform. When the ring reaches the surface of the solution the wire twist and its defection was shown on a scale that is calibrated for the surface tension (Krüss GmbH, 2007). Surface tension was measured three times for all polymer solutions.

3.2.2.3   Viscosity

The viscosity characterization was measured using the IKA® Viscometers Rotavisc hi-vi II Complete (KG, USA). Around 10 ml of polymer solution was filled in the sample container. Then the sample container was inserted to a container at the bottom of the viscometer. To conduct the measurement, the spindle "TL 6" was inserted and centered in the sample and attached to the viscometer. Rotating speed was set to rpm 20.00 and after one minute, the viscosity value (in mPas) was written down. Viscosity was measured three times for all polymer solutions.

3.2.3   Electrospinning of polymer solutions

The ES process was carried out using the Elmarco Nanospider™ ES machine (Liberec, Czech Republic). The instrument is applicable for NF-ES processes with a roll-to-roll collector. The machine has an adjustable spinning distance of between 120-240 mm, a substrate speed of 0- 5000 mm/min and a power supply capable of delivering 80 kV current. A volume of 50 mL polymer solution was transferred to the 50 mL carriage reservoir. The metal insert used had an orifice size of 0.8 mm. The average temperature and RH was, 22 ± 2 °C and 32 ± 8 %, respectively.

All polymer solutions were electrospun for 1 hour 20 minutes and the carriage reservoir was refilled every 20 minutes. The ES was conducted at maximum voltage of 80 kV and at a carriage speed of 300 mm/s. The substrate speed was set at 2 mm/min and distance from the electrode to the collector was 24 cm. Humidity and temperature was measured to be within the preset limits by using a TES-1364 Humidity-Temperature meter (TES Electrical Electronic Corp, Taipei, Taiwan).

3.2.4 Characterization of nanofibers

All the electrospun nanofibrous were characterized in terms of absorption capacity, tensile properties, nanofiber morphology, diameter and *in vitro* cell toxicity. In addition, CAM incorporated nanofibrous scaffolds were evaluated for CAM-content and *in vitro* CAM release.

3.2.4.1 Absorption capacity of nanofibers

All electrospun nanofibers with CHI in the formulation were examined for absorption capacity. To proceed this test, simulated wound fluid (SWF) was prepared by using a modified method (Bradford et al., 2009). SWF was composed of 292.2 mg sodium chloride, 168.02 mg sodium bicarbonate, 14.91 mg potassium chloride, 18.38 mg calcium chloride dihydrate, 8.25 ml Albunorm® and 50 mL distilled water. The absorption time was set to 5 minutes.

Fiber mats were cut with a scalpel into 2 x 2 cm samples, using a plastic template. Three specimens were cut at a predetermined area from all mats and left in a desiccator overnight, to decrease the humidity and to assure that they were completely dry. The dried nanofiber samples were weighed (W_d) and merged into 2000 μL of SWF in a small weighing boat for all the samples and a tool to remove the nanofiber was laid in it. After 5 minutes, the nanofibers were carefully removed and passed on a tissue paper. The excess fluid was blotted gently with a tissue paper before the absorbed nanofiber was weighed (W_s). The test was conducted in triplicate for each fiber mats and the percentage absorption capacity (C_a) was calculated using the following equation:

$$C_a(\%) = \frac{W_s - W_d}{W_d} \, x \, 100 \qquad\qquad \textbf{Eq. 1}$$

Where W_s is the weight of the absorbed nanofiber sample and W_d indicates the weight of the dry fiber sample.

3.2.4.2 Tensile properties of nanofibers

A TA.XT plus texture analyzer (Stable Micro Systems, Surrey, UK) was used to determine tensile strength of the electrospun nanofibrous at room temperature. The method was in accordance with ASTM-standard D882-18, the standard test method for tensile properties of thin plastic sheeting (ASTM-International, 2018). A 5 kg weight was used to calibrate the instrument. To hold the test specimens a pair of tensile grips was screwed to the machine. Then height calibration was executed with a return distance of 10 mm, return speed of 10 mm/sec and contact force of 1 kg. The starting position was set to a grip distance of 50 mm and a test speed of 0.08 mm/sec, which is the rate of separation of the two tensile grips.

In total five specimens at predetermined positions were cut from all fiber mats using a suitable razor blade and a plastic template to ensure uniform strips with a width of 10 mm and length of 80 mm. These specimens were placed in a desiccator overnight with silica to remove humidity. The thickness of the nanofibrous was measured by utilizing an IP54 Digital Micrometer (Wilson Wolpert Instruments, Aachen, Germany). The thickness of specimens was determined by measuring some pieces around already cut specimens, and the average value was entered to adjust for variations in thickness for the specimens. The tensile grips were lined with cardboard and parafilm to prevent fracture on the test sample. Then the specimen was placed in the tensile grips and it was tightened evenly before the test was run. Tensile strength, and percent elongation at break were measured by utilizing Exponent Connect software v. 6.1.16.0 (Stable Micro Systems, Surrey, UK), through the obtained tensile stress-strain curve (Figure 12).

$$TS = \frac{\text{Maximum force}}{\text{Crossectional area of specimen}}$$

$$PEB = \frac{\text{Extension at moment of rupture}}{\text{Initial length of specimen}} \times 100$$
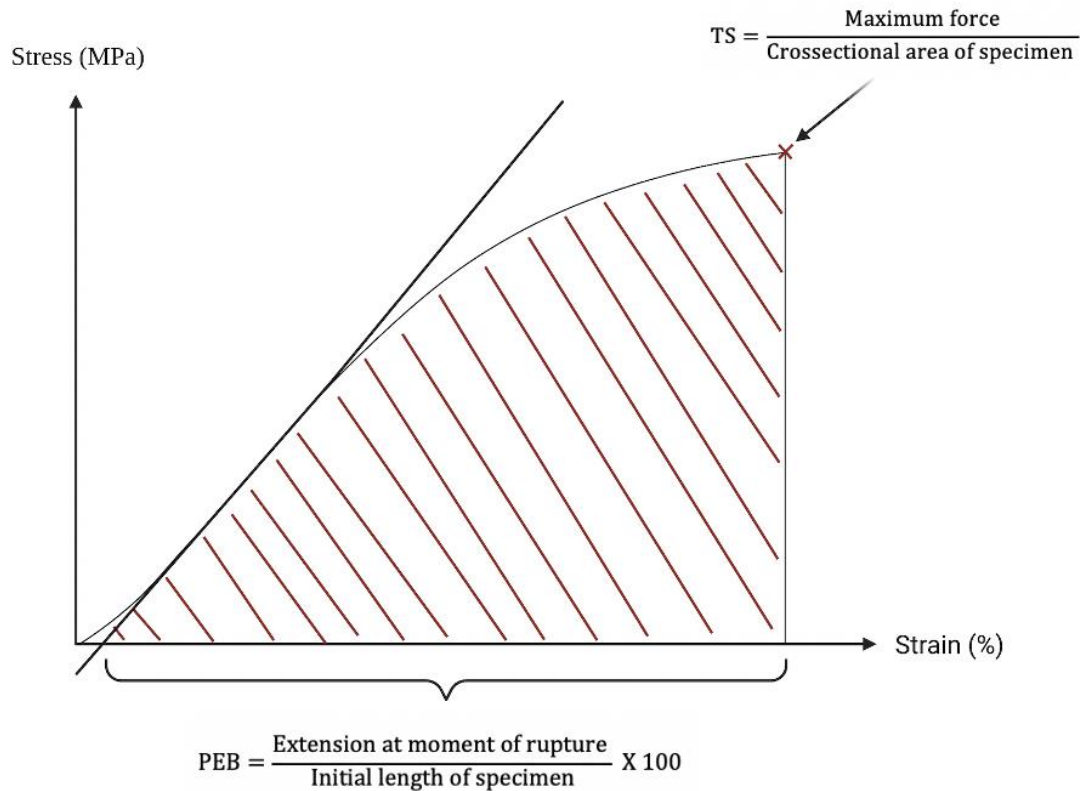
Figure 12: A typical strain-stress curve, present behavior of a specimen when it is subjected to a load. *TS stands for tensile strength, PEB stands for percent elongation at break.* Created with Biorender.com.

3.2.4.3   Diameter and morphology of nanofibers

All nanofibers were examined for surface morphology applying Field Emission Scanning Electron Microscopy (FE-SEM). The instrument used was a Zeiss Sigma FE-SEM (Carl Zeiss, Oberkochen, Germany), with an accelerating voltage of 2 kV. The fibers were cut into small specimens and put-on metallic studs with double-sided carbon tape and placed in a desiccator overnight to dry. Before examination, the specimens were sputter-coated with delicate coat of gold-palladium applying a Polaron SC7640 (Quorum Technologies LTD, Kent, UK). The examination was carried out under high vacuum. At least five images were made per specimen with different magnifications: 1, 3, and 15 kX. The average diameter of each nanofiber mat was determined using the ImageJ software (NIH, MD, USA). In total three images from each nanofiber mat were analyzed. The fiber diameter was measured for 100 randomly selected individual fibers per image. Thus, in total 300 individual fibers were measured for each fiber specimen, to ensure a representative average nanofiber diameter.

3.2.4.4 Chloramphenicol content

All the spun nanofibers that contained CAM were analyzed for their CAM-content. The day before conducting the experiment five specimens were cut at a predetermined area from each fiber mat using a 2 x 2 cm plastic template. These samples were left in a desiccator overnight, to dry.

The dry nanofiber specimens were weighed and thereafter transferred to glass vials. And dissolved in 1000 µL of distilled water followed with 1000 µL acetic acid. The samples were mixed by vortexing in this process. The vials were then left on a magnetic stirrer for 30 minutes to assure completely dissolved fibers. To centrifuge undissolved polymers, 1.5 g of the mixture was weighed in a centrifuge tube and placed in the Biofuge Stratos centrifuge (Kendro Laboratory Products, Germany) for 1 hour with a speed of 4000 g^{-1} and the temperature was set to 4 ℃.

The supernatant was carefully transferred to a small plastic vial and vortexed. Finally, 3 x 200 µL of the sample was transferred to a microplate and the CAM-content was measured utilizing Spark® Microplate readers (Tecan Trading AG, Switzerland). A wavelength of 276 nm was selected. Provided UV-absorbance was read from the SparkControl™ software and used for further calculate the percentage concentration of CAM in the nanofiber using the following the following equation:

$$CAM - content(\%) = \frac{A}{B} x\ 100\ \%$$ **Eq. 2**

Where A= measured average chloramphenicol (CAM) content in nanofibers, and B= theoretical CAM-content in the nanofibers (1 %).

3.2.4.5 *In vitro* release of chloramphenicol

The *in vitro* testing of the CAM release from the nanofibers was performed utilizing a Franz diffusion cell (PermeGear´s V6-CA Manual Diffusion System, PermeGear Inc, Hellertown, USA) with a receptor chamber with a capacity of approximately 5 mL and a donor surface of 0.64 cm^2. On the day prior to the test, nanofibers were cut into a small circular disc of 0.9/0.8 cm in diameter and placed in a desiccator overnight, to assure complete dry samples. The temperature of the receptor solution was maintained by the water jacket, which is connected to a water bath so it could provide a skin surface temperature of 32 °C (Zhang et al., 2017).

As acceptor solution phosphate-buffered saline (PBS) (pH 7.4) was prepared according to the European Pharmacopoeia. PBS was composed of 8 g/L sodium chloride, 0.19 g/L of potassium phosphate monobasic and 2.38 g/L of sodium phosphate dibasic dihydrate in milli-Q water. The buffer was left to sonicate (Bransonic® Ultrasonic cleaner 5510R-DTH, Branson ultrasonics, Danbury, USA) for approximately 2 hours, to make sure all the substances were dissolved. Before setting the experiment, the cellulose membrane, which was used to separate the acceptor and donor chamber to test the release out of the nanofibers, was cut in an appropriate size range, so it fitted the diffusion cell diameter and was then moistened in PBS for 30 minutes. Prior to the experiment nanofibers were weighed.

Franz cell was filled with approximately 5 mL of PBS and was continuously stirred utilizing built-in bar, to assure uniform temperature. Then, the soaked cellulose membrane (Einmach-Fix Zellglas, Max Bringmann KG, Wendelstein, Germany) was mounted between the receptor and donor chamber. Afterwards, 10 mL of PBS was added to the donor chamber. Then, nanofibers were placed upon the membrane. Right after, the sampling port and donor compound were sealed with parafilm to avoid that the receptor solution evaporates.

CAM release test was conducted for 6 hours, and 500 µL of sample was withdrawn after 10, 20, 30, 40, 60, 120, 180, and 360 minutes. The withdrawn volume was replaced with fresh PBS, to maintain the sink-condition through the examination. Lastly, samples were analyzed using Spark® (Tecan Trading AG, Switzerland) at the wavelength of 278 nm. Results were obtained with help from SparkControl™ software. The release studies were performed in duplicate for all the fiber mats that contained CAM. CAM release was calculated using the following equitation:

$$CAM\ release\ (\%) = \frac{A}{B} x\ 100\ \%$$

Eq. 3

Where A= Cumulative amount of chloramphenicol (CAM), and B= measured CAM-content in nanofiber.

3.2.4.6   *In vitro* cell toxicity

Cell viability test was performed on human immortalized keratinocytes (HaCaT) cell lines by using Cell Counting Kit-8 (CCK-8) (Sigma-Aldrich, St. Louis, MO, USA). To prepare adherent HaCaT cells, Dulbecco`s modified Eagle`s medium-High Glucose (Biowest, Riverside, MO, USA) with Fetal Bovine Serum (Sigma-Aldrich, St. Louis, MO, USA) and Penicillin-Streptomycin (Sigma-Aldrich, St. Louis, MO, USA) was warmed up at 37 ℃ for 1 hour. Dulbecco`s PBS (Sigma-Aldrich, St. Louis, MO, USA) solution was gently added to the cell culture and aspirated. Afterward, the trypsin-EDTA (Sigma-Aldrich, St. Louis, MO, USA) was added and tilted to mix, followed by aspiration, and then incubated for 5 minutes, so cells could come off from the plate. Lastly, the media was added to stop the trypsinization reaction. Before adding the desired volume of the cell suspension to a bottle, cell counting was performed using a counting chamber, a hemocytometer.

Figure 13 describes how the cell viability test was conducted. The cell viability test was performed in a 96-well plate. As shown in step 1, 90 µL of cell suspension (corresponding to 10^5 cells/well) was added to each cell. The plate was thereafter incubated in a humidified incubator at 37 ℃ with 5 % CO_2 for 24 hours. Meanwhile, 10 mg/mL nanofiber solution was prepared for both nanofibers with and without CAM. In a 2 mL measuring flask 20 mg of nanofiber was weighed and then wetted with some drops of milli-Q water followed by vortexing. Further, 20 µL of 10 % acetic acid in milli-Q water was added and vortexed well. Lastly, some drops of milli-Q water were added and vortexed before the solution was sonicated for approximately 2 hours. After sonication, the nanofiber solution was filled with milli-Q water to a total volume of 2 mL and vortexed before it was kept in the refrigerator overnight.
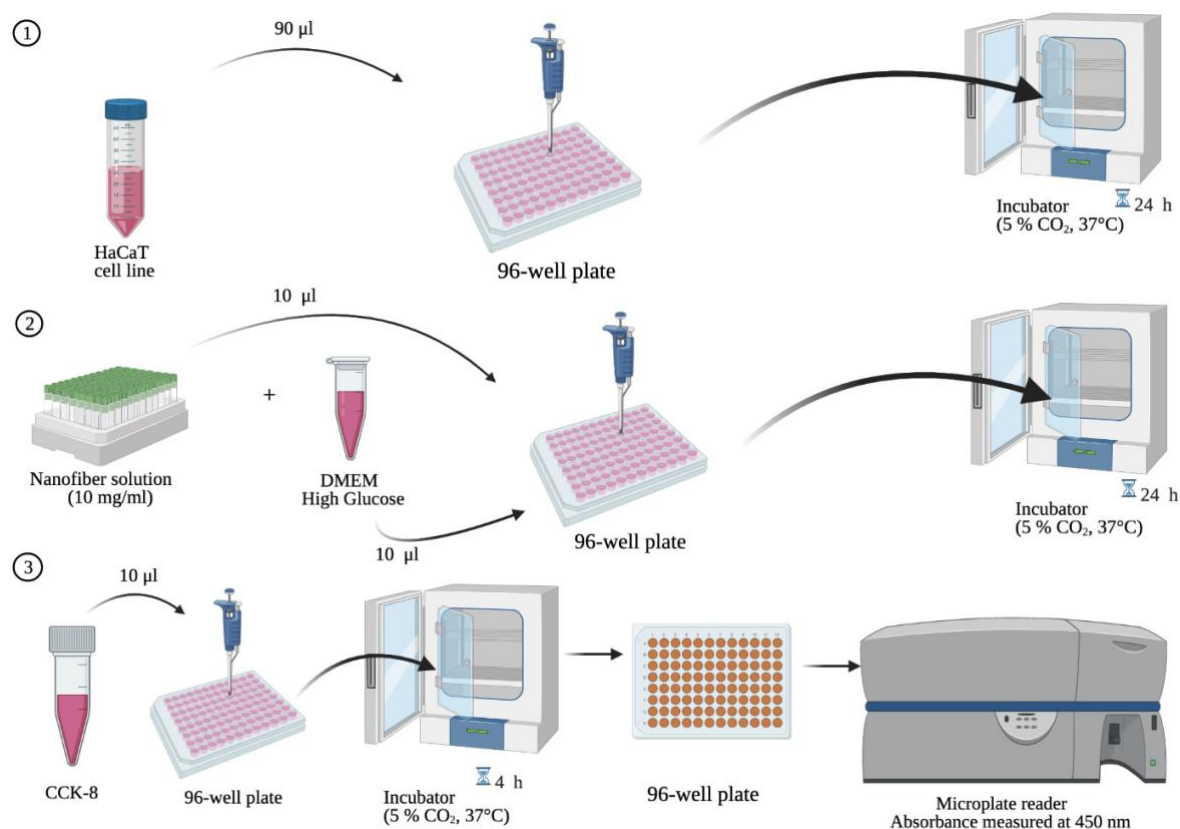
Figure 13: A schematic illustration of how the cell viability test was done. *HaCaT stands for human immortalized keratinocytes, DMEM stands for Dulbecco`s modified Eagle`s medium, CCK-8 stands for cell Counting Kit-8.* Created with Biorender.com.

The day after, nanofiber solutions were stored at room temperature for 30 minutes before 10 µL with three duplicate wells for every nanofiber formulation and media (control) was pipetted into the cell suspension in the 96-well plate and incubated for 24 hours, as shown in step 2 (Figure 13). Step 3 shows that 10 µL of CCK-8 was added to each well of the plate carefully to ensure no bubbles to the wells. The plate was incubated for 4 hours and then the absorbance was measured at 450 nm utilizing Spark®. The percentage of cell viability (CV) was calculated using the following equation:

$$CV(\%) = \frac{A_S}{A_C} x \ 100 \qquad\qquad \textbf{Eq. 4}$$

Where, A_s is the absorbance of sample and A_C is the absorbance of control.

3.2.5 Statistical analysis

The results are presented as the mean ± standard deviation (SD) of the mean from three independent experiments. A two tailed unpaired t-test was utilized to determine the difference between formulations and polymer solutions. A p value of < 0.05 was considered the significant difference.

4 Results and discussion

4.1 Characterization of polymer solutions

Polymer solution properties can affect the ES process, thus impact the final fabricated nanofibers (Haider et al., 2018). Properties such as conductivity, pH, surface tension, and viscosity were properties examined in this project.

4.1.1 Conductivity and pH

The conductivity of the polymer solution is an important parameter for the ES process. This parameter affects the establishment of a surface charge on the fluid droplet, which is necessary for the formation of a Taylor cone (Pelipenko et al., 2015). The polymers utilized in this project are HPMC, PEO, βG and CHI. The three first mentioned polymers are easily dissolved in water, wheras CHI, is not easily soluble directly in water. CHI is soluble at pH less than 6 due to the protonation of $-NH_2$ groups, therefore it was dissolved in acetic acid.

The conductivity plotted against all polymer is shown in Figure 14. These results clearly show that the conductivity of the polymer solutions is unaffected by CAM ($p > 0.05$). For comparison, teicoplanin-loaded CHI/PEO nanofibers for local antibiotic delivery and wound healing reported increased conductivity due to the presence of ionized drug molecules, meanwhile decreased conductivity of the CHI/PEO solution was reported (Amiri et al., 2020). In our study, CAM is utilized as an antibiotic and in the polymer solution it is non-ionic. Therefore, the described increased conductivity in mentioned article cannot be expected in our study.

Figure 14: Conductivity of the different polymer solution without and with chloramphenicol (CAM) (n=3). *"All" indicate that all the polymers (CHI, βG and co-polymers) were included, CHI stands for Chitosan, βG stands for β-glucan, "Ref" indicate that only the co-polymers (polyethylene oxide and hydroxypropyl methylcellulose) were included, "Sol" indicates Solution.*

As expected, the conductivity is higher for polymer solutions containing CHI than those without and it is statistically significant ($p < 0.05$). Similar data reported a magnitude higher conductivity for CHI solution than PEO solution, also a significant increase with increasing CHI concentration was presented (Duan et al., 2004). Two articles reported increasing conductivity of polymer solutions with increasing concentration of CHI (Rošic et al., 2012; Van der Schueren et al., 2012). These results can be explained due to the pKa value of CHI being 6.5. Thus, in an acidic media CHI protonates, it becomes a cationic polyelectrolyte and soluble (Koosha & Mirzadeh, 2015). Hence, acetic acid enables the solubilization and protonation of CHI, and as a result the polymer conducts electricity.

The other polymers applied in our polymer solutions, PEO, HPMC and βG do not function as polyelectrolytes. Therefore, an increase in concentrations of these polymers will not affect the conductivity of the polymer solutions.

Figure 15: pH of the different polymer solution without and with chloramphenicol (CAM) (n=3). *"All" indicate that all the polymers (CHI, βG and co-polymers) were included, CHI stands for Chitosan, βG stands for β-glucan, "Ref" indicate that only the co-polymers (polyethylene oxide and hydroxypropyl methylcellulose) were included, "Sol" indicates Solution.*

The measures pH for the different polymer solutions is demonstrated in Figure 15. The pH difference between CHI containing solutions and polymer solutions without CHI was significant ($p < 0.05$). Acetic acid is dissociating, forming hydronium ions and acetate. Therefore, $-NH_2$ groups on CHI can get protonated and soluble, hence acting as a base (Figure 4, Page 15). This results gives a higher pH for polymer solutions containing CHI since there are less free H^+ ions present here than in the other polymer solution, thus more acidic (Roberts, 1992).

4.1.2 Surface tension

The surface tension of the polymer solution is a critical parameter that interferes with the ES process. This parameter is the primary force acting against Taylor cone production and further jet elongation (Pelipenko et al., 2015). The surface tension indicates the force required from the electrical forces to overcome it (Bhardwaj & Kundu, 2010). The surface tension of the different polymers solutions could therefore theoretically be utilized to predict the spinnability of the solutions into nanofibers.
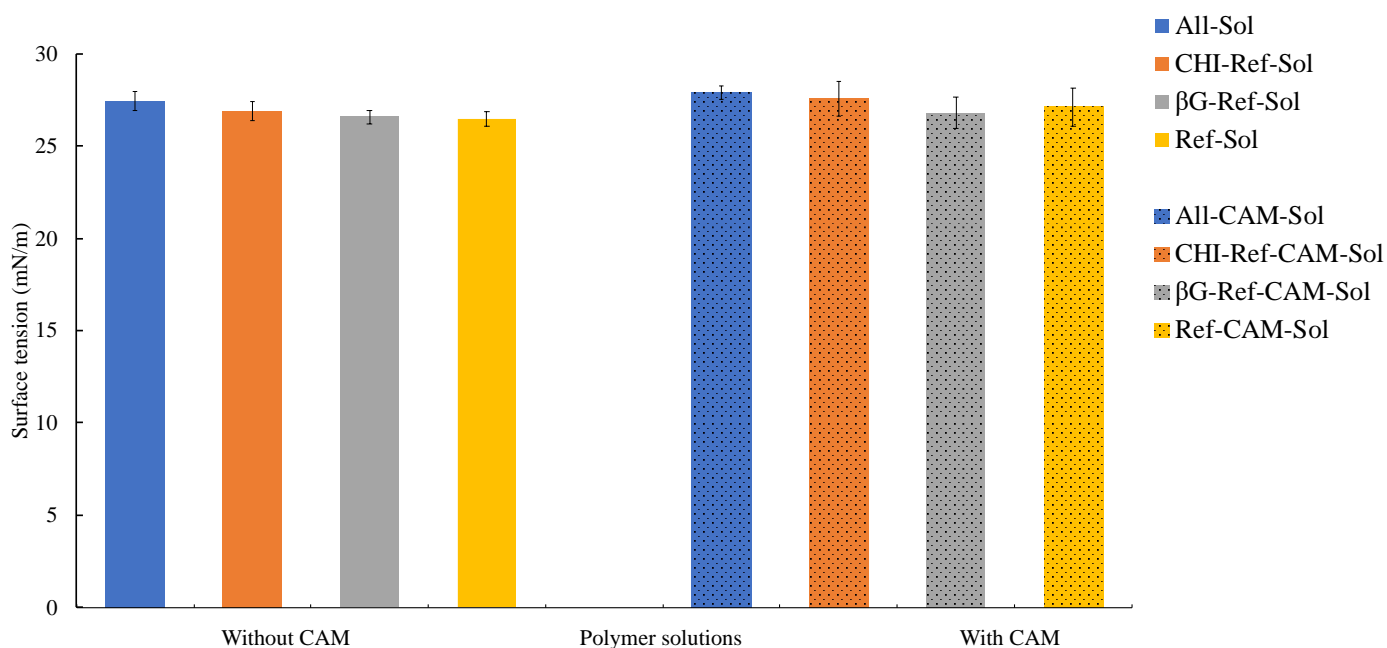
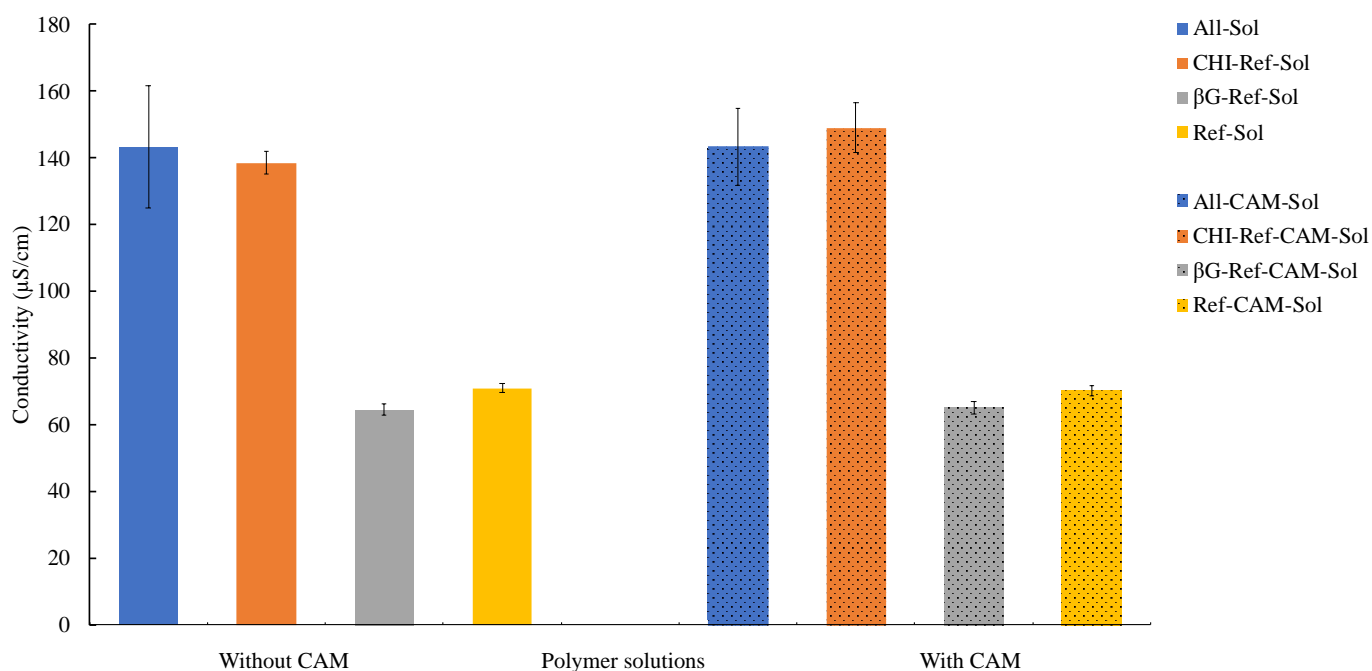**Figure 16:** Surface tension of the different polymer solution without and with chloramphenicol (CAM) (n=3). *"All" indicate that all the polymers (CHI, βG and co-polymers) were included, CHI stands for Chitosan, βG stands for β-glucan, "Ref" indicate that only the co-polymers (polyethylene oxide and hydroxypropyl methylcellulose) were included, "Sol" indicates Solution.*

The surface tension of polymer solutions without and with CAM is shown in Figure 16. The results clearly show that the surface tension of all the polymer was the same, and no difference was observed ($p > 0.05$). This was expected sine the same total mass of polymers, acetic acid and water was utilized within formulations as presented in Table 1-3 (Page 32-33). An article reported surface tension varying with EtOH concentration (Khattab et al., 2012). This finding is not in accordance with our result since the same EtOH concentration was added in all polymer solutions, therefore the surface tension did not change among the different solutions.

4.1.3 Viscosity

The extent of the polymer molecule chain entanglement in the polymer solution influences the viscosity. To produce homogenous nanofibers, polymer molecules have to be entangled. Or else, beads or droplets are deposited on the collector because the low viscoelastic force will not counterbalance the stretching force that enables jet instability (Kriegel et al., 2008). The viscosity of a polymer solutions is depended on several factors, polymer type, concentration of polymer and solvent type (Aydogdu et al., 2018). For example, a moderate concentration of CHI exhibits high viscosity due to the rigid D-glucosamine repeat unit and their high hydrogen bonding affinity (Çay et al., 2014; Li & Hsieh, 2006).

In order to investigate the influence of different polymers and CAM incorporation, the viscosity of the polymer solutions were measured utilizing IKA$^\circledR$ Viscometers Rotavisc hi-vi II Complete (KG, USA) with spindle "TL 6" at 20 rpm. The association between viscosity and polymer solutions is presented in Figure 17.

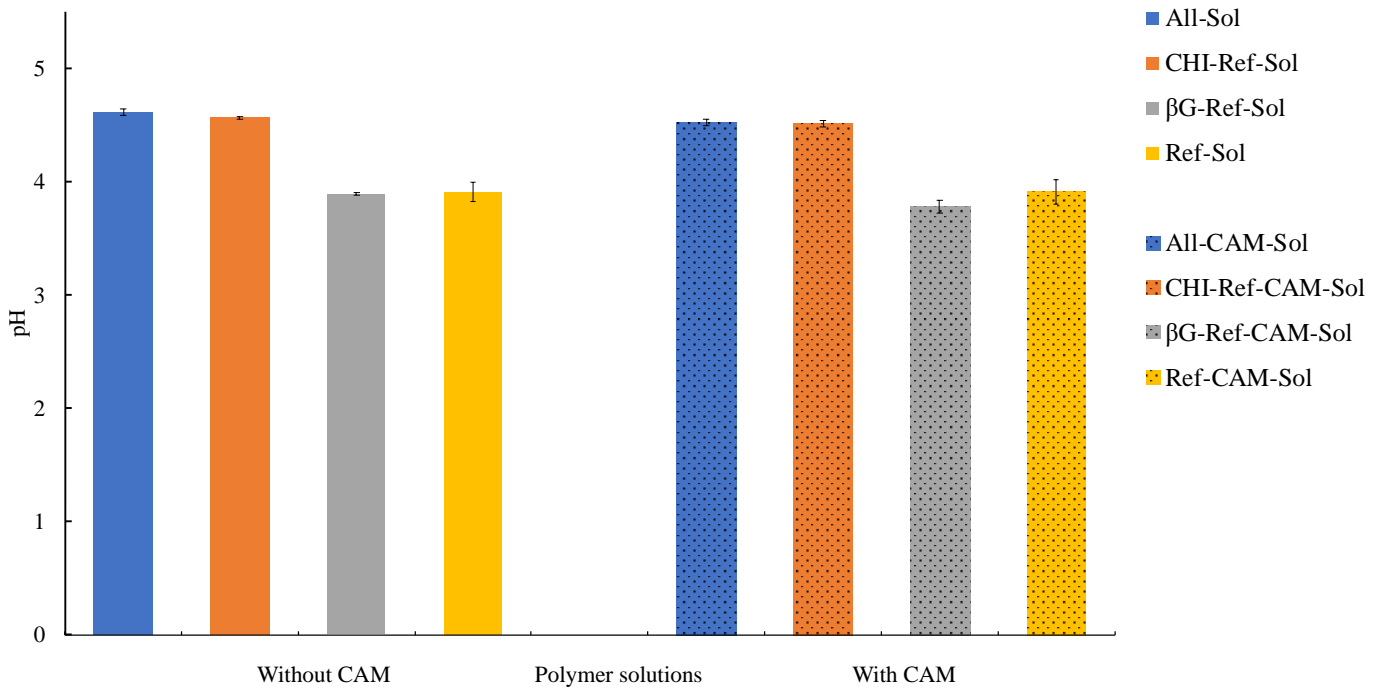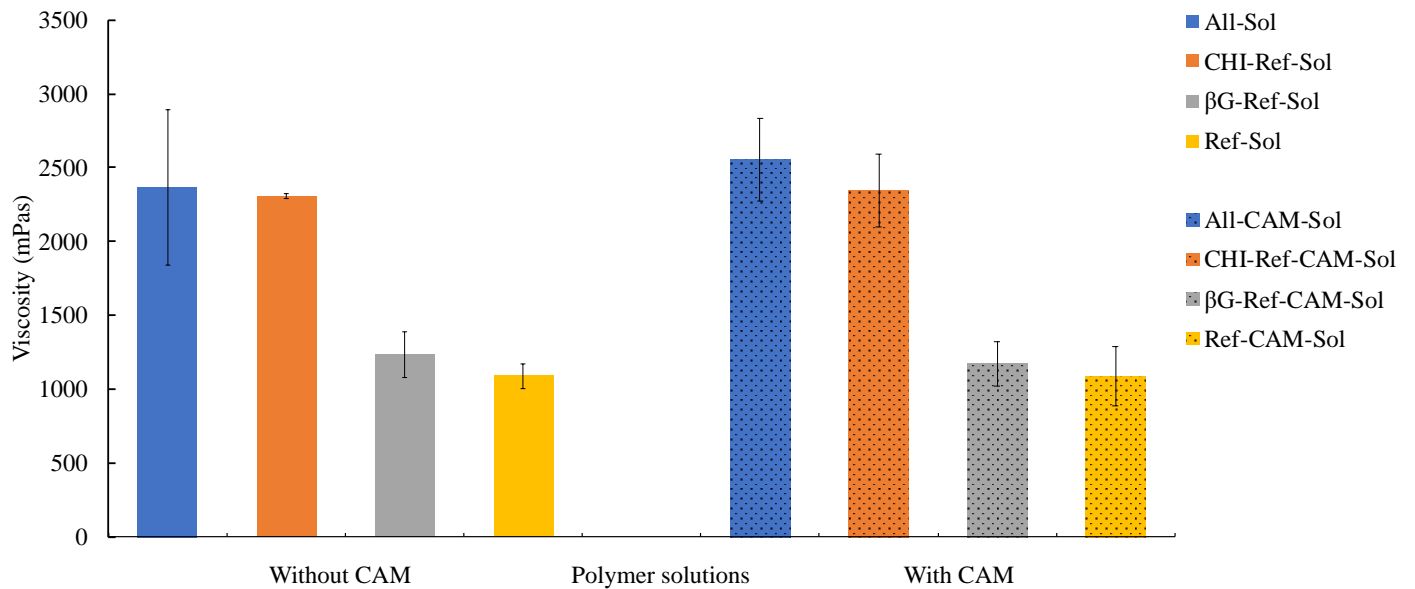**Figure 17:** Viscosity of the different polymer solutions without and with chloramphenicol (CAM) (n=3). *"All" indicate that all the polymers (CHI, βG and co-polymers) were included, CHI stands for Chitosan, βG stands for β-glucan, "Ref" indicate that only the co-polymers (polyethylene oxide and hydroxypropyl methylcellulose) were included, "Sol" indicates Solution.*

These results reveal that the viscosity is not affected by CAM ($p > 0.05$). This indicate that 1 % CAM presence in the polymer solution does not affect the viscosity, and obviously higher concentrations are needed to gain an effect.

Figure 17 shows noticeable differences in viscosity for polymer solutions containing CHI than those without ($p < 0.05$). A article reported an increase in the viscosity with increasing amount of CHI (Çay et al., 2014). In our study the CHI content was kept constants for all the polymer solutions containing CHI, as described in Table 1 and Table 2 (Page 32), thus the observed effect from CHI is only seen when comparing the polymer solutions containing CHI (All-CAM-Sol, All-Sol, CHI-Ref-Sol, CHI-Ref-CAM-Sol) with those that do not contain CHI (βG-Ref-CAM-Sol, βG-CAM-Sol, Ref-CAM-Sol, Ref-Sol). Polymer solutions without CHI show less viscosity compared to the ones with CHI, as mentioned above, the chain entanglement has a critical role in the viscosity. Therefore, CHI containing solutions most probably show higher viscosity due to the strong hydrogen bonds between -NH$_2$ and OH groups of its polymer chain (Figure 4, Page 15) (Bhattarai et al., 2005).

Grip et al observed a lower viscosity for polymer solution without βG containing HPMC, PEO and EtOH in comparison with polymer solution containing βG, HPMC, PEO, EtOH and distilled water. This observation was due to the absence of βG and lower volume of water, since the hydrophilic polymers swell less in EtOH compared to water (Grip et al., 2018). However, the water and EtOH content was constant (Table 3, Page 33) in our study and that is probably why we do not see this effect.

4.2 Electrospinning

All nanofibers were fabricated using the Elmarco Nanospider™ ES machine (Liberec, Czech Republic). This equipment is a needle-free electrospinning (NF-ES) machine enabling the NF-ES process for fabrication of nanofibers directly from a free surface of liquid (Yu et al., 2017). The stationary wire is coated with polymer solution during the ES process by a closed carriage. NF-ES exhibit advantages as it enables to fabricate higher volume of nanofiber mat and there is no problem with needle clogging (El-Newehy et al., 2011; Nayak et al., 2012). This technology has also reported fabrication of fibers with small diameters and uniform distribution (Yalcinkaya, 2019). Previous article published by our research group utilized Nanospider™ for making nanofiber with β-glucan as the active ingredient (Grip et al., 2018).

In this study, the ES duration was standardized with a spinning time of 1 hour and 20 minutes. The equipment was set to maximum voltage of 80 kv, the carriage speed of 300 mm/s, substrate speed at 2 mm/min and distance from the electrode to the collector was 24 cm. These settings were chosen due to an earlier project done by Julie Wik Olaussen where the ES process was optimized (Olaussen, 2020). During the ES process we wanted to control the ambient temperature and relative humidity. This was therefore the first method optimization made in the project.

4.2.1 Controlling environmental parameters

Ambient temperature and RH are two environmental parameters that have a major influence on diameter and morphology of electrospun nanofibers. Therefore, both parameters were tried to control at 24 ± 2 °C and 28 ± 3 %, RH, respectively. This was done to assure that all fibers were spun at the same conditions. The average temperature and RH during the fabrication of bacth 1, 2 and 3 nanofibers and their SD is presented in Table 4 and Table 5.

Table 4: The recorded temperature during electrospinning for batch 1, 2 and 3 of all the polymer solutions (n=3). *"All" indicate that all the polymers (CHI, βG and co-polymers) were included, CHI stands for Chitosan, βG stands for β-glucan, "Ref" indicate that only the co-polymers (polyethylene oxide and hydroxypropyl methylcellulose) were included, CAM stands for chloramphenicol.*

		Temperature (°C)			
		All-Nanofiber	**CHI-Ref-Nanofiber**	**βG-Ref-Nanofiber**	**Ref-Nanofiber**
Without CAM	**1**	22.14 ± 0.45	22.86 ± 0.68	23.74 ± 0.05	23.80 ± 0.53
	2	22.48 ± 0.39	22.56 ± 0.36	23.00 ± 0.65	23.62 ± 0.07
	3	22.52 ± 0.23	22.76 ± 0.36	23.20 ± 0.28	23.48 ± 0.18
With CAM	**1**	24.34 ± 0.51	23.08 ± 0.55	23.06 ± 0.36	22.88 ± 0.51
	2	24.66 ± 0.19	24.16 ± 0.36	24.18 ± 0.31	24.48 ± 0.12
	3	24.38 ± 0.77	24.14 ± 0.42	24.26 ± 0.74	23.62 ± 0.56

The temperature can influence the average diameter of the nanofibers by increasing the evaporation rate of solvents and decrease the viscosity of the solution. The measured temperature (Table 4) during ES process, shows that minimum and maximum temperature was at 22.14 ± 0.45 °C and 24.66 ± 0.19 °C, respectively. This indicated that all nanofibers were prepared in the predetermined temperature range of 24 ± 2 °C and the ambient temperature was successfully controlled.

Table 5: The recorded relative humidity (RH) during electrospinning for batch 1, 2 and 3 of all the polymer solutions (n=3). *"All" indicate that all the polymers (CHI, βG and co-polymers) were included, CHI stands for Chitosan, βG stands for β-glucan, "Ref" indicate that only the co-polymers (polyethylene oxide and hydroxypropyl methylcellulose) were included. CAM stands for chloramphenicol.*

Relative humidity (%)					
		All-Nanofiber	**CHI-Ref-Nanofiber**	**βG-Ref-Nanofiber**	**Ref-Nanofiber**
Without CAM	**1**	25.66 ± 3.70	26.66 ± 2.25	27.58 ± 2.17	27.44 ± 0.42
	2	26.66 ± 1.79	27.84 ± 2.56	27.78 ± 1.89	29.22 ± 0.59
	3	24.64 ± 0.46	26.10 ± 2.14	25.74 ± 1.32	26.42 ± 2.31
With CAM	**1**	24.38 ± 0.57	40.28 ± 2.03	39.36 ± 0.48	26.66 ± 1.77
	2	27.90 ± 0.49	28.28 ± 2.50	29.12 ± 0.71	28.20 ± 0.82
	3	27.82 ± 1.81	26.90 ± 1.92	28.26 ± 1.40	25.98 ± 1.24

RH affects nanofiber diameter by adjusting the solidification performance of the charged jet. This is dependent on the chemical nature of utilized polymers. Table 5 shows the RH during ES process, the minimum and maximum measurement was 24.38 ± 0.57 % and 40.28 ± 2.03 %, respectively. Only three measurements were without the predetermined range of 28 ± 3 % and that was for batch 1 All-CAM-Nanofiber, CHI-Ref-CAM-Nanofiber and βG-Ref-CAM-Nanofiber. This might indicate that it was difficult to control the RH that day of ES. However, all the other measurements were within the determined range and therefore it can be concluded that RH was successfully controlled. In other articles, it was observed differences in nanofiber diameter when utilizing different polymers and varying RH during the ES process (Pelipenko, Kocbek, et al., 2013). It was reported that the nanofiber diameter decreased with increasing RH for several nanofiber mats. Also, bead formation was reported due to an increase in humidity (Pelipenko, Kristl, et al., 2013). Similar articles observed decrease in the nanofiber diameter with increase in humidity. This is due to slower solidification of nanofibers, that leads to thinner fibers (De Vrieze et al., 2009; Park & Lee, 2010). An article reported opposite finding, increased RH resulted in increased average diameter. This is attributed too high ambient humidity that cause more water to be absorbed or make contact with the jet during the ES process. It is suggested that this precipitates the fibers in the jet quickly and inhibit the elongation of the jet, developing larger fiber diameter (De Vrieze et al., 2009; Park & Lee, 2010).

4.3   Characterization of nanofibers

All the electrospun nanofibers were characterized for absorption capacity, tensile properties, morphologies, diameters, CAM-content, *in vitro* CAM-release from nanofibers and *in vitro* cell toxicity.

4.3.1   Absorption capacity of nanofibers

Wound exudate is produced during the inflammatory and proliferative stages of the wound healing. It has an important function in the wound healing process, as it provides a moist wound environment (Cutting, 2017). In chronic wound beds, the volume of exudate is moderate to heavy, which can increase the risk of infection. The fabricated nanofiber dressing is meant to be used directly onto the high to moderately exudation wound. That enables to mask the unpleasant visual features of exudate, absorb adequate amounts of exudate while maintaining a moist and an optimal environment. This first mentioned can also be a disadvantage since the wound cannot be seen properly due to the nanofiber.

The ability to absorb exudate from the wound is critical for an ideal therapy and was thus examined. Table 6 present the absorption capacity as a function of nanofibers without and with CAM.

Table 6: Absorption capacity of all the prepared nanofibers (n=3). ***βG-Ref-Nanofiber and Ref-Nanofiber was not possible to examine. *"All" indicate that all the polymers (CHI, βG and co-polymers) were included, CHI stands for Chitosan, βG stands for β-glucan, "Ref" indicate that only the co-polymers (polyethylene oxide and hydroxypropyl methylcellulose) were included. CAM stands for chloramphenicol.*

Absorption capacity of nanofibers (%)				
	All-Nanofiber	**CHI-Ref-Nanofiber**	**βG-Ref-Nanofiber**	**Ref-Nanofiber**
Without CAM	842 ± 13	862 ± 46	***	***
With CAM	1055 ± 318	779 ± 242	***	***

An article investigated CHI/PEO-nanofibers with metronidazole that were immersed in 500 mL phosphate buffer in the dissolution apparatus for 1 hour. Here, the reported absorption capacity of the fibers were almost 1000 %. The same article exposed CHI/PEO-nanofiber with metronidazole into Franz diffusion for 5 minutes. It was then reported an absorption capacity of 870 % (Špela Zupančič et al., 2016). Other articles reported absorption capacity for CHI containing nanofiber between 350-1000 % depending on the fiber composition (Çay et al., 2014; Li et al., 2011; Sencadas et al., 2012). Similar level of absorption capacity was reported in our study, 842 ± 13 %, 1055 ± 318 %, 862 ± 46 % and 779 ± 242 % for All-Nanofiber, All-CAM-Nanofiber, CHI-Ref-Nanofiber and CHI-Ref-CAM-Nanofiber, respectively. Several studies reported more than 1000 % of absorption capacity for CHI containing nanofibers (Archana et al., 2013; Stie et al., 2020).

An article with βG-nanofiber composed of the same copolymers as the nanofibers fabricated in this study, reported an absorption capacity of 1287 ± 109 % for βG/HPMC/PEO- nanofiber and 1537 ± 141 % for HPMC/PEO-nanofiber, respectively (Grip et al., 2018). Table 6 does not report the absorption capacity for βG-Ref-Nanofiber and Ref-Nanofiber both without and with CAM. This is because while examining these nanofibers in SWF for 5 minutes, these fibers were totally liquefied, and it was therefore impossible to take them out, and to measure the absorption capacity of these fibers. This might indicate that these polymers are easily soluble in water, resulting in the formation of hydrogel right after immersing them in SWF. Moreover, CHI in nanofibers increases the stability of the fiber in SWF since it was possible to measure the absorption capacity. This might be due to CHI that has good swelling abilities and intra- and intermolecular interactions with molecules in SWF (Stie et al., 2020). Due to the concern with βG-nanofiber, Grip et al allowed nanofibers to absorb in the SWF for only 60 seconds (Grip et al., 2018). In our study, the absorption capacity of nanofibers without CHI would have given us more beneficial information; their ability to absorb exudate from the wound bed and whether there is a difference among the different nanofibers.

No previous study included all the same polymers and the exact same method utilized in our study. Therefore, referred articles cannot be directly compared with our results due to differences in nanofiber compositions and used methods. Differences observed in other studies are choice of absorption time, SWF and process of removal of excess fluid from the nanofiber sample, all these parameters could influence measured absorption capacity.

Nanofibers in our study displayed a high degree of absorption capacity in contact with SWF. The high degree of absorption capacity is suggested for treatment of wounds with moderate to high exudate production.

4.3.2 Tensile properties

Mechanical properties of electrospun nanofiber mats should be examined in accordance with the intended application. The fabricated nanofibers should have the ability to withstand the external forces by growing tissue. In addition, fabricated nanofibers should cope with the handling and replacement of the dressing. Hence, nanofibers should exhibit appropriate mechanical properties (Alishahi et al., 2020). Tensile strength and elongation at break are examples of measurable mechanical properties. These mechanical properties of nanofiber mats should enable degradation of the fibers in the wound when the new ECM begin regenerating. To high tensile strength could possibly enable the fibers to last in the wound bed after regeneration and result to hindering tissue development. Contrariwise, nanofibers with low tensile strength might not promote the regenerative process for the recommended time (Chandrasekaran et al., 2011).

The tensile testing was carried out to determine the mechanical properties of the formed nanofibers. Tensile properties such as tensile strength and elongation at break were evaluated from the stress-strain curve, the results are shown in Figure 18 and 19, respectively.

Tensile strength expresses the amount of stress that a material can hold up to before experiencing permanent deformations. The tensile strength is plotted as a function of nanofibers without and with CAM in Figure 18.

Figure 18: Tensile strength of our nanofibers without and with chloramphenicol (CAM) (n=3). *"All" indicate that all the polymers (CHI, βG and co-polymers) were included, CHI stands for Chitosan, βG stands for β-glucan, "Ref" indicate that only the co-polymers (polyethylene oxide and hydroxypropyl methylcellulose) were included.*

Tensile strength was different for the different nanofibers, however this observed difference was not statistically significant ($p > 0.05$). The observed difference among all nanofibers can be explained due to the large SD within the measurements. It is well known that CHI naturally is rigid and brittle, this is due to the strong intra- and intermolecular hydrogen bonds in the backbone of it. PEO exhibits flexible chains due to its linear structure and absence of bulky side groups. Higher concentration of PEO with decreased content of CHI can decrease the tensile strength of nanofiber (Wahba, 2020). An article, reported for CHI/PEO nanofiber that the tensile strength decreased with increasing PEO, from 1.1 ± 0.5 to 0.9 ± 0.4 MPa, with a PEO/CHI ratio of 1:1 and 2:1, respectively (Yuan et al., 2016). The tensile strength values for CHI containing nanofibers are higher in our study compared to Yuan et al. This might be because the test was performed differently, in the article the specimen was cut into 40 mm x 25 mm and the speed was set at a rate of 1 mm min^{-1} (Yuan et al., 2016). The heightened tensile strength in our study might be due to the presence of HPMC in the nanofibers. As mentioned earlier, only few articles are found to utilize HPMC for fabrication of nanofibers and these articles have not examined for the tensile properties of the produced nanofibers (Aydogdu et al., 2018; Frenot et al., 2007; Grip et al., 2018). Meanwhile, several have presented high tensile strength for production of films with HPMC (Pooponpun et al., 2015; Saringat et al., 2005).

Differences in tensile strength among nanofibers without and with CAM is not significant ($p > 0.05$). An article reported decrease in tensile strength for nanofiber with PEO/gelatin-poly (vinyl alcohol)/CHI incorporated with glucantime drug. In addition, the article utilized different drug concentrations and observed decrease in tensile strength with increasing concentration (Alishahi et al., 2020). This was not observed in our study since the concentration of CAM was kept constant for all nanofibers. In comparison, an article reported slightly increased tensile strength for nanofibers incorporated with 4 % (w/w) of CAM (Lanno et al., 2020). Another article is in accordance with this observation, the antibacterial drug linezolid incorporated into polycaprolactone nanofibers reported improved mechanical properties (Tammaro et al., 2015).

This results and previous reported observations might indicate that drug encapsulation can either increase or decrease the tensile strength of nanofibers. It is important to take into consideration that these articles used different solvent, polymers, and antibiotic, in addition the content of these varied. The drug-polymer interactions affect the mechanical properties of electrospun nanofibers, and solvent utilized might influence this interaction (Chou & Woodrow, 2017).

The materials used in nanofibers should possess good mechanical properties such as tensile strength, this is required for handling and replacement of the wound dressing. The skin has a tensile strength of 20 MPa (Chen et al., 2017). The tensile strength in our study was in the range of 17-23 MPa and 9-21 MPa for nanofibers without CAM and with CAM, respectively. This indicate that produced nanofibers have good strength.

Elongation at break is the ratio between changed length and original length after breakage of the test specimen. This tensile property described the ability of the nanofibers to withstand changes in shape without breaking (Wahba, 2020). Figure 19 shows the elongation at break of the different nanofibers. The elongation at break for different nanofibers without and with CAM show no significant differences ($p > 0.05$).

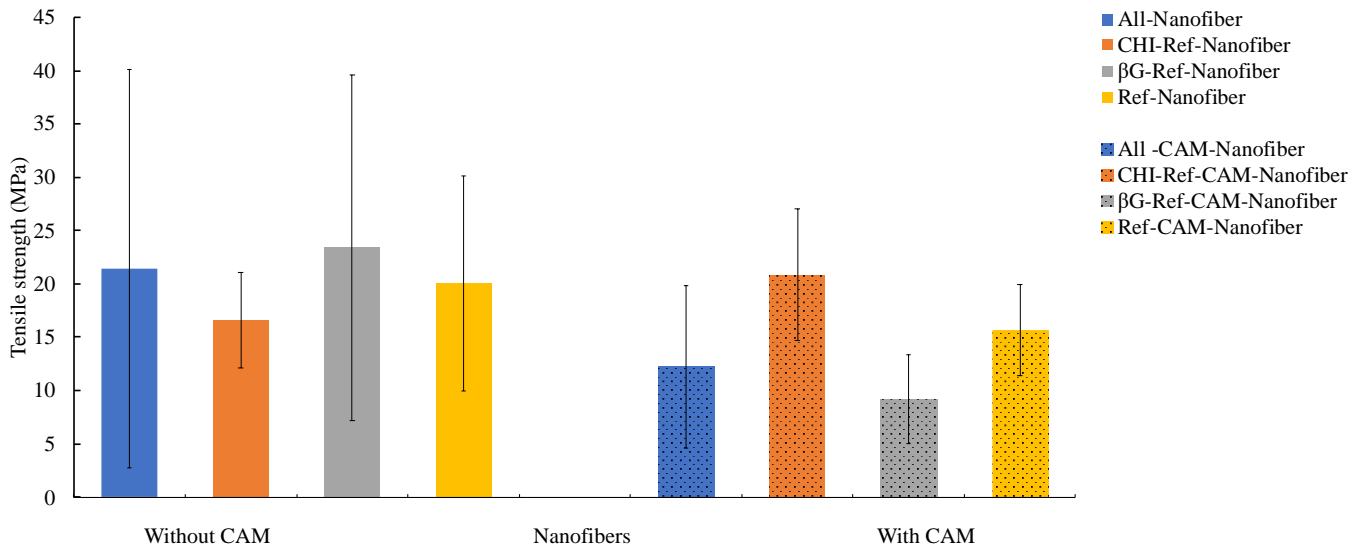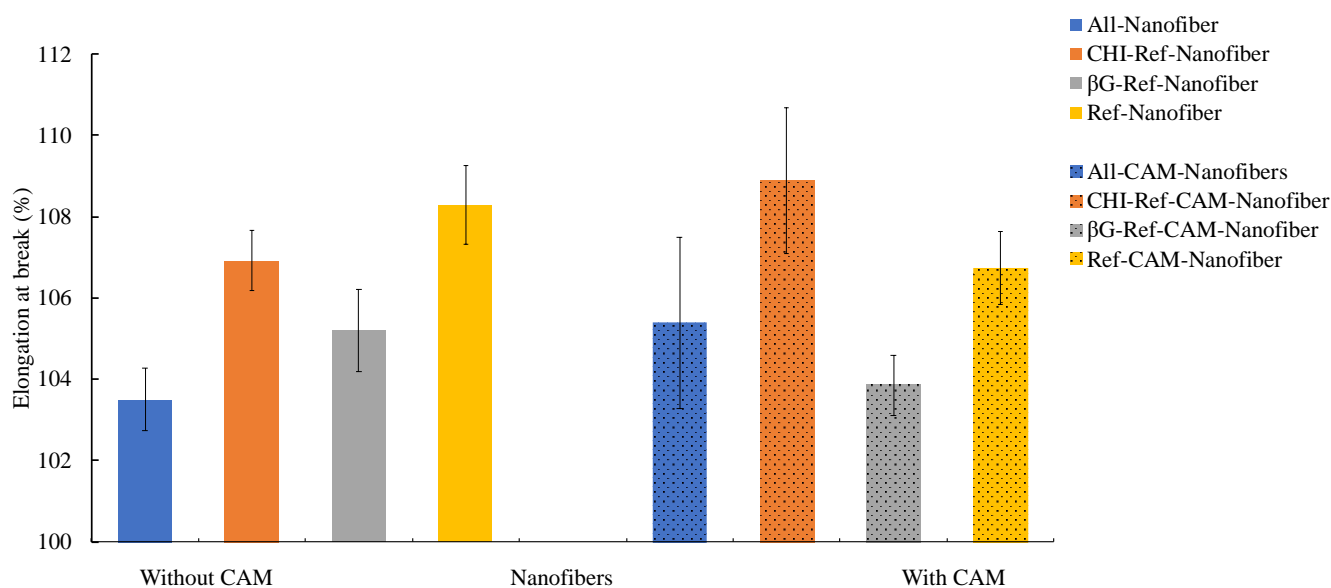**Figure 19:** Elongation at break (%) of our nanofibers without and with chloramphenicol (CAM) (n=3). *"All" indicate that all the polymers (CHI, βG and co-polymers) were included, CHI stands for Chitosan, βG stands for β-glucan, "Ref" indicate that only the co-polymers (polyethylene oxide and hydroxypropyl methylcellulose) were included.*

Nanofibers should be strong enough to keep their structure when applied on the wounded area and be easily removable without damaging the newly forms tissue. The native skin has elongation at break values in the range 35-115 % (Chen et al., 2017). In our study, elongation at break was set to start from 100 %, which refers to "0 %". The elongation at break was in the range of 4-8 % and 4-9 % for nanofibers without and with CAM, respectively. This indicates poor elasticity, thus it can be hard to handle and replace from the wound.

4.3.3 Diameter and morphology of nanofibers

Nanofibers are defined as solid fibers with a diameter in the nanometer range, and theoretically unlimited length. Within this size range can electrospun nanofibers mimic the fibrillar elements of a natural ECM. Therefore, nanofiber contributes both biological and physical support for cell attachment, proliferation, migration, and differentiation (Pelipenko, Kocbek, et al., 2013). Thus, accelerate wound healing.

The surface morphology, diameter, and topography of our nanofibers were investigated using a high-resolution FE-SEM (Carl Zeiss, Oberkochen, Germany). Average diameters of nanofibers were measured utilizing ImageJ (NIH, MD, USA), and the result are presented in Table 7. Histogram of diameter distribution of each nanofiber formulation are presented in Figure A 1-A 8 in Appendix. The result presented in the table is for batch 1 and batch 2, it was not possible to examine the morphology and diameter for batch 3 due to a damaged instrument.

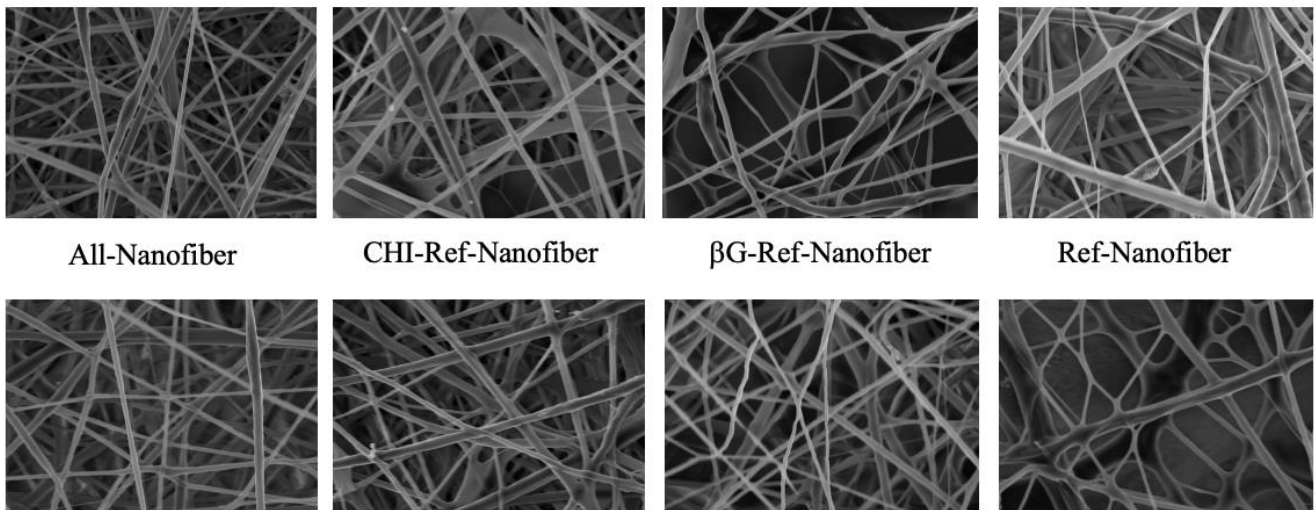**Table 7:** The mean diameter (nm) of nanofibers presented with SD (n=2). *"All" indicate that all the polymers (CHI, βG and co-polymers) were included, CHI stands for Chitosan, βG stands for β-glucan, "Ref" indicate that only the co-polymers (polyethylene oxide and hydroxypropyl methylcellulose) were included. CAM stands for chloramphenicol.*

Diameter (nm)				
	All-Nanofiber	**CHI-Ref-Nanofiber**	**βG-Ref-Nanofiber**	**Ref-Nanofiber**
Without CAM	129.5 ± 54.8	174.5 ± 81.9	136.1 ± 61.9	200.9 ± 110.0
With CAM	158.9 ± 58.2	158.2 ± 59.7	151.1 ± 59.3	161.6 ± 82.1

Both nanofiber mats without CAM and with CAM had a uniform structure and white color in appearance (Table A 3 and Table A 4 in Appendix). The FE-SEM images show that uniform nanofibers were obtained (Figure 20). The average diameter for different nanofiber formulations ranged from 129.5 to 200.9 nm and SD for some of the formulations, especially CHI-Ref-Nanofiber, Ref-Nanofiber and Ref-CAM-Nanofiber were large. However, there was no significant differences in diameter between electrospun nanofibers without and with CAM ($p > 0.05$). For example, the average diameter of All nanofibers was 129.54 ± 54.76 nm and of All-CAM nanofibers was 158.87 ± 58.23 nm. This indicates that addition of CAM into polymer solution does not have that noticeable effect on nanofiber morphology ($p > 0.05$).

Figure 20: FE-SEM images of all the different nanofibers (n=2). *"All" indicate that all the polymers (CHI, βG and co-polymers) were included, CHI stands for Chitosan, βG stands for β-glucan, "Ref" indicate that only the co-polymers (polyethylene oxide and hydroxypropyl methylcellulose) were included. CAM stands for chloramphenicol.*

However, it is well known that addition of a drug into polymer solution may affect viscosity, surface tension or other solution parameters, which can affect the ES process and resulting morphology of the fibers. In our study, CHI containing polymer solutions had increased conductivity, pH and viscosity (Figure 14-15, 17), these properties seem not to affect the nanofiber diameter. CAM and βG containing polymer solutions with their properties was not observed to influence the fiber diameter. RH for batch 1 All-CAM-Nanofiber, CHI-Ref-CAM-Nanofiber and βG-Ref-CAM-Nanofiber was outside the predetermined range of 28 ± 3 % (Table 5). However, the RH of these fibers did not show decreased diameter nor thinner fibers, as would actually be expected at high RH. Several studies have reported no differences in average diameter of electrospun nanofibers without and with CAM but these studies have not investigated the influence of the drug agent in the polymer solutions (Preem et al., 2017; Tamm et al., 2016). These studies fabricated nanofibers with different polymer compositions, therefore results are difficult to compare directly. One article reported an average diameter of 496 ± 306 nm and 496 ± 339 nm for polycaprolactone and polycaprolactone/CAM nanofibers (Preem et al., 2017). Another article has also commented that there were no differences found in the average diameters of nanofibers containing CAM compared with pure nanofibers (without CAM) (Tamm et al., 2016).

The diameter of the electrospun nanofibers was 136.1 ± 61.9 nm and 200.9 ± 110.0 nm for nanofibers βG-Ref-Nanofiber and Ref-Nanofiber. Similar level of average diameter was observed in a an article with βG-nanofiber composed of the same copolymers as the nanofibers fabricated in this study reported 110 ± 74 nm and 180 ± 95 nm for nanofibers βG-Ref and Ref (Grip et al., 2018).

4.3.4 Chloramphenicol content

Throughout ES process, CAM is exposed to a short-term physical stress including high voltage, electrostatic repulsion forces, and high evaporation rate of solvents. This can result to the loss of active ingredients in the electrospun nanofiber mats (Bertoncelj et al., 2014). Therefore, it is important to investigate the amount of CAM present in fabricated nanofiber mats after the formation. CAM-content of drug loading within electrospun nanofibers were determined using Spark® Microplate readers (Tecan Trading AG, Switzerland). UV-absorbance was read from the SparkControl™ software and used to further calculate the percentage concentration of CAM in the nanofiber (Eq. 2, Page 41).

The actual CAM-content in nanofibers is presented in Table 8. The CAM-content of all fabricated nanofibers was observed to be similar to the added amount of CAM, which was 1 % of the polymer material. This indicate that CAM is stable in all nanofibers and tolerates the ES process good. These values were used further to calculate the amount of drug released under the test *in vitro* CAM release.

Table 8: Chloramphenicol (CAM) content (% of the polymer material in all nanofibers). Theoretical CAM-content was 1 % of the polymer material. *"All" indicate that all the polymers (CHI, βG and co-polymers) were included, CHI stands for Chitosan, βG stands for β-glucan, "Ref" indicate that only the co-polymers (polyethylene oxide and hydroxypropyl methylcellulose) were included.*

Nanofibers	CAM-content (%)
All-CAM-Nanofiber	1.07 ± 0.04
CHI-Ref-CAM-Nanofiber	0.92 ± 0.05
βG-Ref-CAM-Nanofiber	1 ± 0.02
Ref-CAM-Nanofiber	0.91 ± 0.06

Also Tamm et al reported no significant loss of CAM in the final electrospun fibers (Tamm et al., 2016). Here, a CAM-loss of between 9 and 13 % was observed during ES (Tamm et al., 2016). In our study, the quantified amount of CAM in the nanofibers indicate close to 100 % recovery, and no significant degradation, taking the limitation of the analytical method into account.

4.3.5 *In vitro* release of chloramphenicol

The antibacterial activity of a drug has a direct connection to its drug release behavior. The release kinetics of a drug from electrospun nanofiber mats is therefore important to evaluate. This includes simulation of the application site to assess the potential *in vivo* performance. In this study, the *in vitro* release test of CAM from electrospun nanofiber mats were conducted utilizing the release method, Franz diffusion cell due to the low fluid volume available at local infection site, that resembles the *in vivo* conditions (Brown et al., 2011).

The cumulative CAM release profiles of nanofibers in PBS as a function of time (hours) are shown in Figure 21. There was only a minor difference between the fiber mats. In PBS at pH 7.4 and 32 °C, a burst release of CAM nanofibers occurred in the first 2 hours, followed by a release of remaining CAM from the nanofibers for 4 hours. Burst release may be attributed to some drug molecules on the outer surface of the nanofibers and can also be explained due to the small diameter and high surface area of nanofibers. The drug molecules can therefore have rapid desorption and a short diffusion pathway from the nanopores (Amiri et al., 2020). The observed burst release of CAM could also be due to the hydrophilic polymers used in this project. The initial burst release of CAM at the wound site is crucial for the acute phase of injuries, to eliminate primary bacteria (Amiri et al., 2020). After approximately 2 hours, the release rate slowed down for all the fibers. At this stage 58.08 to 86.67 % of the drug is released from the fibers, thus there is less drug left available for release from the fiber. The slow drug release after burst release is explained by drug diffusion that occurs from the core of the nanofiber scaffolds. A significant burst release was reported up to 15 minutes of release testing for nanofibers containing polycaprolactone/PEO/CAM and polycaprolactone/CAM (Preem et al., 2019). It is important to mention that this article used a dissolution apparatus, 20 mL PBS and that the test was conducted at 37 °C. Another article with the same composition and method as the last referred one, reported a burst release whereas 92 % and 95 % of CAM was released from polycaprolactone/PEO/CAM nanofiber after 15 minutes and 1 hour (Preem et al., 2017).
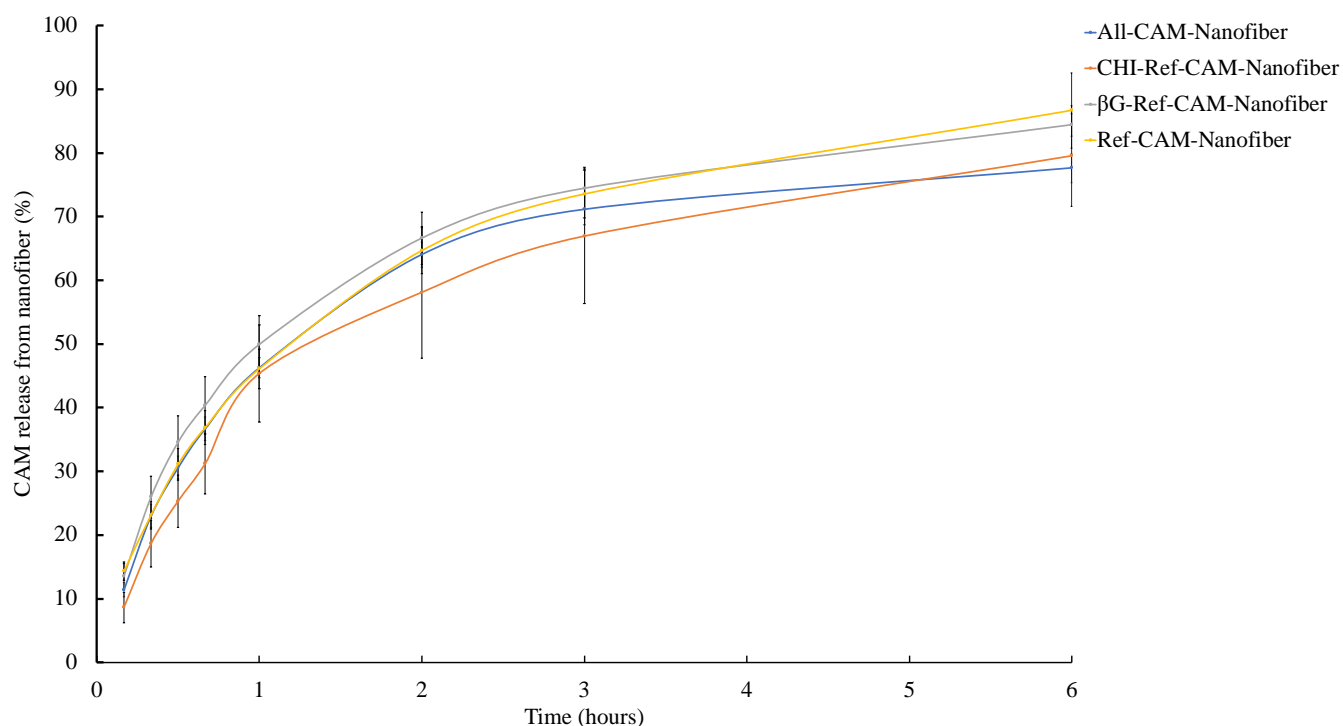
Figure 21: Relative cumulative release of chloramphenicol (CAM) (%) from nanofiber mats. (n=2). *"All" indicate that all the polymers (CHI, βG and co-polymers) were included, CHI stands for Chitosan, βG stands for β-glucan, "Ref" indicate that only the co-polymers (polyethylene oxide and hydroxypropyl methylcellulose) were included.*

The release of CAM after 6 hours was 77.63 %, 79.52 %, 84.42 % and 86.67 % for All-CAM-Nanofiber, CHI-Ref-CAM-Nanofiber, βG-Ref-CAM-Nanofiber and Ref-CAM-Nanofiber, respectively. The remaining content of CAM from the nanofibers was further investigated shortly after Franz diffusion and the total recovery amount of CAM is shown in Figure 22. This figure includes the amount released from Franz diffusion cell referred as "release", remained CAM in the nanofibers referred as "rest" and content on cellulose membrane referred as "membrane". It can be seen from these results (Figure 22) that CHI-Ref-CAM-Nanofiber, βG-Ref-CAM-Nanofiber and Ref-CAM-Nanofiber had recovery over 90 % and absence of 5.61± 7.19 %, 2.39 ± 1.57 % and 0.64 ± 10.18 % of CAM. This indicate that nearly full amount of the drug can be tracked in the nanofibers, except All-CAM-Nanofiber. The release and amount retained in both membrane and fibers were calculated, using the measured CAM-content as reference value. All-CAM-Nanofiber had a low recovery rate. The measured CAM-content of these fibers was above the theoretical content and might therefor have lead to the calculation of a lower recovery rate.
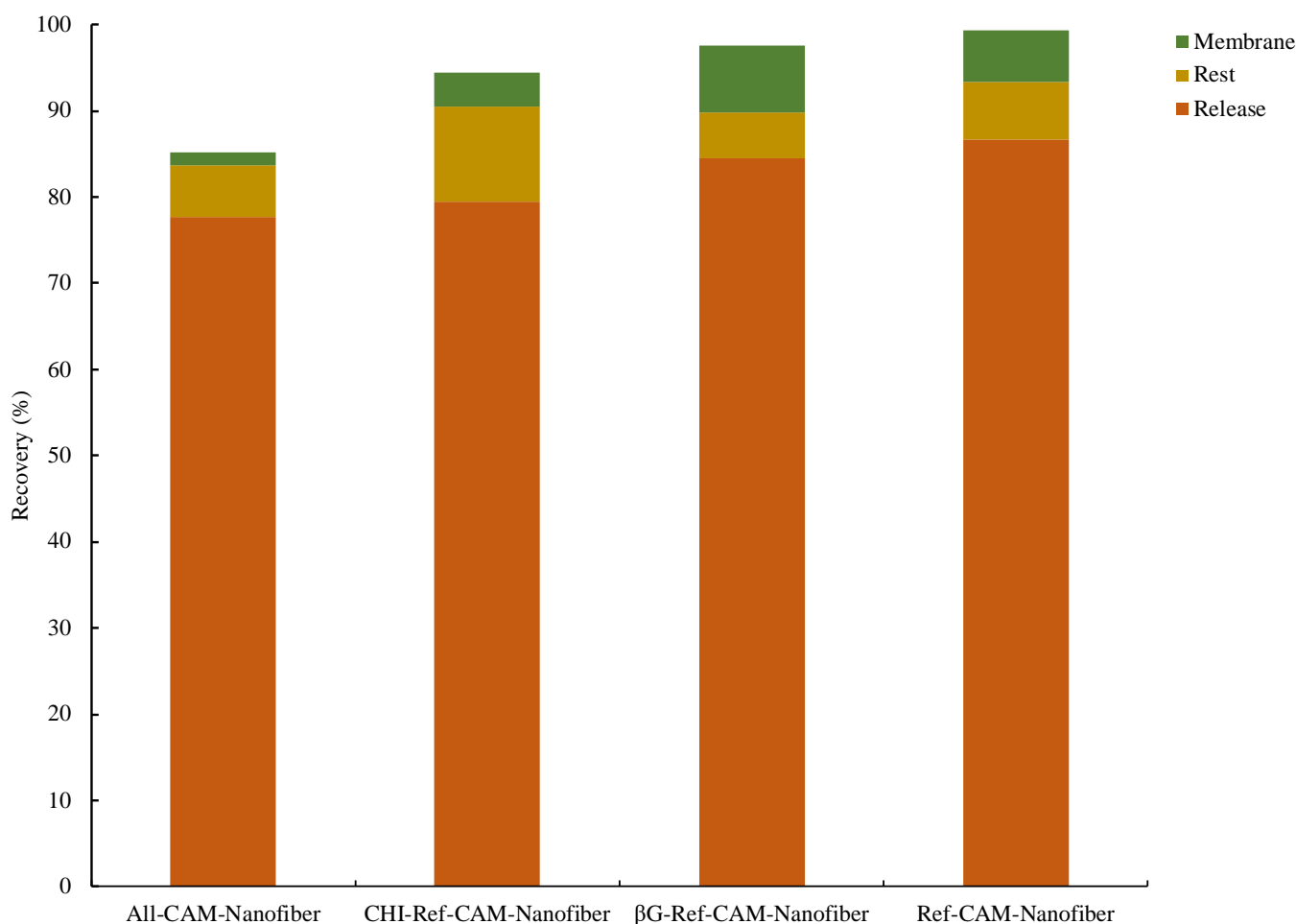
Figure 22: Recovery of chloramphenicol (CAM) during the release testing, showing CAM content in cellulose membrane (Membrane), in the remaining nanofibers (Rest) and the released amount found in the acceptor compartment of the Franz diffusion cells after the 6 hours test period (Release) (n=2). *"All" indicate that all the polymers (CHI, βG and co-polymers) were included, CHI stands for Chitosan, βG stands for β-glucan, "Ref" indicate that only the co-polymers (polyethylene oxide and hydroxypropyl methylcellulose) were included.*

The All-CAM-Nanofiber had a recovery of 85.16 % and 14.84 ± 2.23 % of CAM is in absence. The report is not in accordance with the CAM content examination, where the total dry CAM-content of 1.07 % in the fibers was reported. In comparison with the other nanofibers, content of CAM was only found 1.46 ± 1.34 % in the cellulose membrane and 6.07 ± 3.00 % remained in nanofiber. Earlier it was reported that CAM might be stable during the ES process. However, it was discussed that visualization of CAM distribution would have been advantageous. The absence of 14.84 ± 2.23 % of CAM might be due to not uniform CAM distribution within All-CAM-Nanofiber or an error in the measurement.

The incorporation of drug into nanofibers to sustain its release over one week or minimal burst effect is often most desirable (Chou et al., 2015). Sustained release of an antibiotic in the wound bed for a sufficient duration can prevent infectious diseases, complicated postoperative infectious and tissue damages (Arbade et al., 2018). In our study, initially high burst release was observed for CAM and nearly all the CAM content was released after 6 hours. Therefore, the use of hydrophobic polymers would have been imperative to prolong and retard the rate of drug release (Š Zupančič et al., 2016).

4.3.6   *In vitro* cell toxicity

Nanofiber as wound dressings should possess great biomedical properties, among them cytocompatibility and non-toxicity (Yang et al., 2019). The cell viability of nanofibers without and with CAM was examined *in vitro* using CCK-8 assay method on HaCaT cells. Metabolically active cells interact with tetrazolium salt in CCK-8 and produce a soluble formazan dye.

A pre-cell viability test was done, whereas four different fiber concentrations of 0.5, 1.25, 2.5 and 10 mg/mL for all nanofibers were investigated and CAM in an aqueous solution was applied on HaCaT cells as a reference (Figure A 9, Appendix). In control samples, the cells were seeded with medium only (negative control), and the viability of these cells was regarded as 100 % viable. The viability of HaCaT cells cultured with nanofiber solutions without and with CAM, and CAM solutions were over 90 %. This indicated no toxicity up to concentration of 10 mg/mL. Therefore, this concentration was used further in cell viability test.

The result of cell viability of cells exposed for dissolved nanofibers is shown in Figure 23. Nanofibers without and with CAM displayed almost similar viability in comparison with HaCaT cells in medium. All the HaCaT cells exposed for the nanofibers in this cell viability study showed over 100 % viability. For some of them, the SD is large, for example CHI-Ref-Nanofiber. No statistically significant ($p > 0.05$) differences could however be seen among the cells treated with nanofibers with different compositions, or between nanofiber without and with CAM. Similar results were reported by Grip et al; nanofibers with βG/HPMC/PEO and HPMC/PEO did not show toxicity up to a fiber concentration of 100 µg/mL (Grip et al., 2018). This indicates that nanofibers both without and with CAM had an excellent cytocompatibility and that the presence of CAM in nanofibers are nontoxic.
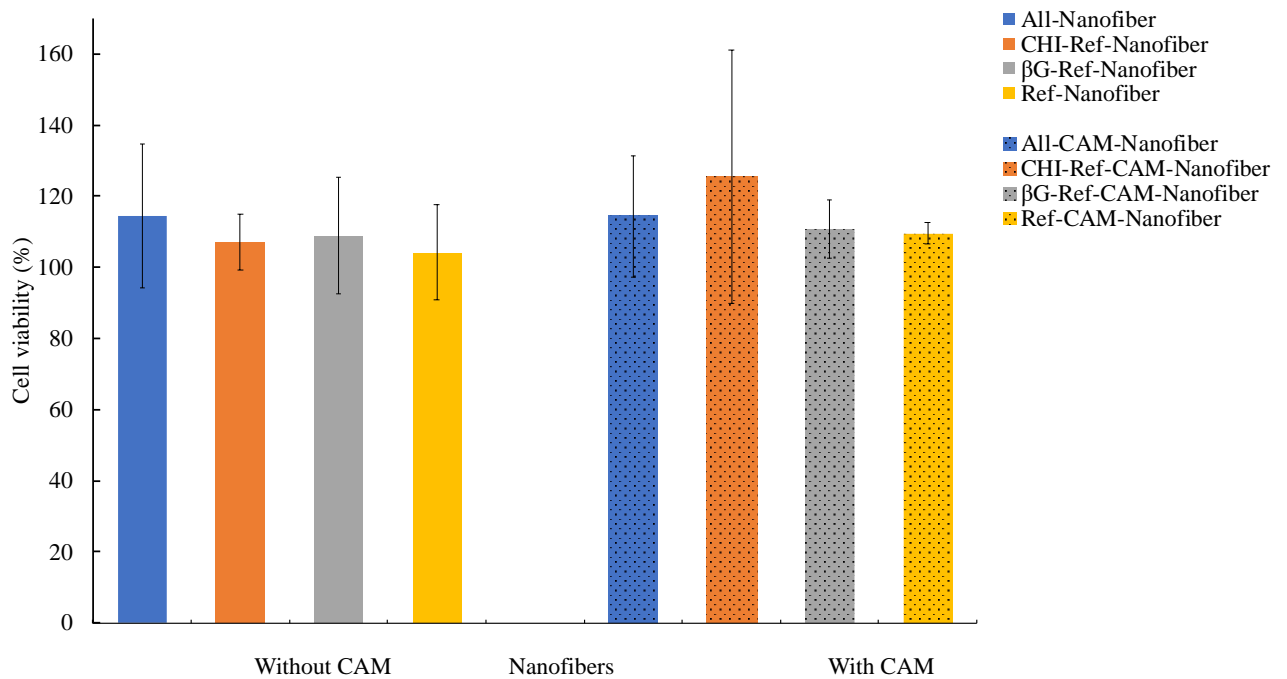
Figure 23: Human immortalized keratinocytes (HaCaT) viability (%) evaluated utilizing CCK-8 assay for 10 mg/mL nanofibers without and with chloramphenicol (CAM) (n=3). *"All" indicate that all the polymers (CHI, βG and co-polymers) were included, CHI stands for Chitosan, βG stands for β-glucan, "Ref" indicate that only the co-polymers (polyethylene oxide and hydroxypropyl methylcellulose) were included.*

An article investigated cell viability of Human Dermal Fibroblasts for CHI/PEO-nanofiber loaded with teicoplanin. This article used Alamar Blue to dye each well otherwise the same method to examine the toxicity and cytocompatibility was utilized as described in this project. The article reported that the cell viability was alike for CHI/PEO-nanofibers loaded with teicoplanin compared to nanofibers without (Amiri et al., 2020). Another study used ciprofloxacin as antibiotic for potential wound dressing application and reported that the cell viability was over 120 % for drug loaded nanofiber and without drug (Yang et al., 2019). Similar observation was also seen in our study (Figure 23). However, the article utilized another form for antibiotic compared to our study.

It was observed that cell viability was higher for CAM incorporated in nanofibers compared to CAM in water. For example, the cell viability was 114 ± 17 % and 104 ± 37 % for 10 mg/ml All-CAM-Nanofiber and CAM solution, respectively (Figure A 9, Appendix). This might indicate that the encapsulation of CAM in nanofibers reduce drug toxicity by controlling the release of CAM from nanofibers. The same observation was reported by Amiri et al (Amiri et al., 2020).

All nanofibers exhibited cell viability over 100 %, indicating that nanofiber with CAM did not affect the viability of HaCaT cells. These results specify that nanofibers with CAM were relatively nontoxic and showed excellent cytocompatibility.

5 Conclusion

In the present study, nanofibers with different compositions, including the active ingredients chitosan (CHI), β-glucan (βG) and chloramphenicol (CAM), and the selected co-polymers polyethylene oxide (PEO) and hydroxypropyl methylcellulose (HPMC), were successfully fabricated by needle-free electrospinning (Nanospider^{TM}). CAM and βG did not change the solution properties, whereas CHI-containing polymer solutions had increased conductivity, pH, and viscosity, which supposable were attributed to the polycationic nature of CHI. No effect on the electrospinning spinnability was observed from adding any of the active ingredients to the polymer solutions. The temperature and relative humidity were successfully controlled, and all nanofibers were spun at the same ambient conditions, assuring the same known ambient influences on the nanofibers morphology and diameter.

All obtained nanofibers were uniform. The nanofiber diameter was in the range from 129.5 to 200.9 nm, for all fabricated nanofibers. Nanofibers containing CHI retained their structure in simulated wound fluid (SWF) and could be examined for absorption capacity. These fibers had up to 1055 % absorption capacity, thus suggested for treatment of wounds with moderate to high exudate. The absorption capacity could not be examined for nanofibers without CHI, as these nanofibers dissolved rapidly in SWF. The tensile strength of all nanofibers was found to be in the same range as native skin, and was judged good. Moreover, all nanofibers did have a poor elongation at break and exhibited poor elasticity compared to the native skin. CHI and βG nanofibers did not influence the *in vitro* CAM release, as all nanofibers showed an initial burst release. The high recovery of CAM from the release test, from 85 to 99 %, indicates that CAM is stable within all nanofibers, and tolerate the electrospinning process well. All nanofibers had an excellent cytocompatibility on human immortalized keratinocytes (HaCaT) cell lines, as no cytotoxicity could be seem.

The results in this project are promising and can provide as a strong base for further utilization of the nanofibers in wound healing.

6 Perspectives

Firstly, tensile properties of fabricated nanofibers should be enhanced since all nanofibers exhibited poor elongation at break. This would give more information of their mechanical properties in a dry state at the wound bed. To enhance tensile properties of all nanofibers crosslinking can be utilized. The improved nanofibers can be further investigated for absorption capacity.

Furthermore, visualization of CAM distribution within produced nanofibers should be interesting, since it can give more information on how the drug is distributed. This can be evaluated using for example Raman scattering microspectroscopy.

A further optimization of nanofibers with CAM to obtain sustain release and minimal burst release can be desirable to prevent infectious diseases. This might be achieved by utilizing hydrophobic polymers.

Nanofibers with CAM should further be evaluated for antimicrobial efficiency, testing them *in vitro* against bacteria strains frequently found in wounds. In addition, the inflammatory potential of produced nanofibers would be interesting to evaluate.

Moreover, *in vivo* studies should be done to investigate the effect and safety of produced nanofibers in appropriate animal model and finally also in humans.

7 References

Ahmed, S., & Ikram, S. (2016). Chitosan based scaffolds and their applications in wound healing. *Achiev. Life. Sci., 10*, 27-37.

Albanna, M., & IV, J. H. H. (2016a). Chapter 1 - Anatomy, physiology, histology, and immunohistochemistry of human skin. In J. Fenner & R. A. F. Clark (Eds.), *Skin tissue engineering and regenerative medicine* (1st ed., pp. 1-17). Elsevier Science & Technology.

Albanna, M., & IV, J. H. H. (2016b). Chapter 12 - Wound healing: a comprehensive wound assessment and reatment approach. In W. J. Ennis & D. Hill (Eds.), *Skin tissue engineering and regenerative medicine* (1st ed., pp. 239-263). Elsevier Science & Technology.

Ali, A., & Ahmed, S. (2018). A review on chitosan and its nanocomposites in drug delivery. *Int. J. Biol. Macromol., 109*, 273-286.

Alishahi, M., Khorram, M., Asgari, Q., Davani, F., Goudarzi, F., Emami, A., Arastehfar, A., & Zomorodian, K. (2020). Glucantime-loaded electrospun core-shell nanofibers composed of poly(ethylene oxide)/gelatin-poly(vinyl alcohol)/chitosan as dressing for cutaneous leishmaniasis. *Int. J. Biol. Macromol., 163*, 288-297.

Ambekar, R. S., & Kandasubramanian, B. (2019). Advancements in nanofibers for wound dressing: a review. *Eur. Polym. J., 117*, 304-336.

Amiri, N., Ajami, S., Shahroodi, A., Jannatabadi, N., Amiri Darban, S., Fazly Bazzaz, B. S., Pishavar, E., Kalalinia, F., & Movaffagh, J. (2020). Teicoplanin-loaded chitosan-PEO nanofibers for local antibiotic delivery and wound healing. *Int. J. Biol. Macromol., 162*, 645-656.

Arbade, G. K., Jathar, S., Tripathi, V., & Patro, T. U. (2018). Antibacterial, sustained drug release and biocompatibility studies of electrospun poly(caprolactone)/chloramphenicol blend nanofiber scaffolds. *Biomed. Phys. Eng. Express., 4*, 1-15.

Archana, D., Dutta, J., & Dutta, P. K. (2013). Evaluation of chitosan nano dressing for wound healing: characterization, in vitro and in vivo studies. *Int. J. Biol. Macromol., 57*, 193- 203.

Ashcroft, G. S., Greenwell-Wild, T., Horan, M. A., Wahl, S. M., & Ferguson, M. W. (1999). Topical estrogen accelerates cutaneous wound healing in aged humans associated with an altered inflammatory response. *Am. J. Pathol., 155*, 1137-1146.

Ashcroft, G. S., Mills, S. J., & Ashworth, J. J. (2002). Ageing and wound healing. *Biogerontology., 3*, 337-345.

ASTM-International. (2018). *Standard test method for tensile properties of thin plastic sheeting*. https://www.astm.org

Aurélie, O., Nabyl, K., Laurence, S., Dominique C, A., & Hélène, G. (2018). Optimization of meta-aramid electrospun nanofibers productivity through wire-based electrospinning setup scale up. *J. Ind. Text., 48*, 236-254.

Aydogdu, A., Sumnu, G., & Sahin, S. (2018). A novel electrospun hydroxypropyl methylcellulose/polyethylene oxide blend nanofibers: morphology and physicochemical properties. *Carbohydr. Polym., 181*, 234-246.

Balogh, A., Farkas, B., Verreck, G., Mensch, J., Borbás, E., Nagy, B., Marosi, G., & Nagy, Z. K. (2016). AC and DC electrospinning of hydroxypropylmethylcellulose with polyethylene oxides as secondary polymer for improved drug dissolution. *Int. J. Pharm., 505*, 159-166.

Bashir, K. M. I., & Choi, J. S. (2017). Clinical and physiological perspectives of β-Glucans: the past, present, and future. *Int. J. Mol. Sci., 18*, 1-48.

Baum, C. L., & Arpey, C. J. (2005). Normal cutaneous wound healing: clinical correlation with cellular and molecular events. *Dermatol. Surg., 31*, 674-686.

Bertoncelj, V., Pelipenko, J., Kristl, J., Jeras, M., Cukjati, M., & Kocbek, P. (2014). Development and bioevaluation of nanofibers with blood-derived growth factors for dermal wound healing. *Eur. J. Pharm. Biopharm., 88*, 64-74.

Bhardwaj, N., & Kundu, S. C. (2010). Electrospinning: a fascinating fiber fabrication technique. *Biotechnol. Adv., 28*, 325-347.

Bhattacharya, D., Ghosh, B., & Mukhopadhyay, M. (2019). Development of nanotechnology for advancement and application in wound healing: a review. *IET. Nanobiotechnol., 13*, 778-785.

Bhattarai, N., Edmondson, D., Veiseh, O., Matsen, F. A., & Zhang, M. (2005). Electrospun chitosan-based nanofibers and their cellular compatibility. *Biomaterials., 26*, 6176- 6184.

Bhattarai, R. S., Bachu, R. D., Boddu, S. H. S., & Bhaduri, S. (2019). Biomedical applications of electrospun nanofibers: drug and nanoparticle delivery. *Pharmaceutics., 11*, 1-30.

Boateng, J., & Catanzano, O. (2015). Advanced therapeutic dressings for effective wound healing: a Review. *J. Pharm. Sci., 104*, 3653-3680.

Boateng, J. S., Matthews, K. H., Stevens, H. N. E., & Eccleston, G. M. (2008). Wound healing dressings and drug delivery systems: a review. *J. Pharm. Sci., 97*, 2892-2923.

Bradford, C., Freeman, R., & Percival, S. L. (2009). In vitro study of sustained antimicrobial activity of a new silver alginate dressing. *J. Am. Col. Certif. Wound. Spec., 1*, 117- 120.

Brown, C. K., Friedel, H. D., Barker, A. R., Buhse, L. F., Keitel, S., Cecil, T. L., Kraemer, J., Morris, J. M., Reppas, C., Stickelmeyer, M. P., Yomota, C., & Shah, V. P. (2011). FIP/AAPS joint workshop report: dissolution/in vitro release testing of novel/special dosage forms. *AAPS. PharmSciTech., 12*, 782-794.

Buch, P. J., Chai, Y., & Goluch, E. D. (2021). Bacterial chatter in chronic wound infections. *Wound. Repair. Regen., 29*, 106-116.

Çay, A., Miraftab, M., & Perrin Akçakoca Kumbasar, E. (2014). Characterization and swelling performance of physically stabilized electrospun poly(vinyl alcohol)/chitosan nanofibres. *Eur. Polym. J., 61*, 253-262.

Chandrasekaran, A. R., Venugopal, J., Sundarrajan, S., & Ramakrishna, S. (2011). Fabrication of a nanofibrous scaffold with improved bioactivity for culture of human dermal fibroblasts for skin regeneration. *Biomed. Mater., 6*, 1-10.

Chen, S., Liu, B., Carlson, M. A., Gombart, A. F., Reilly, D. A., & Xie, J. (2017). Recent advances in electrospun nanofibers for wound healing. *Nanomedicine., 12*, 1335-1352.

Chitinor. (2020). *Chitosan*. https://chitinor.com/about-chitosan/#chitosan

Chou, S.-F., & Woodrow, K. A. (2017). Relationships between mechanical properties and drug release from electrospun fibers of PCL and PLGA blends. *J. Mech. Behav. Biomed. Mater., 65*, 724-733.

Chou, S. F., Carson, D., & Woodrow, K. A. (2015). Current strategies for sustaining drug release from electrospun nanofibers. *J. Control. Release., 220*, 584-591.

Croitoru, A.-M., Ficai, D., Ficai, A., Mihailescu, N., Andronescu, E., & Turculet, C. F. (2020). Nanostructured fibers containing natural or synthetic bioactive compounds in wound dressing applications. *Materials., 13*, 1-19.

Cutting, K. F. (2017). The cost-effectiveness of a novel soluble beta-glucan gel. *J. Wound. Care., 26*, 228-234.

Dai, C., Shih, S., & Khachemoune, A. (2020). Skin substitutes for acute and chronic wound healing: an updated review. *J. Dermatolog. Treat., 31*, 639-648.

De Vrieze, S., De Vrieze, S., Van Camp, T., Van Camp, T., Nelvig, A., Nelvig, A., Hagström, B., Hagström, B., Westbroek, P., Westbroek, P., De Clerck, K., & De Clerck, K. (2009). The effect of temperature and humidity on electrospinning. *J. Mater. Sci., 44*, 1357- 1362.

Demidova-Rice, T. N., Hamblin, M. R., & Herman, I. M. (2012). Acute and impaired wound healing: pathophysiology and current methods for drug delivery, part 1: normal and chronic wounds: biology, causes, and approaches to care. *Adv. Skin. Wound. Care., 25*, 304-314.

Diegelmann, R. F., & Evans, M. C. (2004). Wound healing: an overview of acute, fibrotic and delayed healing. *Front. Biosci., 9*, 283-289.

Du, B., Bian, Z., & Xu, B. (2014). Skin health promotion effects of natural beta-glucan derived from cereals and microorganisms: a review. *Phytother. Res., 28*, 159-166.

Duan, B., Dong, C., Yuan, X., & Yao, K. (2004). Electrospinning of chitosan solutions in acetic acid with poly(ethylene oxide). *J. Biomater. Sci. Polym. Ed., 15*, 797-811.

Dwivedi, A., Agarwal, N., Ray, L., & Tripathi, A. K. (2019). Chapter 1 - Skin anatomy and morphology In N. Yadav, S. Parveen, S. Chakravarty, & M. Banerjee (Eds.), *Skin aging & cancer: ambient UV-R exposure* (1st ed., pp. 1-10). Springer Singapore: Imprint: Springer.

Eatemadi, A., Daraee, H., Zarghami, N., Melat Yar, H., & Akbarzadeh, A. (2016). Nanofiber: synthesis and biomedical applications. *Artif. Cell. Nanomed. B., 44*, 111-121.

El-Newehy, M. H., Al-Deyab, S. S., Kenawy, E.-R., & Abdel-Megeed, A. (2011). Nanospider technology for the production of nylon-6 nanofibers for biomedical applications. *J. Nanomater., 2011*, 1-8.

Elsabee, M. Z., Naguib, H. F., & Morsi, R. E. (2012). Chitosan based nanofibers. *Mater. Sci. Eng. C., 32*, 1711-1726.

Fras Zemljič, L., Maver, U., Kraševac Glaser, T., Bren, U., Knez Hrnčič, M., Petek, G., & Peršin, Z. (2020). Electrospun composite nanofibrous materials based on (poly)-phenol-polysaccharide formulations for potential wound treatment. *Materials., 13*, 1- 26.

Frenot, A., Henriksson, M. W., & Walkenström, P. (2007). Electrospinning of cellulose-based nanofibers. *J. Appl. Polym. Sci., 103*, 1473-1482.

Frykberg, R. G., & Banks, J. (2015). Challenges in the treatment of chronic wounds. *Adv. Wound. Care., 4*, 560-582.

Grip, J. (2018). *Development of novel wound dressings with soluble beta-glucan (SBG) as an active ingredient* [Ph.D, University of Tromsø].

Grip, J., Engstad, R. E., Skjæveland, I., Škalko-Basnet, N., Isaksson, J., Basnet, P., & Holsæter, A. M. (2018). Beta-glucan-loaded nanofiber dressing improves wound healing in diabetic mice. *Eur. J. Pharm. Sci., 121*, 269-280.

Haider, A., Haider, S., & Kang, I.-K. (2018). A comprehensive review summarizing the effect of electrospinning parameters and potential applications of nanofibers in biomedical and biotechnology. *Arab. J. Chem., 11*, 1165-1188.

Halim, A. S., Emami, A., Salahshourifar, I., & Kannan, T. P. (2012). Keloid scarring: understanding the genetic basis, advances, and prospects. *Arch. Plast. Surg., 39*, 184- 189.

Henderson, G., Flower, R. J., Loke, Y. K., Ritter, J. M., MacEwan, D., & Rang, H. P. (2018). Chapter 52 - Antibacterial drugs In *Rang and Dale's Pharmacology* (9th ed., pp. 661- 677). Elsevier.

Hosseinnejad, M., & Jafari, S. M. (2016). Evaluation of different factors affecting antimicrobial properties of chitosan. *Int. J. Biol. Macromol., 85*, 467-475.

Iacob, A. T., Drăgan, M., Ionescu, O. M., Profire, L., Ficai, A., Andronescu, E., Confederat, L. G., & Lupașcu, D. (2020). An overview of biopolymeric electrospun nanofibers based on polysaccharides for wound healing management. *Pharmaceutics., 12*, 1-49.

Khattab, I. S., Khattab, I. S., Bandarkar, F., Bandarkar, F., Fakhree, M. A. A., Fakhree, M. A. A., Jouyban, A., & Jouyban, A. (2012). Density, viscosity, and surface tension of water+ethanol mixtures from 293 to 323K. *Korean. J. Chem. Eng., 29*, 812-817.

Koosha, M., & Mirzadeh, H. (2015). Electrospinning, mechanical properties, and cell behavior study of chitosan/PVA nanofibers. *J. Biomed. Mater. Res. A., 103*, 3081- 3093.

Kriegel, C., Arecchi, A., Kit, K., McClements, D. J., & Weiss, J. (2008). Fabrication, functionalization, and application of electrospun biopolymer nanofibers. *Crit. Rev. Food. Sci. Nutr., 48*, 775-797.

Lanno, G. M., Ramos, C., Preem, L., Putrinš, M., Laidmäe, I., Tenson, T., & Kogermann, K. (2020). Antibacterial porous electrospun fibers as skin scaffolds for wound healing applications. *ACS. Omega., 5*, 30011-30022.

Lannutti, J., Reneker, D., Ma, T., Tomasko, D., & Farson, D. (2007). Electrospinning for tissue engineering scaffolds. *Mater. Sci. Eng. C., 27*, 504-509.

Leaper, D., Assadian, O., & Edmiston, C. E. (2015). Approach to chronic wound infections. *Br. J. Dermatol., 173*, 351-358.

Legentil, L., Paris, F., Ballet, C., Trouvelot, S., Daire, X., Vetvicka, V., & Ferrières, V. (2015). Molecular interactions of β-(1→3)-glucans with their receptors. *Molecules., 20*, 9745- 9766.

Li, C. L., Martini, L. G., Ford, J. L., & Roberts, M. (2005). The use of hypromellose in oral drug delivery. *J. Pharm. Pharmacol., 57*, 533-546.

Li, L., & Hsieh, Y. L. (2006). Chitosan bicomponent nanofibers and nanoporous fibers. *Carbohydr. Res., 341*, 374-381.

Li, M., Han, B., & Liu, W. (2011). Preparation and properties of a drug release membrane of mitomycin C with N-succinyl-hydroxyethyl chitosan. *J. Mater. Sci. Mater. Med., 22*, 2745-2755.

Limbert, G. (2019). Chapter 1 - Human Skin: composition, structure and visualisation Methods. In H. K. Graham, A. Eckersley, M. Ozols, K. T. Mellody, & M. J. Sherratt (Eds.), *Skin Biophysics : from experimental characterisation to advanced modelling* (1st ed., pp. 1-18). Springer International Publishing : Imprint: Springer.

Liu, H., Wang, C., Li, C., Qin, Y., Wang, Z., Yang, F., Li, Z., & Wang, J. (2018). A functional chitosan-based hydrogel as a wound dressing and drug delivery system in the treatment of wound healing. *RSC. Adv., 8*, 7533-7549.

Lyons, J., Li, C., & Ko, F. (2004). Melt-electrospinning part I: processing parameters and geometric properties. *Polymer., 45*, 7597-7603.

Ma, J., & Underhill, D. M. (2013). β-Glucan signaling connects phagocytosis to autophagy. *Glycobiology., 23*, 1047-1051.

Majtan, J., & Jesenak, M. (2018). β-Glucans: multi-functional modulator of wound healing. *Molecules., 23*, 1-15.

Martin, J. M., Zenilman, J. M., & Lazarus, G. S. (2010). Molecular microbiology: new dimensions for cutaneous biology and wound healing. *J. Invest. Dermatol., 130*, 38- 48.

Mast, B. A., & Schultz, G. S. (1996). Interactions of cytokines, growth factors, and proteases in acute and chronic wounds. *Wound. Repair. Regen., 4*, 411-420.

Matabola, K. P., & Moutloali, R. M. (2013). The influence of electrospinning parameters on the morphology and diameter of poly(vinyledene fluoride) nanofibers- effect of sodium chloride. *J. Mater. Sci., 48*, 5475-5482.

Matica, M. A., Aachmann, F. L., Tøndervik, A., Sletta, H., & Ostafe, V. (2019). Chitosan as a wound dressing starting material: antimicrobial properties and mode of action. *Int. J. Mol. Sci., 20*, 1-33.

Nayak, R., Padhye, R., Kyratzis, I. L., Truong, Y. B., & Arnold, L. (2012). Recent advances in nanofibre fabrication techniques. *Text. Res. J., 82*, 129-147.

Nitzan, O., Kennes, Y., Colodner, R., Saliba, W., Edelstein, H., Raz, R., & Chazan, B. (2015). Chloramphenicol use and susceptibility patterns in Israel: a national survey. *Isr. Med. Assoc. J., 17*, 27-31.

Ohkawa, K., Kim, H., & Lee, K. (2004). Biodegradation of electrospun poly-(ε-caprolactone) non-woven fabrics by pure-cultured soil filamentous fungi. *J. Polym. Environ., 12*, 211- 218.

Olaussen, J. W. (2020). *Electrospinning of nanofibers with chitosan and beta-glucan as active wound healing ingredients* [Master's thesis, The Arctic University of Norway].

Oliveira, S., Rosowski, E. E., & Huttenlocher, A. (2016). Neutrophil migration in infection and wound repair: going forward in reverse. *Nat. Rev. Immunol., 16*, 378-391.

Pakravan, M., Heuzey, M.-C., & Ajji, A. (2011). A fundamental study of chitosan/PEO electrospinning. *Polymer., 52*, 4813-4824.

Park, J. Y., & Lee, I. H. (2010). Relative humidity effect on the preparation of porous electrospun polystyrene fibers. *J. Nanosci. Nanotechnol., 10*, 3473-3477.

Partheniadis, I., Nikolakakis, I., Laidmae, I., & Heinamaki, J. (2020). A mini-review: needleless electrospinning of nanofibers for pharmaceutical and biomedical applications. *Processes., 8*, 1-20

Pastar, I., Nusbaum, A. G., Gil, J., Patel, S. B., Chen, J., Valdes, J., Stojadinovic, O., Plano, L. R., Tomic-Canic, M., & Davis, S. C. (2013). Interactions of methicillin resistant Staphylococcus aureus USA300 and Pseudomonas aeruginosa in polymicrobial wound infection. *PLoS. One., 8*, 1-11.

Pelipenko, J., Kocbek, P., Govedarica, B., Rošic, R., Baumgartner, S., & Kristl, J. (2013). The topography of electrospun nanofibers and its impact on the growth and mobility of keratinocytes. *Eur. J. Pharm. Biopharm., 84*, 401-411.

Pelipenko, J., Kocbek, P., & Kristl, J. (2015). Critical attributes of nanofibers: preparation, drug loading, and tissue regeneration. *Int. J. Pharm., 484*, 57-74.

Pelipenko, J., Kristl, J., Janković, B., Baumgartner, S., & Kocbek, P. (2013). The impact of relative humidity during electrospinning on the morphology and mechanical properties of nanofibers. *Int. J. Pharm., 456*, 125-134.

Periayah, M. H., Halim, A. S., & Saad, A. Z. (2016). Chitosan: a promising marine polysaccharide for biomedical research. *Pharmacogn. Rev., 10*, 39-42.

Pool, J. G. (1977). Normal hemostatic mechanisms: a review. *Am. J. Med. Technol., 43*, 776- 780.

Pooponpun, S., Polnok, A., Paeratakul, O., Kraisit, P., & Sarisuta, N. (2015). Mechanical and adhesive properties of cellulosic film coats containing polymeric additives. *Pharmazie., 70*, 300-305.

Powers, J. G., Higham, C., Broussard, K., & Phillips, T. J. (2016). Wound healing and treating wounds: chronic wound care and management. *J. Am. Acad. Dermatol., 74*, 607-625.

Preem, Bock, Hinnu, Putrinš, Sagor, Tenson, Meos, Østergaard, & Kogermann. (2019). Monitoring of antimicrobial drug chloramphenicol release from electrospun nano- and microfiber mats using UV imaging and bacterial bioreporters. *Pharmaceutics., 11*, 1- 19.

Preem, L., Mahmoudzadeh, M., Putrinš, M., Meos, A., Laidmäe, I., Romann, T., Aruväli, J., Härmas, R., Koivuniemi, A., Bunker, A., Tenson, T., & Kogermann, K. (2017). Interactions between chloramphenicol, carrier polymers, and bacteria–implications for designing electrospun drug delivery systems countering wound infection. *Mol. Pharm., 14*, 4417-4430.

Qin, F., Sletmoen, M., Stokke, B. T., & Christensen, B. E. (2013). Higher order structures of a bioactive, water-soluble (1→3)-β-D-glucan derived from Saccharomyces cerevisiae. *Carbohydr. Polym., 92*, 1026-1032.

Qin, Y. (2016). Chapter 1 - A brief description of the human body. In Y. Qin (Ed.), *Medical textile materials* (1st ed., pp. 1-12). Elsevier Science & Technology.

Rasouli, R., Barhoum, A., Bechelany, M., & Dufresne, A. (2019). Nanofibers for biomedical and healthcare applications. *Macromol. Biosci., 19*, 1-27.

Reinke, J. M., & Sorg, H. (2012). Wound repair and regeneration. *Eur. Surg. Res., 49*, 35-43.

Rieder, A., & Samuelsen, A. B. (2012). Do cereal mixed-linked β-glucans possess immune-modulating activities? *Mol. Nutr. Food. Res., 56*, 536-547.

Rieger, K. A., Birch, N. P., & Schiffman, J. D. (2013). Designing electrospun nanofiber mats to promote wound healing: a review. *J. Mater. Chem. B., 1*, 4531-4541.

Roberts, G. A. F. (1992). Chapter 5 - Chemical behaviour of chitin and chitosan in chitin chemistry (1st ed., pp. 203-273). Palgrave, London.

Rodrigues, M., Kosaric, N., Bonham, C. A., & Gurtner, G. C. (2019). Wound healing: a cellular perspective. *Physiol. Rev., 99*, 665-706.

Rošic, R., Pelipenko, J., Kocbek, P., Baumgartner, S., Bešter-Rogač, M., & Kristl, J. (2012). The role of rheology of polymer solutions in predicting nanofiber formation by electrospinning. *Eur. Polym. J., 48*, 1374-1384.

Sahariah, P., & Másson, M. (2017). Antimicrobial chitosan and chitosan derivatives: a review of the structure-activity relationship. *Biomacromolecules., 18*, 3846-3868.

Saringat, H. B., Alfadol, K. I., & Khan, G. M. (2005). The influence of different plasticizers on some physical and mechanical properties of hydroxypropyl methylcellulose free films. *Pak. J. Pharm. Sci., 18*, 25-38.

Schreml, S., Szeimies, R. M., Prantl, L., Karrer, S., Landthaler, M., & Babilas, P. (2010). Oxygen in acute and chronic wound healing. *Br. J. Dermatol., 163*, 257-268.

Schultz, G. S., Davidson, J. M., Kirsner, R. S., Bornstein, P., & Herman, I. M. (2011). Dynamic reciprocity in the wound microenvironment. *Wound. Repair. Regen., 19*, 134-148.

Schultz, G. S., & Mast, B. A. (1999). Molecular analysis of the environments of healing and chronic wounds: cytokines, proteases and growth factors. *Wounds. Compend. Clin. Res. Pract., 7*, 7-15.

Sencadas, V., Correia, D. M., Ribeiro, C., Moreira, S., Botelho, G., Gómez Ribelles, J. L., & Lanceros-Mendez, S. (2012). Physical-chemical properties of cross-linked chitosan electrospun fiber mats. *Polym. Test., 31*, 1062-1069.

Seo, G., Hyun, C., Choi, S., Kim, Y. M., & Cho, M. (2019). The wound healing effect of four types of beta-glucan. *App. Biol. Chem., 62*, 1-9.

Seyedian, R., Fard, E. S., Hashemi, S. S., Hasanzadeh, H., Assadi, M., & Zaeri, S. (2020). Diltiazem-loaded electrospun nanofibers as a new wound dressing: fabrication, characterization, and experimental wound healing. *Pharm. Dev. Technol., 26*, 167-180

Shen, A. Y., Haddad, E. J., Hunter-Smith, D. J., & Rozen, W. M. (2018). Efficacy and adverse effects of topical chloramphenicol ointment use for surgical wounds: a systematic review. *ANZ. J. Surg., 88*, 1243-1246.

Shi, R., Geng, H., Gong, M., Ye, J., Wu, C., Hu, X., & Zhang, L. (2018). Long-acting and broad-spectrum antimicrobial electrospun poly (ε-caprolactone)/gelatin micro/nanofibers for wound dressing. *J. Colloid. Interface. Sci., 509*, 275-284.

Siefert, S. A., & Sarkar, R. (2012). Matrix metalloproteinases in vascular physiology and disease. *Vascular., 20*, 210-216.

Sill, T. J., & von Recum, H. A. (2008). Electrospinning: applications in drug delivery and tissue engineering. *Biomaterials., 29*, 1989-2006.

Singh, S., Young, A., & McNaught, C. E. (2017). The physiology of wound healing. *Surgery., 35*, 473-477.

Sorg, H., Krueger, C., & Vollmar, B. (2007). Intravital insights in skin wound healing using the mouse dorsal skin fold chamber. *J. Anat., 211*, 810-818.

Stie, M. B., Gätke, J. R., Wan, F., Chronakis, I. S., Jacobsen, J., & Nielsen, H. M. (2020). Swelling of mucoadhesive electrospun chitosan/polyethylene oxide nanofibers facilitates adhesion to the sublingual mucosa. *Carbohydr. Polym., 242*, 116428- 116428.

Sun, B., Long, Y. Z., Zhang, H. D., Li, M. M., Duvail, J. L., Jiang, X. Y., & Yin, H. L. (2014). Advances in three-dimensional nanofibrous macrostructures via electrospinning. *Prog. Polym. Sci., 39*, 862-890.

Sun, L., & Zhao, Y. (2007). The biological role of dectin-1 in immune response. *Int. Rev. Immunol., 26*, 349-364.

Tamm, I., Heinämäki, J., Laidmäe, I., Rammo, L., Paaver, U., Ingebrigtsen, S. G., Škalko- Basnet, N., Halenius, A., Yliruusi, J., Pitkänen, P., Alakurtti, S., & Kogermann, K. (2016). Development of suberin fatty acids and chloramphenicol-loaded antimicrobial electrospun nanofibrous mats intended for wound therapy. *J. Pharm. Sci., 105*, 1239- 1247.

Tammaro, L., Saturnino, C., D'Aniello, S., Vigliotta, G., & Vittoria, V. (2015). Polymorphic solidification of linezolid confined in electrospun PCL fibers for controlled release in topical applications. *Int. J. Pharm., 490*, 32-38.

Toledo-Pereyra, L. H., Lopez-Neblina, F., & Toledo, A. H. (2004). Reactive oxygen species and molecular biology of ischemia/reperfusion. *Ann. Transplant., 9*, 81-83.

Tsioufis, C., Bafakis, I., Kasiakogias, A., & Stefanadis, C. (2012). The role of matrix metalloproteinases in diabetes mellitus. *Curr. Top. Med. Chem., 12*, 1159-1165.

van Asten, S. A., La Fontaine, J., Peters, E. J., Bhavan, K., Kim, P. J., & Lavery, L. A. (2016). The microbiome of diabetic foot osteomyelitis. *Eur. J. Clin. Microbiol. Infect. Dis., 35*, 293-298.

Van der Schueren, L., Steyaert, I., De Schoenmaker, B., & De Clerck, K. (2012). Polycaprolactone/chitosan blend nanofibres electrospun from an acetic acid/formic acid solvent system. *Carbohydr. Polym., 88*, 1221-1226.

Vig, K., Chaudhari, A., Tripathi, S., Dixit, S., Sahu, R., Pillai, S., Dennis, V. A., & Singh, S. R. (2017). Advances in skin regeneration using tissue engineering. *Int. J. Mol. Sci., 18*, 1-19.

Wahba, M. I. (2020). Enhancement of the mechanical properties of chitosan. *J. Biomater. Sci. Polym. Ed., 31*, 350-375.

Walker, S., Diaper, C. J. M., Bowman, R., Sweeney, G., Seal, D. V., & Kirkness, C. M. (1998). Lack of evidence for systemic toxicity following topical chloramphenicol use. *Eye., 12*, 875-879.

Wallace, L. A., Gwynne, L., & Jenkins, T. (2019). Challenges and opportunities of pH in chronic wounds. *Ther. Deliv., 10*, 719-735.

Wang, J., Planz, V., Vukosavljevic, B., & Windbergs, M. (2018). Multifunctional electrospun nanofibers for wound application: novel insights into the control of drug release and antimicrobial activity. *Eur. J. Pharm. Biopharm., 129*, 175-183.

Wilgus, T. A. (2008). Immune cells in the healing skin wound: influential players at each stage of repair. *Pharmacol. Res., 58*, 112-116.

Yalcinkaya, F. (2019). Preparation of various nanofiber layers using wire electrospinning system. *Arab. J. Chem., 12*, 5162-5172.

Yang, S., Zhang, X., & Zhang, D. (2019). Electrospun chitosan/poly (vinyl alcohol)/graphene oxide nanofibrous membrane with ciprofloxacin antibiotic drug for potential wound dressing application. *Int. J. Mol. Sci., 20*, 1-16.

Yu, M., Dong, R. H., Yan, X., Yu, G. F., You, M. H., Ning, X., & Long, Y. Z. (2017). Recent advances in needleless electrospinning of ultrathin fibers: from academia to industrial production. *Macromol. Mater. Eng., 302*, 1-19.

Yuan, T. T., Jenkins, P. M., DiGeorge Foushee, A. M., Jockheck-Clark, A. R., & Stahl, J. M. (2016). Electrospun chitosan/polyethylene oxide nanofibrous scaffolds with potential antibacterial wound dressing applications. *J. Nanomater., 2016*, 1-10.

Zhang, Q., Murawsky, M., LaCount, T., Hao, J., Kasting, G. B., Newman, B., Ghosh, P., Raney, S. G., & Li, S. K. (2017). Characterization of temperature profiles in skin and transdermal delivery system when exposed to temperature gradients in vivo and in vitro. *Pharm. Res., 34*, 1491-1504.

Zhao, G., Usui, M. L., Lippman, S. I., James, G. A., Stewart, P. S., Fleckman, P., & Olerud, J. E. (2013). Biofilms and inflammation in chronic wounds. *Adv. Wound. Care., 2*, 389- 399.

Zhao, R., Liang, H., Clarke, E., Jackson, C., & Xue, M. (2016). Inflammation in chronic wounds. *Int. J. Mol. Sci., 17*, 1-14.

Zhu, F., Du, B., & Xu, B. (2016). A critical review on production and industrial applications of beta-glucans. *Food. hydrocoll., 52*, 275-288.

Zupančič, Š., Potrč, T., Baumgartner, S., Kocbek, P., & Kristl, J. (2016). Formulation and evaluation of chitosan/polyethylene oxide nanofibers loaded with metronidazole for local infections. *Eur. J. Pharm. Sci., 95*, 152-160.

Zupančič, Š., Sinha-Ray, S., Sinha-Ray, S., Kristl, J., & Yarin, A. L. (2016). Controlled release of ciprofloxacin from core-shell nanofibers with monolithic or blended core. *Mol. Pharm., 13*, 1393-1404.

Zykova, S. N., Balandina, K. A., Vorokhobina, N. V., Kuznetsova, A. V., Engstad, R., & Zykova, T. A. (2014). Macrophage stimulating agent soluble yeast β-1,3/1,6-glucan as a topical treatment of diabetic foot and leg ulcers: a randomized, double blind, placebo-controlled phase II study. *J. Diabetes. Investig., 5*, 392-399.

8 Appendix

Polymer solutions

Tabel A 1: Theoretical composition of polymers and chloramphenicol (CAM) in the polymer solution.*"All" indicate that all the polymers (CHI, βG and co-polymers) were included, CHI stands for Chitosan, βG stands for β-glucan, "Ref" indicate that only the co-polymers (polyethylene oxide and hydroxypropyl methylcellulose) were included.*

Name of solution	Polymer concentration (%)	CHI (%)	βG (%)	PEO (%)	HPMC (%)	CAM (%)
All-Sol	2.5	20	20	30	30	
CHI-Ref-Sol	2.5	20		40	40	
βG-Ref-Sol	2.5		20	40	40	
Ref-Sol	2.5			50	50	
All-CAM-Sol	2.5	20	20	29.5	29.5	1
CHI-Ref-CAM-Sol	2.5	20		39.5	39.5	1
βG-Ref-CAM-Sol	2.5		20	39.5	39.5	1
Ref-CAM-Sol	2.5			49.5	49.5	1

Tabel A 2: Exact composition of polymers and chloramphenicol (CAM) in the polymer solution. *"All" indicate that all the polymers (CHI, βG and co-polymers) were included, CHI stands for Chitosan, βG stands for β-glucan, "Ref" indicate that only the co-polymers (polyethylene oxide and hydroxypropyl methylcellulose) were included.*

| Name of solution	Polymer concentration (%)	CHI (%)	βG (%)	PEO (%)	HPMC (%)	CAM (%)
All-Sol	2.5	20	20	30	30	
All-Sol	2.5	20	20	30	30	
All-Sol	2.5	19.9	19.9	30.2	30	
CHI-Ref-Sol	2.5	20		40	40	
CHI-Ref-Sol	2.5	20		40	40	
CHI-Ref-Sol	2.51	20		40	40	
βG-Ref-Sol	2.5		20	40	40	
βG-Ref-Sol	2.5		20	40	40	
βG-Ref-Sol	2.5		20	40	40	
Ref-Sol	2.5			50	50	
Ref-Sol	2.5			50	50	
Ref-Sol	2.5			50	50	
All-CAM-Sol	2.5	20	20	29.5	29.5	1
All-CAM-Sol	2.5	20	20	29.5	29.5	1
All-CAM-Sol	2.5	20	20	29.5	29.5	1
CHI-Ref-CAM-Sol	2.5	20		39.5	39.5	1
CHI-Ref-CAM-Sol	2.5	20		39.5	39.5	1
CHI-Ref-CAM-Sol	2.5	20		39.5	39.5	1
βG-Ref-CAM-Sol	2.5		20	39.5	39.5	1
βG-Ref-CAM-Sol	2.5		20	39.5	39.5	1
βG-Ref-CAM-Sol	2.5		20	39.5	39.5	1
Ref-CAM-Sol	2.5			49.5	49.5	1
Ref-CAM-Sol	2.5			49.5	49.5	1
Ref-CAM-Sol	2.5			49.5	49.5	1

Diameter distribution
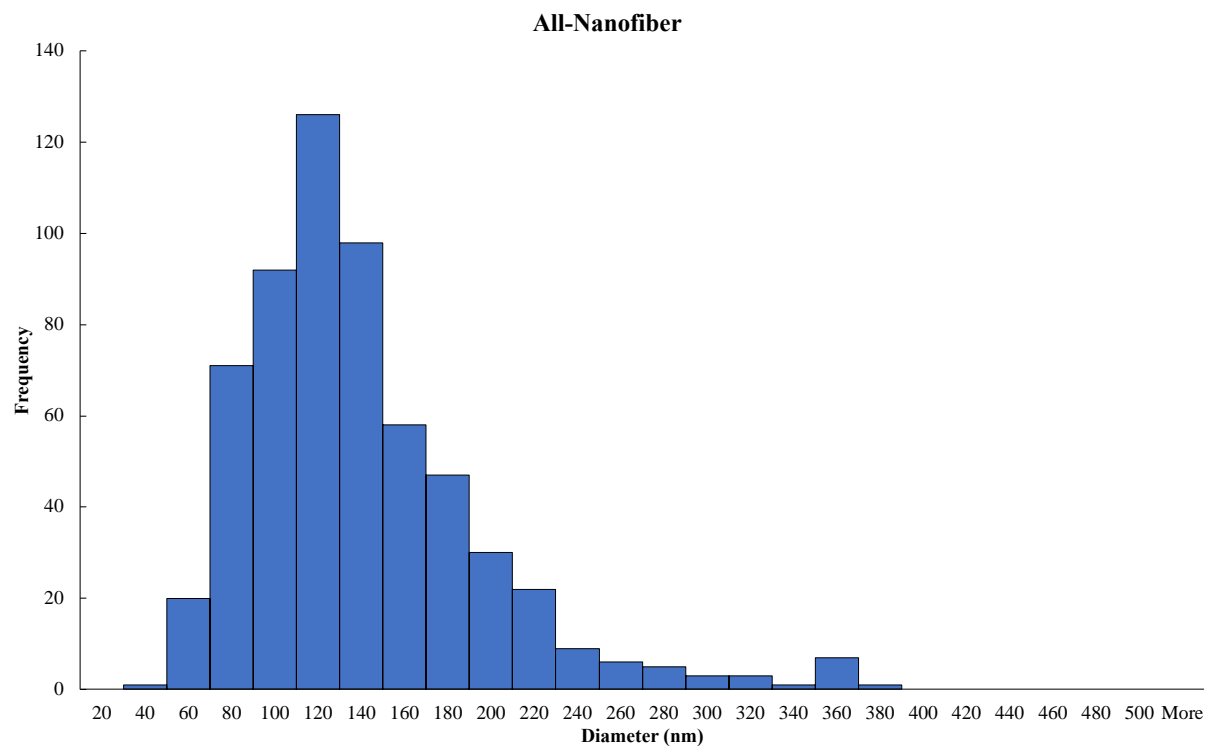
Figure A 1: Diameter distribution histogram for All-Nanofiber. *"All" indicate that all the polymers (CHI, βG and co-polymers) were included, CHI stands for Chitosan, βG stands for β-glucan, "Ref" indicate that only the co-polymers (polyethylene oxide and hydroxypropyl methylcellulose) were included.*
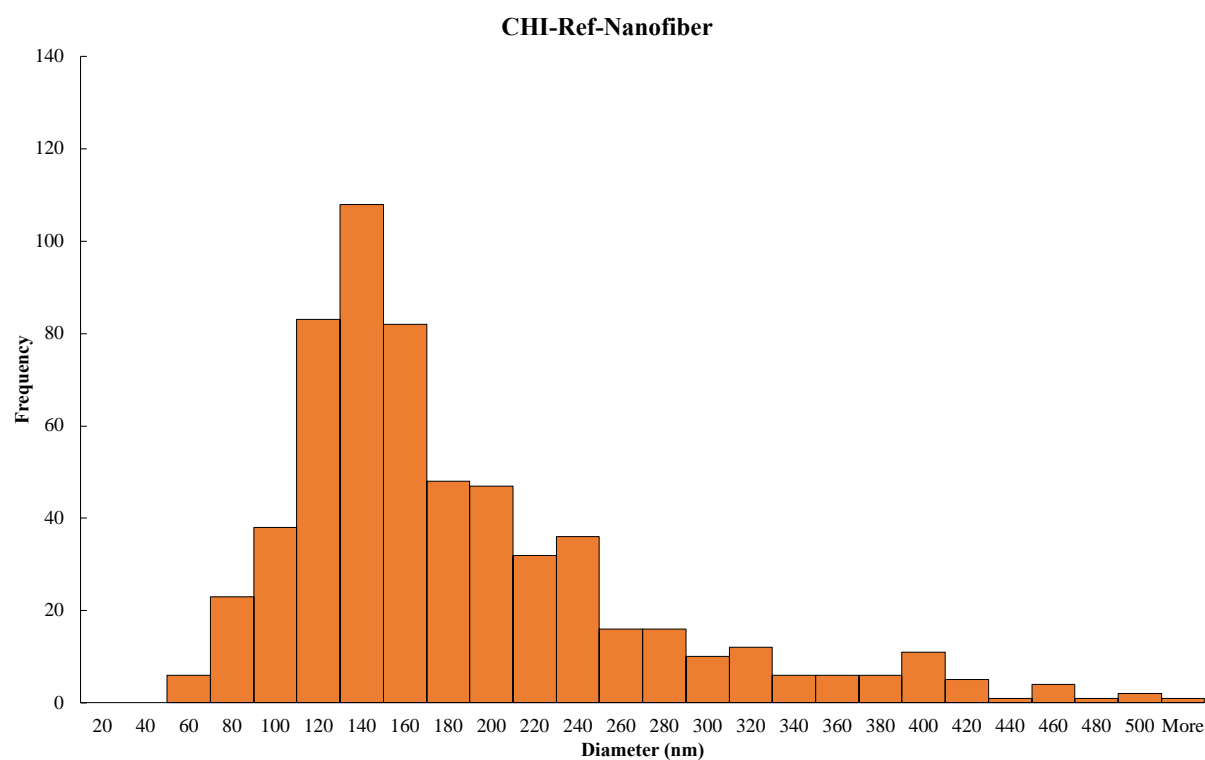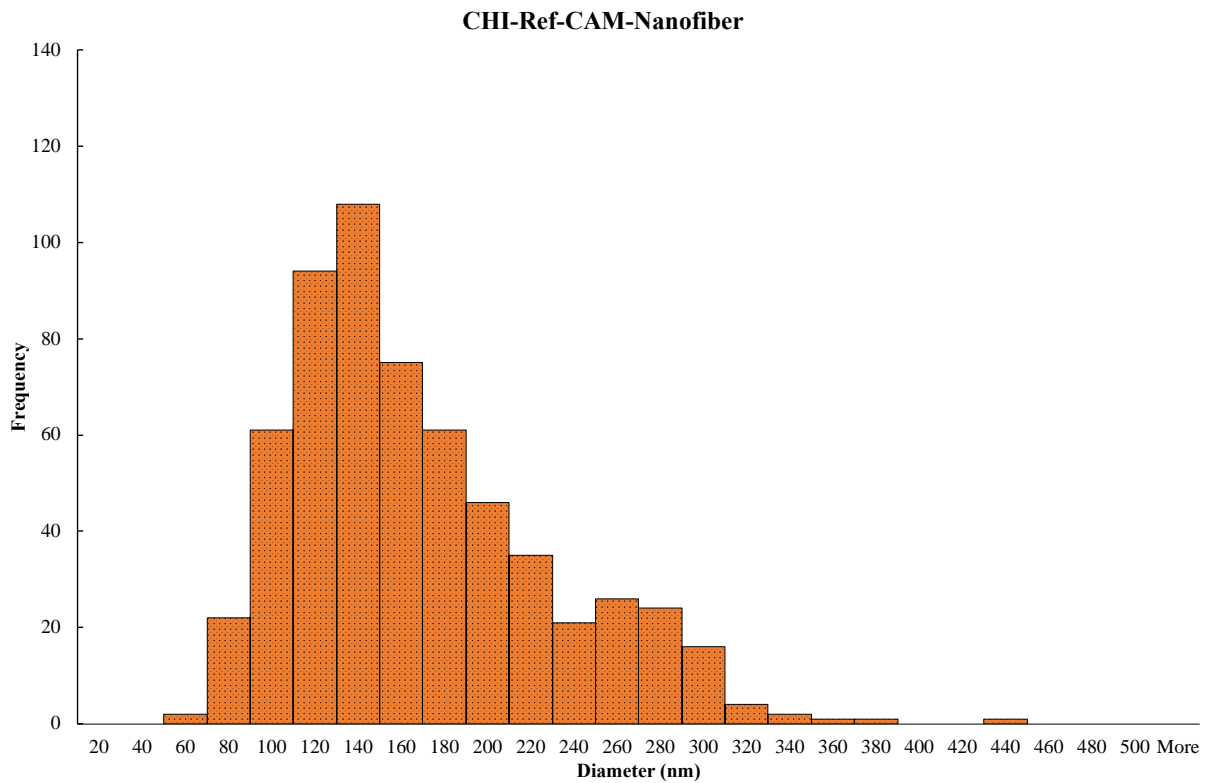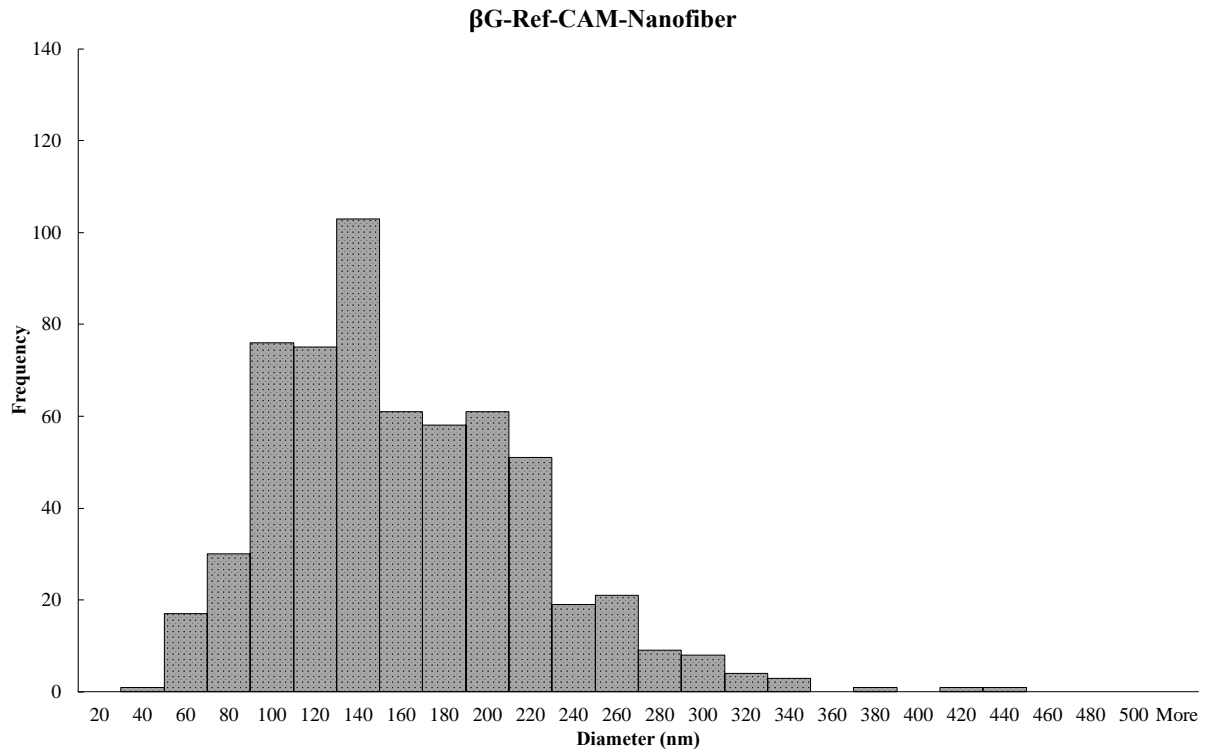

Figure A 2: Diameter distribution histogram for CHI-Ref-Nanofiber. *CHI stands for Chitosan, βG stands for β-glucan, "Ref" indicate that only the co-polymers (polyethylene oxide and hydroxypropyl methylcellulose) were included.*
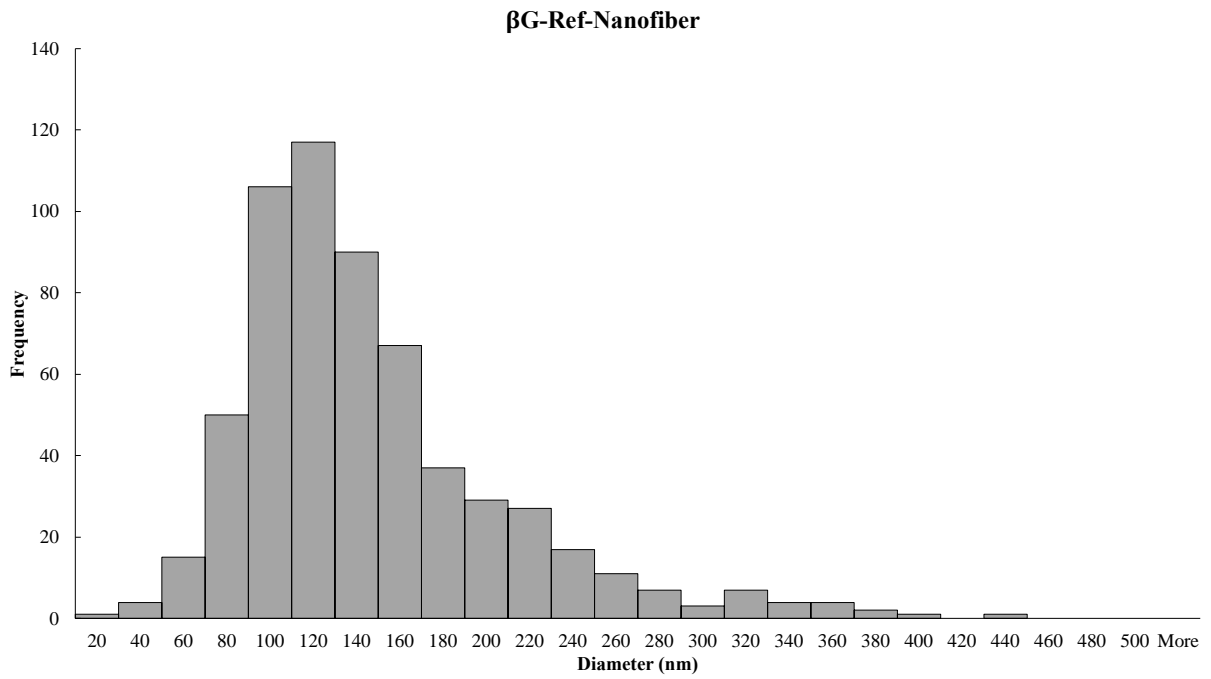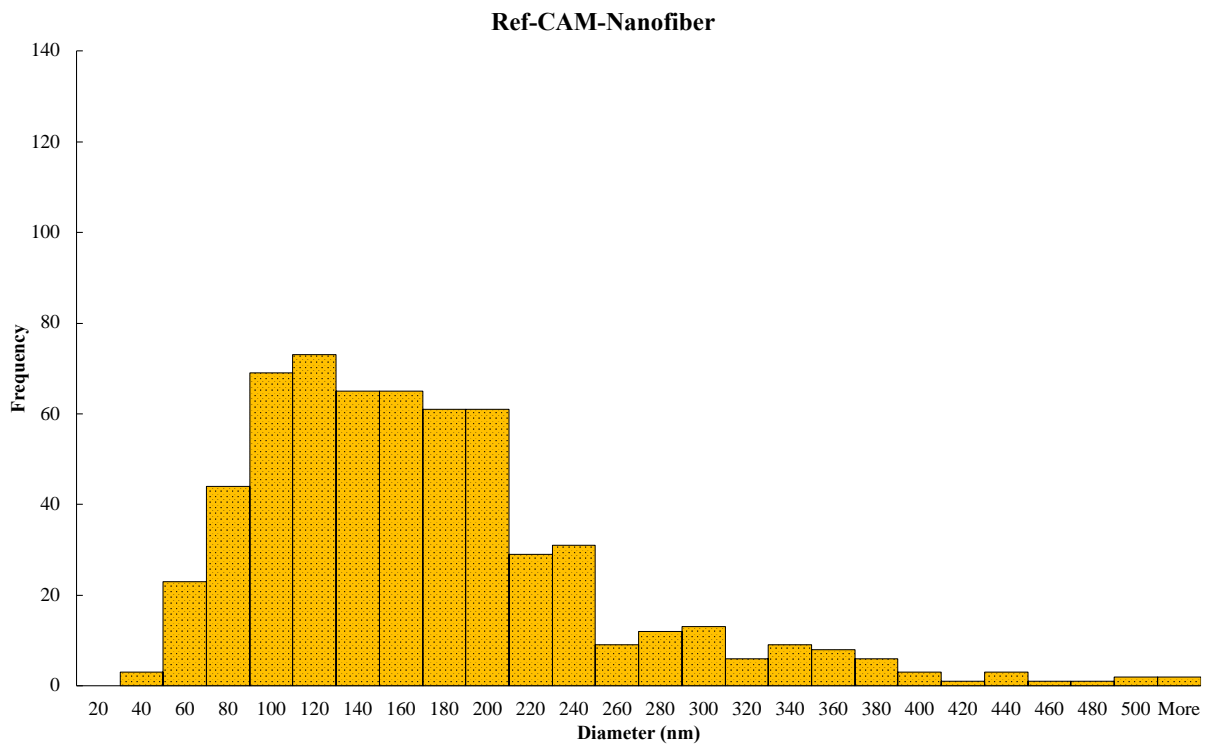
βG-Ref-Nanofiber

Figure A 3: Diameter distribution histogram for βG-Ref-Nanofiber. *βG stands for β-glucan, "Ref" indicate that only the co-polymers (polyethylene oxide and hydroxypropyl methylcellulose) were included.*
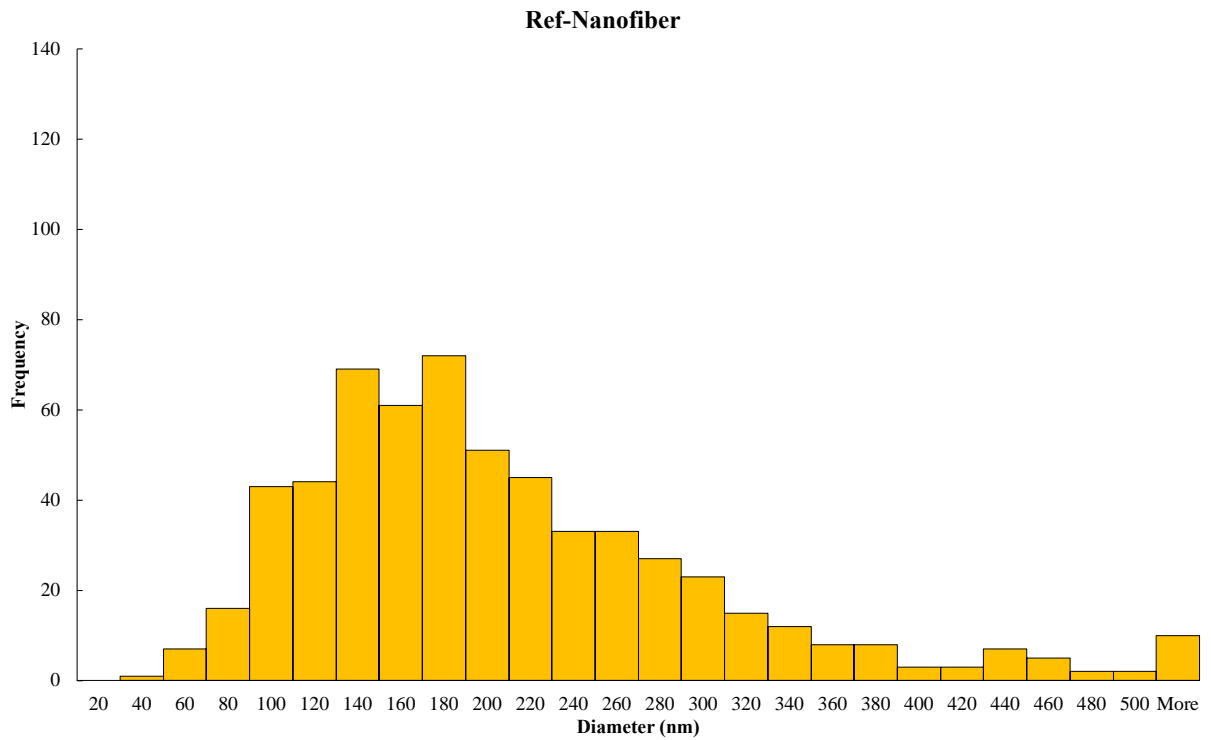
Ref-Nanofiber

Figure A 4: Diameter distribution histogram for Ref-Nanofiber. *"Ref" indicate that only the co-polymers (polyethylene oxide and hydroxypropyl methylcellulose) were included.*
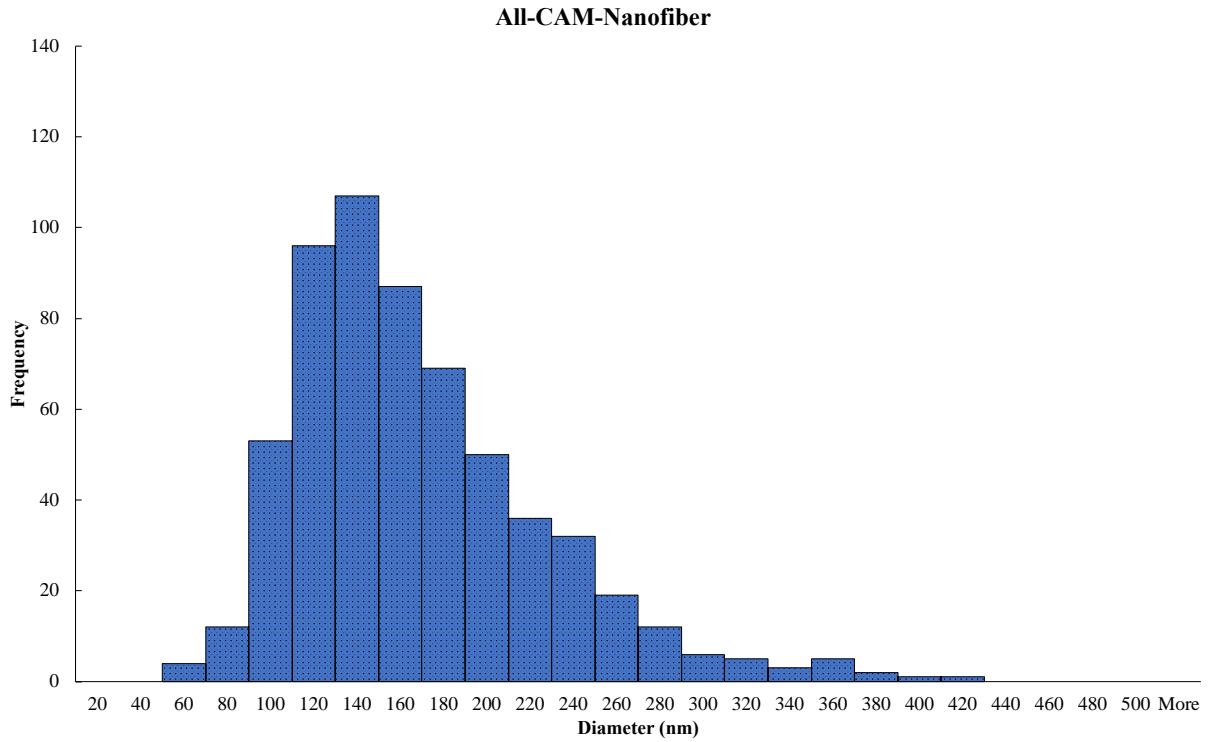
Figure A 5: Diameter distribution histogram for All-CAM-Nanofiber. *"All" indicate that all the polymers (CHI, βG and co-polymers) were included, CHI stands for Chitosan, βG stands for β-glucan, "Ref" indicate that only the co-polymers (polyethylene oxide and hydroxypropyl methylcellulose) were included. CAM stands for chloramphenicol.*
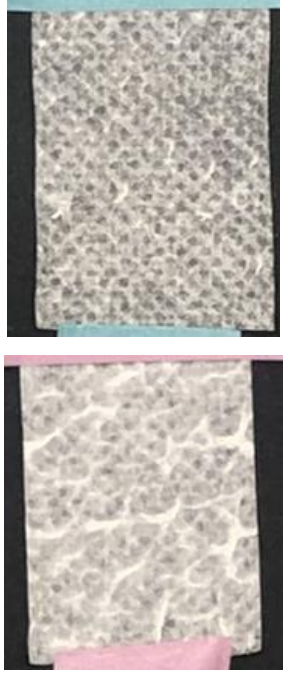

Figure A 6: Diameter distribution histogram for CHI-Ref-CAM-Nanofiber. *CHI stands for Chitosan, βG stands for β-glucan, "Ref" indicate that only the co-polymers (polyethylene oxide and hydroxypropyl methylcellulose) were included. CAM stands for chloramphenicol.*

Figure A 7: Diameter distribution histogram for βG-Ref-CAM-Nanofiber. *CHI stands for Chitosan, βG stands for β-glucan, "Ref" indicate that only the co-polymers (polyethylene oxide and hydroxypropyl methylcellulose) were included. CAM stands for chloramphenicol.*
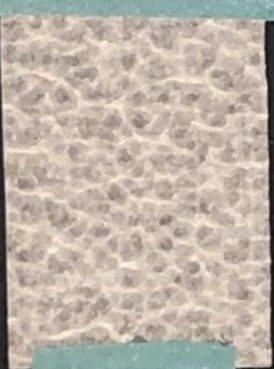

Figure A 8: Diameter distribution histogram for Ref-CAM-Nanofiber. *"Ref" indicate that only the co-polymers (polyethylene oxide and hydroxypropyl methylcellulose) were included. CAM stands for chloramphenicol.*

Nanofibers

Tabel A 3: Picture of electrospun nanofibers. *."All" indicate that all the polymers (CHI, βG and co-polymers) were included, CHI stands for Chitosan, βG stands for β-glucan, "Ref" indicate that only the co-polymers (polyethylene oxide and hydroxypropyl methylcellulose) were included.*

Nanofiber	iPhone images	Comments
All-Nanofiber		• White appearance • Felt thicker than other electrospun nanofibers • Easy to remove from the substrate
CHI-Ref-Nanofiber		• White appearance • Easy to remove from the substrate
βG-Ref-Nanofiber		• Almost uniform white appearance, both pictures to left show nanofibers obtained after electrospinning • Felt thinner compared to nanofibers containing CHI • Hard to remove from the substrate • Sometimes it was hard to handle since it was brittle than other nanofibers containing CHI.

Ref-Nanofiber		• Almost uniform white appearance. • Felt thinner compared to nanofibers containing CHI. • Hard to remove from the substrate • Sometimes it was hard to handle since it was brittle than other nanofibers containing CHI.
All-CAM-Nanofiber		• White appearance • Felt thicker than other electrospun nanofibers without CHI • Easy to remove from the substrate
CHI-Ref-CAM-Nanofiber		• White appearance • Felt thicker than other electrospun nanofibers without CHI • Easy to remove from the substrate
βG-Ref-CAM-Nanofiber		• Almost uniform white appearance, both pictures to left show nanofibers obtained after electrospinning • Felt thinner compared to nanofibers containing CHI • Hard to remove from the substrate

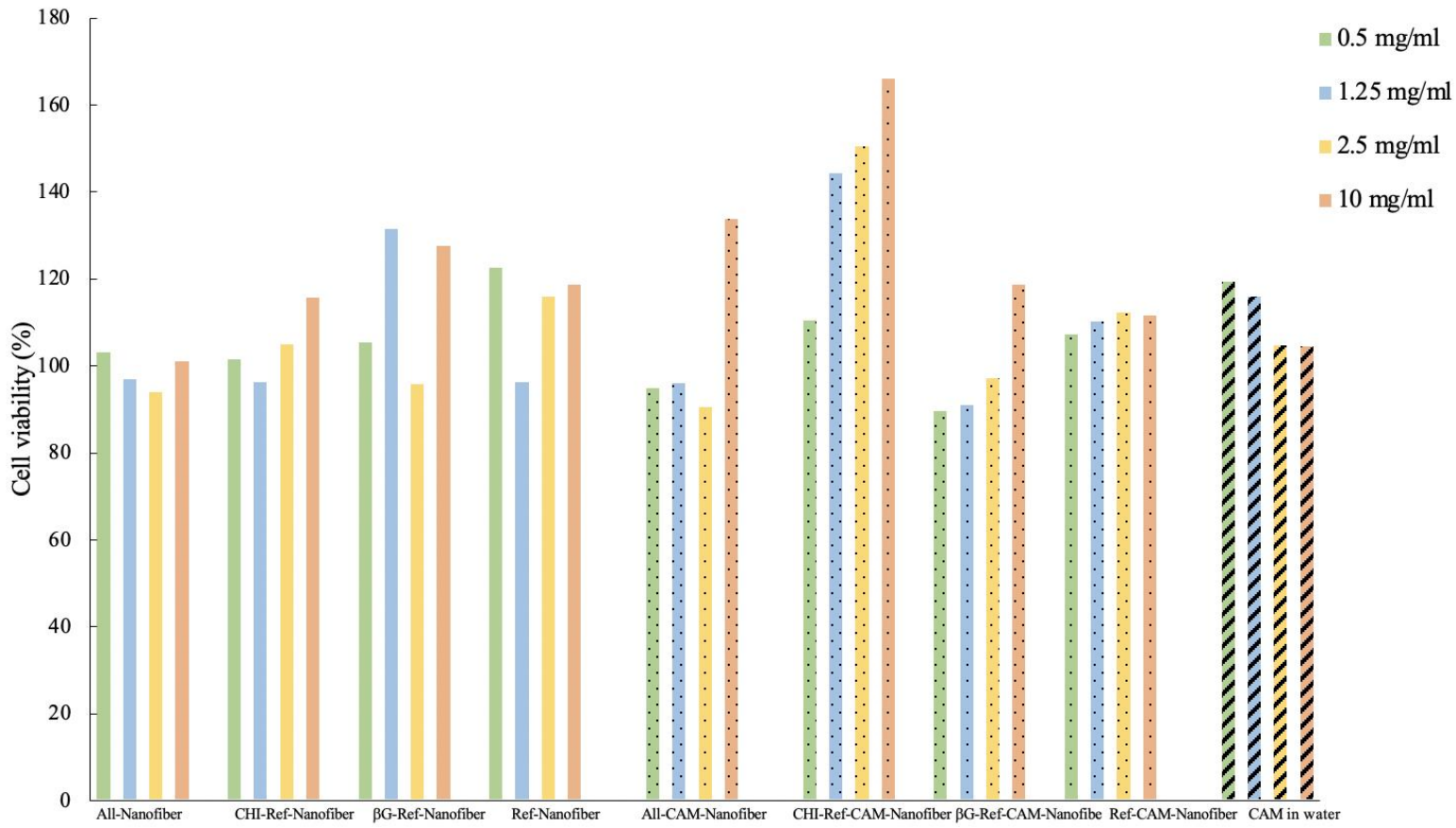|		
		• Sometimes it was hard to handle since it was brittle than other nanofibers containing CHI.
Ref-CAM-Nanofiber		• Almost uniform white appearance. • Felt thinner compared to nanofibers containing CHI. • Hard to remove from the substrate • Sometimes it was hard to handle since it was brittle than other nanofibers containing CHI.

Cell viability

Figure A 9: Cell viability of different nanofibers with different concentrations. *"All" indicate that all the polymers (CHI, βG and co-polymers) were included, CHI stands for Chitosan, βG stands for β-glucan, "Ref" indicate that only the co-polymers (polyethylene oxide and hydroxypropyl methylcellulose) were included.*